Characterization of new Fe^{II} PNP Pincer-Complexes with sterically nondemanding Phosphine-Residues

Master Thesis

Mathias Glatz

0731595

Institute of Chemistry/Inorganic Chemistry
University of Graz

Head: Univ.-Prof. Dipl.-Chem. Dr.rer.nat Nadia Carmen Mösch-Zanetti

Person in Charge: Univ.-Prof. Dipl.-Chem. Dr.rer.nat Nadia Carmen Mösch-Zanetti

and Ao.Univ.Prof. Dipl.-Ing. Dr.techn. Karl Kirchner (Technical University of Vienna)

Graz, September 2013

STATUTORY DECLARATION

I declare that I have authored this thesis independently, that I have not used other than the declared sources / resources and that I have explicitly marked all material which has been quoted either literally or by content from the used sources.

…… ……..

date (signature)

Note of Thanks

Karl Kirchner - ein umgänglicher, freundlicher und zugleich fachlich kompetenter Professor, in einer Kombination wie mir bisher kein Anderer untergekommen ist. Danke Karl für die vielen Erfahrungen die ich in dieser Arbeitsgruppe machen konnte. In diesem ehrgeizigen Umfeld in dem das Ziel „coole, tolle Chemie“ ist, konnte ich meinen durchschnittlichen Erfindergeist uneingeschränkt ausleben. Ganz nebenbei entflammte hier meine Begeisterung für Phosphine – im wahrsten Sinne.

Ich danke dem Dekan der TU Graz, Herrn Gescheidt-Demner, für die Genehmigung der Masterarbeit sowie Nadia Mösch-Zanetti die mir als Betreuerin diese Arbeit überhaupt ermöglicht hat.

Vielen Dank für die Unterstützung meiner Familie über das gesamte Chemiestudium hinweg – auch wenn Sie mit Chemie nicht wirklich was anfangen können. Auch wenn es mal zu kleineren „Vorfällen“ im Labor kommt – mir geht’s gut und ich hab das im Griff– gibt wirklich schlimmeres! Dank an meine Schwester Kata für ihre Fürsorge in Wien und die Abwicklung aller Dinge abseits des Studiums für die ich zu faul/blöd/feig bin.

Dank an die Kollegen Ötzi, Burnman, Matthias, Christian, Nikolaus, Iker, Sathy-Booze und Sara der Arbeitsgruppe für die kompetente fachbezogene Unterstützung im Labor, das freundliche Arbeitsklima und die wunderbaren „sozialen“ Abende in der Küche oder auch Grillabende. Es ist euer verdienst, dass ich mittlerweile mehr auf der Uni bin als sonst wo.

Danke Burnman für die Einweisung in Gerätschaften, Arbeitstechniken und Administratives. Jeder Tag im Labor ist ein Kabarett mit dir. Treib deine Studenten nicht zuviel!

Danke Ötzi für die Hilfe bei Synthesen und Einkristallen, wenn ich schon am verzweifeln war. Du als Aufseher im Labor wirst sehr fehlen.

Danke Christian für die synthetischen Hilfestellungen und Arbeitstechniken.

Danke Matthias für die gute Freundschaft – ich freue mich auf die (hoffentlich) erfolgreiche Zusammenarbeit mit einem organischen Genie wie dir.

Danke „ Team Simmering“ (Burnman, Matthias, Ouda, Daniel, Meister Eder…) für die lustigen Abende auf hohem Niveau mit musikalischer Unterlegung.

Danke unserem „Kirchenwirt“ (Theater Kantine) für das geile Mittagessen sowie unserem Lunchgood für das schöne Wetter.

Dank auch an die hilfreichen Kollegen anderer Arbeitsgruppen Danny, Sven, Big-Fel, Stu-Tang.

Dank an meine feine steirische Selektion an guten Freunden aus meiner Heimat, die ich glücklicherweise in Wien öfter treffen konnte. Lupac, dem talentierten Mediziner und einzigen nicht-Chemiker mit dem ich immer wieder fachliche Diskussionen führen kann. Ich freue mich auf viele weitere Karten-Abende mit gutem Essen und NFL Diskussionen. P-Diddy dem Maschinenbauer, A-Dogg dem Germanisten, meiner Anlaufstelle für Gaming. Hell-Mood der Mathematiker, meine Anlaufstelle für guten Whisky.

Dank an meine großartigen Studienkollegen aus Graz die mir sehr fehlen. Es ist immer wieder eine Freude die 3 lustigen 4 zu treffen – Vielen Dank für die schöne Zeit und die gemeinsamen Lernstunden während unseres Werdegangs. Stefan, der Organiker der sich alles aus den Fingern saugen kann. Auch wenn ich nicht helfen kann, frag Manu und Seppo die fleißigen Arbeitstiere! Wann kommt ihr mich eigentlich mal besuchen?

Dank auch an die ehem. Mitglieder der Spaßfraktion Robin, Lu und Robert.

Abstract

Catalysis based on pincer-complexes has rapidly developed during the last two decades. The field of Fe based pincer-catalysts is also on the rise. The ligand design is crucial when it comes down to the fine-tuning of catalysts. Due to benefits in modification (steric/electronic) and characterization (NMR) phosphine-ligands found great utilization.

In order to extend the scope of PNP pincer ligands, new sterically nondemanding phosphine-precursors with ranging electronic properities, were synthesized. The impact on reactivity of these small residues was tested on a set of Fe^{II} carbonyl complexes $[Fe(PNP)Y_2CO]$ and $[Fe(PNP)Y(CO)_2]^+$ (Y = Cl, Br).

The primary focus was put on a series of octahedral Fe(II) complexes of general type κ^2, κ^3-$[Fe(PNP)_2Y]^+$ (Y = Cl, Br), which have been developed in this study. These new complexes show an unusual bonding modes of two PNP-pincers, one in a bidentate (*N,P*) and one in a regular tridentate (*P,N,P*) bonding manner. The formation of these complexes is highly dependent on the phosphine-residues ($-PR_2$) moiety being formed only with sterically little demanding substituents. Subtle variation of the substituents also resulted in striking differences in reactivity and stability. Utilizing a wide range of different phosphines was essential to understand these behaviors.

Contents

Introduction and Motivation

In the recent decades pincer complexes have received considerable attention in the field of organometallic chemistry. Especially pincer complexes of noble metals (e.g. Pd, Ir, Ru, Pt) have shown high potential in catalysis. Noteworthy applications are various coupling reactions, transfer reactions, and condensations.[1] Although the first pincer ligands were already synthesized and described in 1976 by Moulton and Shaw,[2] it took another decade until they were reexamined. Pincers are neutral or cationic, tridentate ligands which usually adopt in a meridional coordination mode. Due to the large scope of possible structures, a general simplification is made for designation by using the letters of the coordinated atoms. Throughout this study, PNP pincers were used exhibiting the 2,6-diaminopyridine (2,6-DAP) scaffold (**figure 1**).

The formation of P-N bonds has been employed for many decades[3] by reaction of a chlorophosphine with a primary or secondary amine. HCl liberated in the course of this reaction, is trapped by an organic base. The resulting aminophosphine is stable, while di- and triamides tend higher lability.[4]

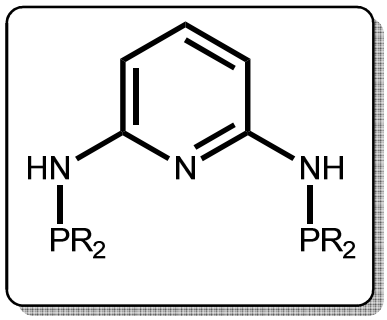

Figure 1. N,N'-bis(diaryl)- and bis(dialkyl) phosphino-2,6-diaminopyridines (PNP), the basic ligands of this study

Despite its simple structure, PNP pincers offer various possibilities for modifications (**figure 2**). Obviously, most of the electronic influence results from the atoms directly coordinated to the metal center (Z, D).

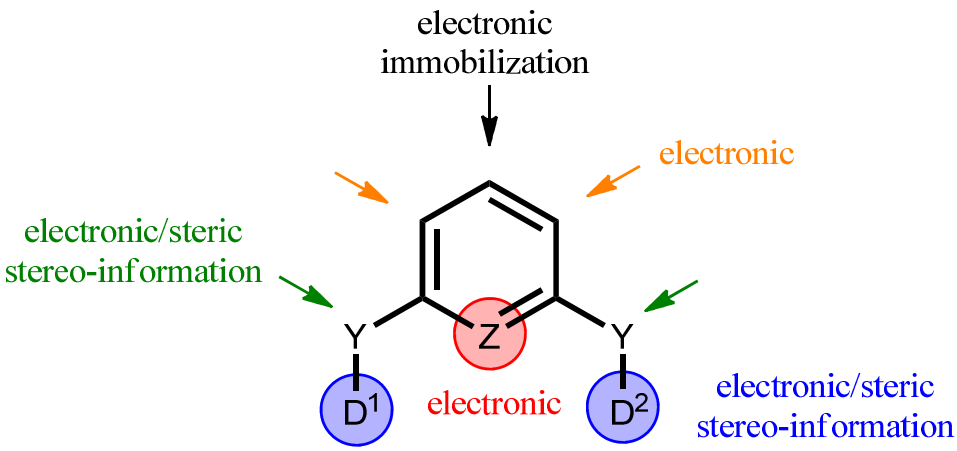

Figure 2. Sites and type of modifications for pincer ligands

Sometimes steric effects are even more important, especially when it comes to chiral information in catalysis. Both D and Y are suitable for steric modification provided that the valency of Y allows steric/chiral modifications in the case of C and N spacers. Electronic influence is also provided by the bridging atoms Y (Y = C, N, O) as well as the substituents attached to them. The striking difference of Y-alkylated (Y = N) PNP-pincers was shown by Kirchner *et al* in a series of Mo and W complexes.[5] Moreover, the aromatic ring can also be modified easily by substitutions or variations in ring-size, but this usually has only minor electronic effects. In this case, the four position of the pyridine is an exception, because it is predestinated for immobilization on selected surfaces. After all, a large variety of ligands can be prepared utilizing inexpensive building-blocks.

The replacement of rare and expensive noble metals catalysts by more earth abundant metals like iron is a desirable goal in chemistry. Among existing Fe-catalysts, hydrogenation and transfer hydrogenation reactions are strongly represented. Lately, the research groups of Casey,[6] Chirik,[7] Morris,[8] and Milstein[9] have successfully demonstrated the potential of Fe-catalysts for hydrogenation of ketones, aldehydes, and even alkenes.

Beside catalytic applications, well defined molecular devices and switches are major goals of organometallic compounds. Various sensors for small molecules like carbon monoxide (CO) have been developed lately. CO is considered as one of the “six common air pollutants” by the Environmental Protection Agency (EPA) besides ozone, particulate matter, nitrogen oxides, sulfur oxide and lead. The gas is usually emitted during incomplete combustion which makes traffic and industry a major source for CO. Since CO is odor- and colorless, the gas is not olfactory recognized by the human organism even at high exposure levels which makes it a potential silent killer. Actually CO has a 200 plus fold higher affinity towards hemoglobin than molecular oxygen. As a result, the oxygen delivery towards essential organs and tissues

is reduced. Depending on the exposure level and time, the hazardous effects range from chronic long term damage to acute harm and death. To handle this issue the EPA set National Ambient Air Quality Standards (NAAQS) for common pollutants as a result of the Clean Air Act. The standards for CO in air were finalized in 2011 and are since yet set to 9 ppm average per 8h or rather 35 ppm average per 1 h not to exceed more than 1/year.[10] A global monitoring of CO therefore requires an innovative, robust and affordable senor system.

Recently numerous materials capable for detection of CO have emerged, most of them consisting of metal oxides (e.g. Zn) with an electrochemical based detection technique.[11] A few research groups published molecular compounds with well-defined structures, binding gaseous CO reversibly resulting in an obvious change in color. These rare chromogenic sensing systems, usually organometallic complexes and clusters, show high selectivity towards CO in solid state and/or in solution. Many of these examples include metals of the 1st transition row as reported for Fe(II) and Co(II) complexes containing hemilabile tridentate PSN-ligands, facial coordinated.[12]

A single example was reported for a planar Ni(II) complex with an immediate color change in solution in the presence of CO.[13] A recent example shows polymeric PSX (X=N,O) coordinated Cu(I) reversible binding CO in solid state.[14] Other examples report 2nd row transition-metals like oxoacetato-bridged Ru_3-clusters, reversibly binding CO in CH_3CN, although induced by photosensitized electron transfer.[15] Few of these examples combine both good detection limit and long term stability which would be essential for a wide range application. However, the most remarkable solid state chromogenic sensing system with an overwhelming detection limit of 0.2 ppm, even recordable with the “naked eye” was reported by Moragues *et al*.[16]

Scheme 1 displays a suitable PNP-system based on iron on molecular level which was already published in 2008 by Kirchner et al.[17] Similar systems, using a modified ring-system were also reported.[18]

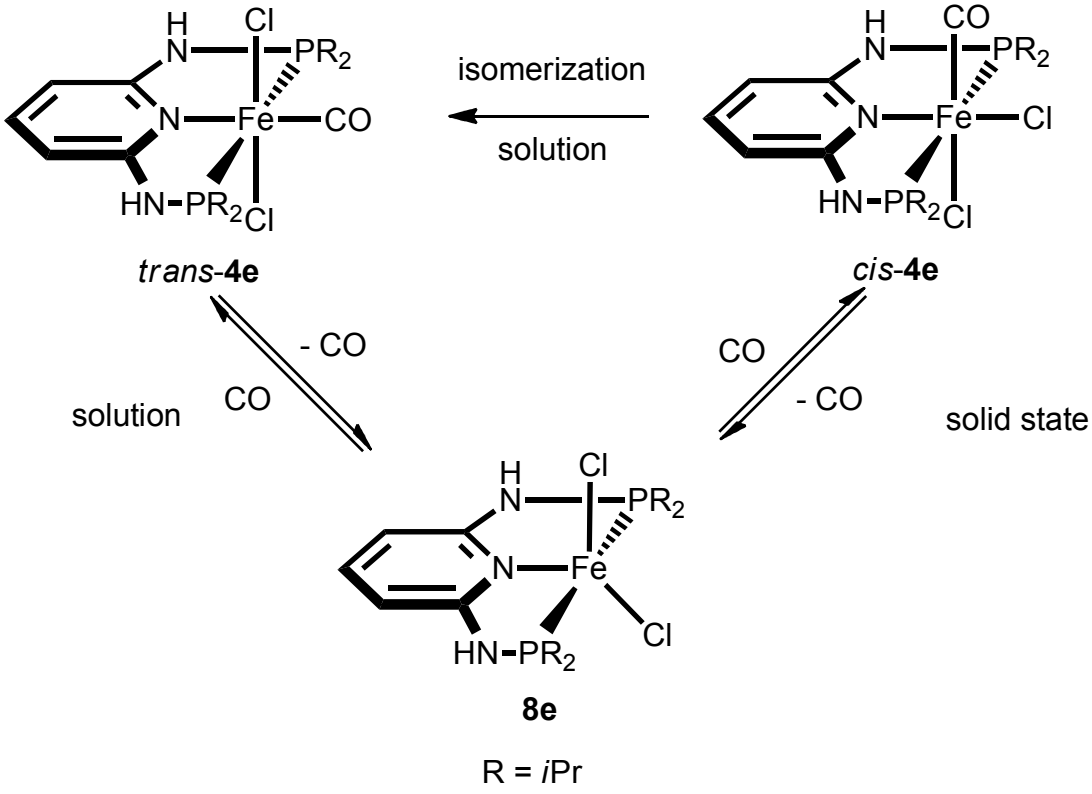

Scheme 1. Reversible binding of CO in solid state and solution by [Fe(PNP-*i*Pr)Cl$_2$] (8e)

The pentacoordinated 16e$^-$-complex (**8e**) with a PNP-*i*Pr ligand is highly selective binding CO in solid state, as well as in solution which is affecting the configuration of the carbonyl-complex formed. The addition of CO is reversible at least up to 5 cycles in solid state and on top of that, the reaction can be indicated by naked eye. Reversibility has critical drawbacks, because harsh conditions of 100°C and 20 mbar are necessary for regeneration of the pentacoordinated complex **8e**. In order to improve the efficiency of such a system, the influence of other phosphine-residues has to be investigated. To achieve this goal the main focus has to be the modification of the Fe-CO bonding strength. The M-C bonding strength in CO-complexes highly relies on the capability of the metal-centers for π-backbonding.

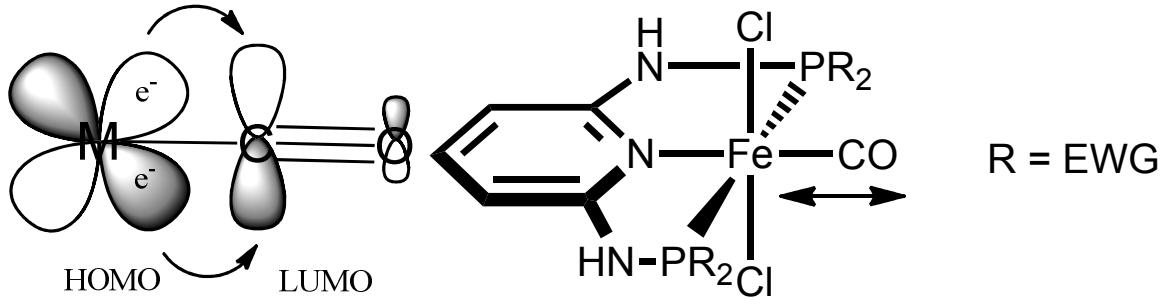

Figure 3. π-backbonding of metal center (M) toward π*-orbital of CO depending on electron density of M

Introduction of electron-withdrawing group groups (EWG's) at the phosphorus-site clearly render the phosphines better π-acceptors (**figure 3**). In return, the phosphines compete with CO for the metal π-electron density resulting in a weakening of the M-C bond.

In regard to potential catalytic reactions like the hydrogenation of carbonyl-compounds phosphite-based PNP ligands became of interest, since in combination with Fe-precursors these are comparatively little investigated so far. Therefore, utilization of a simple phosphite like BIPOL is a nice probe to discover trends in reactivity of these compounds. In addition, when the fundamentals of these compounds are revealed the system can be taken further to chiral phosphites. **Figure 4** presents a series of already prepared and investigated chiral PNP ligands.[19]

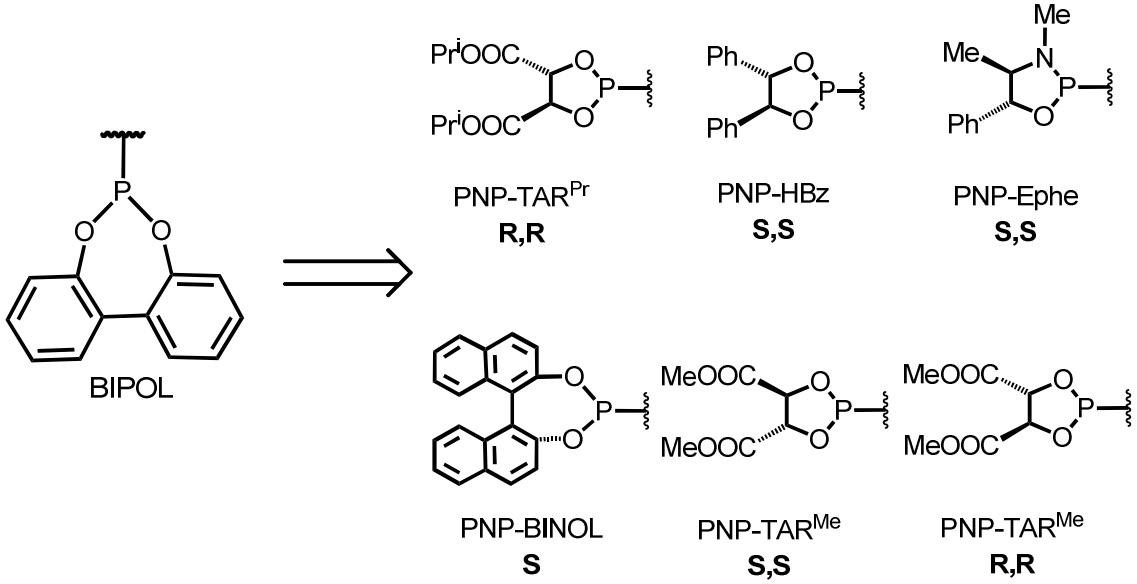

Figure 4. Chiral phosphite-based R_2P- moieties

All of them are readily available and easy to synthesize on a large scale which makes them attractive for asymmetric catalysis.

Ultimately, new types of unexpected octahedral complexes with unique bonding modes emerged from the experiments with these new ligands. This perspective will include characterization of structure and driving forces and reactivities. The new compounds (**figure 5**) combine two PNP ligands with bidentate κ^2-(*P,N*) and tridentate κ^3-(*P,N,P*) bonding modes. The formation of these complexes is highly dependent on the steric properties of the ligand, which can be expressed by the phosphine cone angle.[20]

	R	X	Y
9a	BIPOL	H	Cl
9b	Ph	H	Cl
9c	Ph	Cl	Cl
9d	Et	H	Cl
12d	Et	H	Br

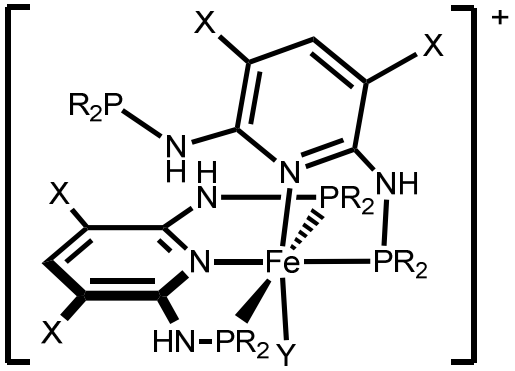

Figure 5. κ^2,κ^3-type complexes of general formula κ^2,κ^3-[Fe(PNP)$_2$Y]$^+$

The occurrence of κ^2 bonding modes of pincers is unusual, but has been reported in the past. In a review of Rietvield[21] the wide scope of bonding modes of NCN-complexes is summarized including κ^3, κ^2 and even κ^1. A notable difference is that these examples arise from a mono-anionic ligand forming one covalent bond in the complex. An example of κ^2 bonding modes by a dianionic CNC pincer is reported by Smith in a square-planar Au-complex.[22] This was achieved following selective cleavage of an Au-C bond with AgOTf (OTf = $CF_3SO_3^-$). More comparable systems using neutral pincers are reported by Dong[23] and Hayashi.[24] In both cases the PNP pincers adopt a κ^2-(*P,P*) bonding mode (**figure 6**).

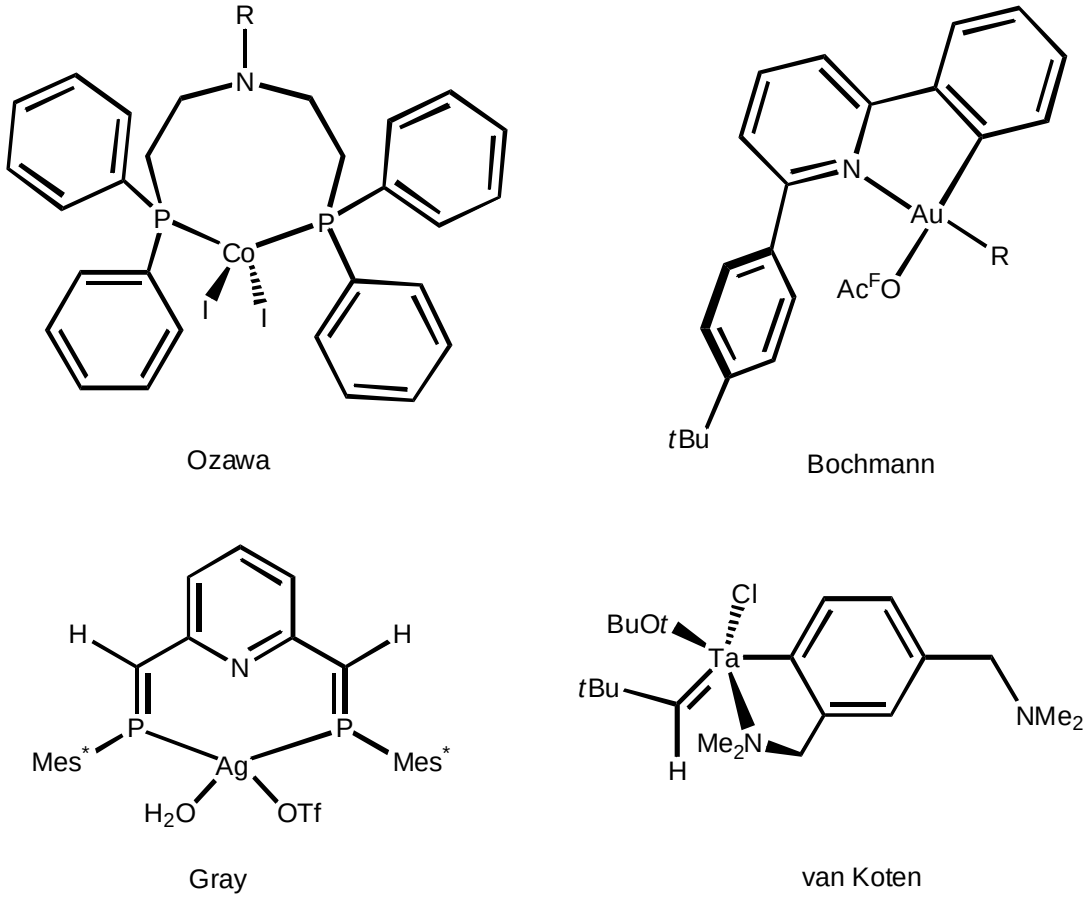

Figure 6. Examples of literature known pincer-complexes with κ^2 bonding mode

Results and Discussion

Synthesis of Ligands

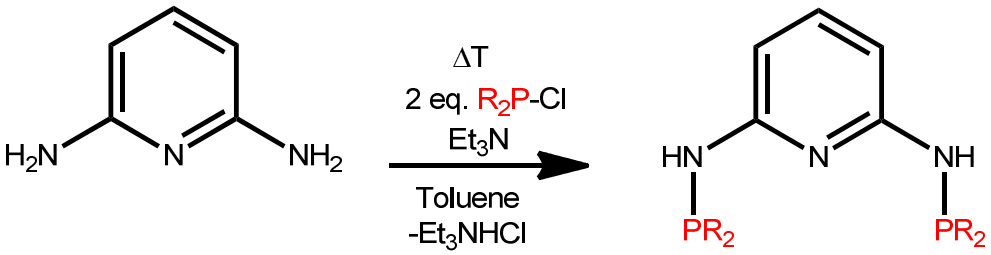

Scheme 2. Synthesis of the 2,6-diaminopyridine based PNP-pincer ligands

The synthesis of the pyridine based PNP-pincers (**scheme 2**) is performed under rather mild conditions starting from 2,6-diaminopyridine (2,6-DAP) and the corresponding chlorophosphine R_2P-Cl (**figure 7**). These fundamental precursors were prepared within the context of a project lab-course.

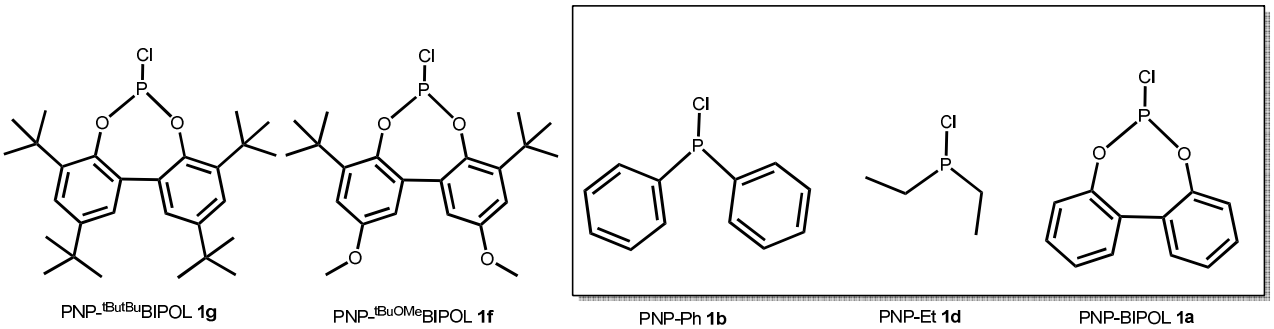

Figure 7. A series of chlorophosphines R_2P-Cl ordered in decreasing bulkyness (cone angle).

Since the amine-groups NH_2 are very acidic, a mild base such as triethylamine NEt_3 is sufficient for deprotonation in most cases.

After nucleophilic attack at the phosphorus, with chloride as a leaving group, the P-N bond then is formed, shown in **figure 8**.

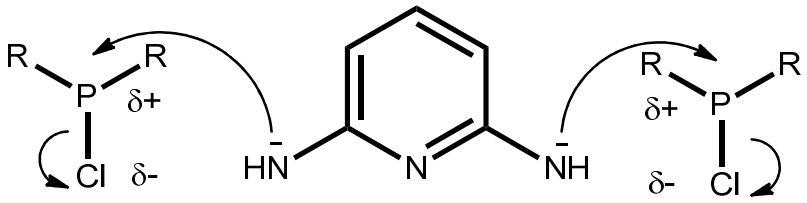

Figure 8. Mechanism of the formation of P-N bonds

Usage of solvents like toluene, Et_2O or THF shifts the equilibrium of the reaction strongly towards the product side as the ammonium-salt (Et_3NHCl) precipitates and can be filtered off afterwards. The 2,6-DAP is poorly soluble in these solvents, even after deprotonation. Heating of the reaction mixture up to 80°C improves the solubility as well as the reaction rates in general. However, higher temperatures may lead to side reactions and entail a shrinkage of selectivity. Major byproducts are diphosphines which in turn influence the stoichiometry of the educts and also lead to mono-phosphorylated compounds. It turned out that addition of the chlorophosphine at 0-5°C and stirring at room temperature and NEt_3 works quantitatively for the less demanding phosphine ligands **2a**-**2d**. On the other hand, the bulkier chlorophosphines show almost no conversion at these conditions. Excess of the chlorophoshine **1f-1g** (1.1 equiv) and NEt_3 (1.5 equiv) at 80°C overnight shows good conversion, but leads to accumulation of significant amounts of byproducts. An alternative method using *n*-butyl-lithium (*n*-BuLi) for deprotonation affords better yields. The procedure is similar, except the addition of *n*-BuLi (instead of NEt_3) below -20°C. The suspension is slowly warmed to RT and stirred at least for 2 hours. With the exception of the PNP-Et, the ligands are comparatively inert to oxidation and can be stored in a freezer or in a glove-box for several weeks. On the other hand, PNP-BIPOL is very sensitive towards hydrolysis and should be kept in a glove-box.

Synthesis of chlorophosphines R_2P-Cl

Ph_2P-Cl was commercially available, the chlorophosphites (**1a, 1f-1g**) and Et_2P-Cl (**1d**) were synthesized according to literature and purified by distillation.

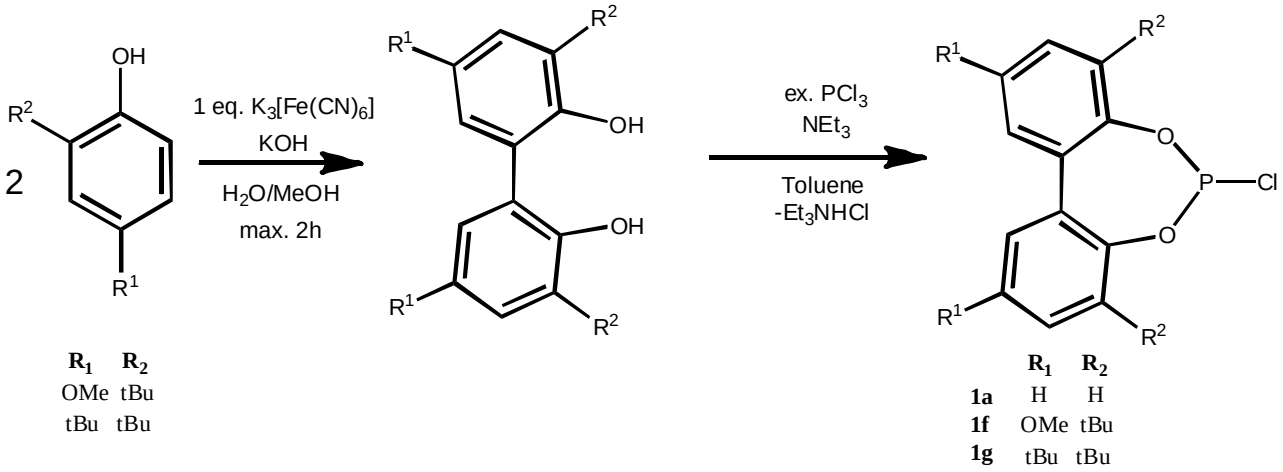

	R_1	R_2
	OMe	tBu
	tBu	tBu

	R_1	R_2
1a	H	H
1f	OMe	tBu
1g	tBu	tBu

Scheme 3. Pathway for the synthesis of cyclic chlorophosphites

Synthesis of Biphenol-PCl 1a, ^{tBuOMe}Biphenol-PCl 1f, ^{tButBu}Biphenol-PCl 1g

First of all, the synthesis requires a 2,2'-dihydroxy-biphenyl structured body as a starting material. The most simple one (R^1 =R^2 = H) was commercially available, while **1f** and **1g** were prepared from the corresponding 2,4-substituted phenol (**scheme 3**). The coupling-reaction was performed under strong basic conditions in a mixture of H_2O/MeOH using stoichiometric amounts of $K_3[Fe(CN)_6]$ as an oxidizing agent.[25] The reaction-time is crucial, because the reaction suffers from red-colored byproducts with increasing reaction time which lowers the yield. A white powder is then obtained by extraction with EtOAc, which is washed with cold acetone and dried properly before the next reaction step. The procedure works well for **1f**, but poorly for **1g**.

According to literature, the 7-membered cyclic chlorophosphites (**1a, 1f-1g**) are obtained after conversion with an excess of PCl_3 in toluene.[26] At room temperature base is required, but reaction-time is still long and large amounts of solvent are consumed for removal of the ammonia-salts by filtration. It is important to add the base either simultaneously with the PCl_3 or afterwards, as the previous deprotonation of the OH leads to large amounts of byproducts. In the case of **2a** a base-free procedure was established. The suspension is stirred at 50-60°C, while the HCl formed is let off through a gas-wash-bottle. This method is less solvent consuming and quicker, but yield is slightly lower. This method did not work out for bulkier substrates (**1f-1g**). In any case, a following purification by bulb-to-bulb distillation is necessary to get rid of the sticky yellow-orange by-products. The temperatures necessary for separation range from 220-260°C. The chlorophosphines are hard as rock afterwards and

inconvenient to handle. After subsequent re-dissolving (Et_2O or *n*-hexane) and evaporation the product can be isolated as a loose powder. The ligand synthesis was not selective for the substituted chlorophosphites and this system was thus not further investigated.

Synthesis of Et_2P-Cl

The synthesis of Et_2P-Cl was achieved via a four-step procedure because, according to literature, simple dialkylation of PCl_3 only works inadequately. Ethylgroups are sterically not very demanding, leading to full alkylation of PCl_3. Therefore another pathway, starting from tetraethyldiphosphine Et_4P_2 is proposed (**scheme 4**). After desulfurization,[27] Et_4P_2 the P-P bond is cleaved by a chloro-arylphosphine to obtain Et_2P-Cl.[28]

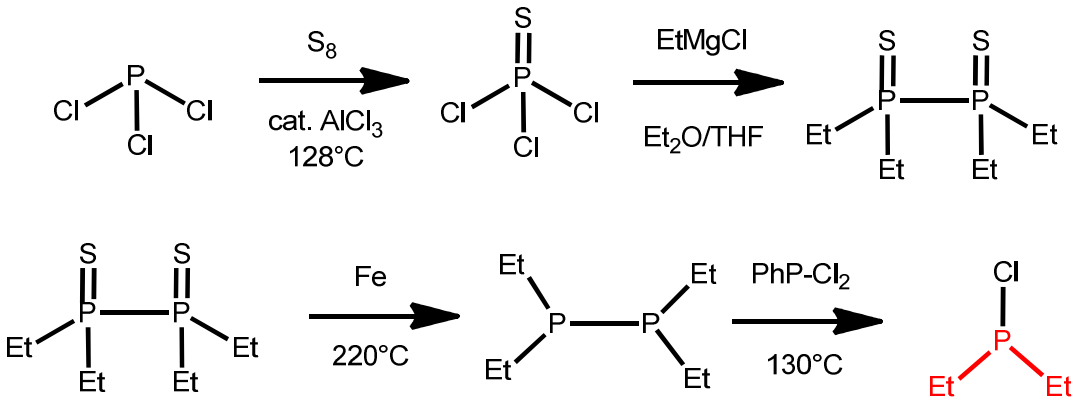

Scheme 4. Synthetic pathway for Et_2P-Cl

The synthesis of Et_4P_2 started by the reaction of PCl_3 with an excess of elemental sulfur at 110°C in the presence of approximately 5 mol% of $AlCl_3$. After a few seconds, the lively reaction is finished and the resulting thiophosphorylchloride ($S{=}PCl_3$) is obtained in good yield after purification by fractional distillation. Unreacted PCl_3 might be left, so the first few mL of the distillate were discarded. Remaining PCl_3 is detectable by $^{31}P\{^1H\}$ NMR, but does not interfere in the next step. Ethylation with a Grignard-reagent leads to tetraethyldiphosphinedisulfide ($Et_4P_2S_2$) which is then recrystallized from EtOH at -20°C. The Grignard reagent was prepared in Et_2O. Addition of THF at a later stage improved the yield up to 70% while in neat Et_2O the yield was limited to 40%. It is expected that THF as a better coordinating solvent enhances the reactivity of the Grignard-reagent by influencing the Schlenk-equilibrium. This is indicated by the exothermic reaction of the reaction-mixture while the drop wise addition of THF. A plausible mechanism for the P-P bond formation is reported by Patel and James Harwood (**scheme 5**).[29]

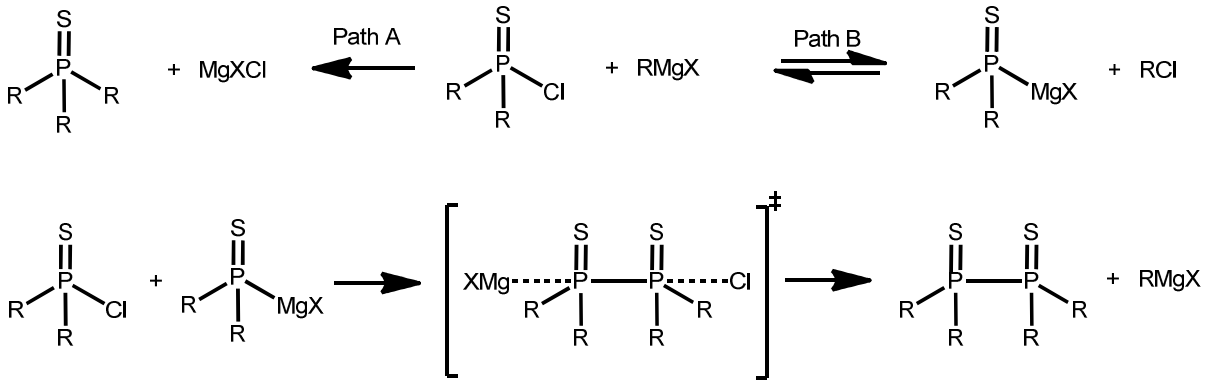

Scheme 5. Proposed mechanism for phosphorus-phosphorus bond formation

Removal of sulfur is achieved by direct reduction with an excess of activated Fe-powder at 220°C. Both starting-materials are mixed neat, and previously homogenized in a mortar. The activation of the Fe was achieved by heating under H_2-atmosphere. Crude characterization for the tetraethyldiphosphine (Et_4P_2) was accomplished by $^{31}P\{^1H\}$ NMR and ^1H NMR. The removal of the first fraction at 60°C, which exhibits no signals in the $^{31}P\{^1H\}$ NMR spectrum and only a few broad peaks in the ^1H NMR spectrum, is important. There were two major compounds identified by $^{31}P\{^1H\}$ NMR at -20 ppm which agrees with literature data for Et_2P-PEt_2 and a resonance at -43 ppm which presumably could be Et_2PH. However, the latter product does not affect the subsequent reaction steps and the follow-up products were obtained in up to 81% yield. Usage of crude non-activated Fe-powder leads to a pale red liquid. After an additional distillation at 220°C the colorless Et_4P_2 is obtained in similar yield. Further it turned out, that the best yields are obtained when the flask is quickly heated up to 200°C. This was achieved with a preheated sandbath. Refluxing before distillation solely led to the volatile by-product of the first fraction. Generally, $Et_4P_2$is highly reactive towards oxygen and self-igniting and should therefore immediately be converted with Ph_2P-Cl. Permanent cooling of the flask is thus also advised. A less expensive way to do so is the usage of PhP-Cl_2 which also works perfectly. In a so-called “scrambling” reaction the phosphine-residues are exchanged and the volatile Et_2P-Cl can be removed by distillation. A further fractional distillation is necessary for purification, where the less volatile oxidized by-products remain in the distillation flask. The ^{1}HNMR of the by-product is similar to the product, but is shifted lowfield, while the $^{31}P\{^1H\}$ resonance is shifted upfield to 86 ppm. After all, Et_2P-Cl was obtained in 40% overall yield on a 10 g scale and can be stored in a freezer for a several weeks.

Mono-CO-complexes [Fe(PNP)Y_2(CO)]

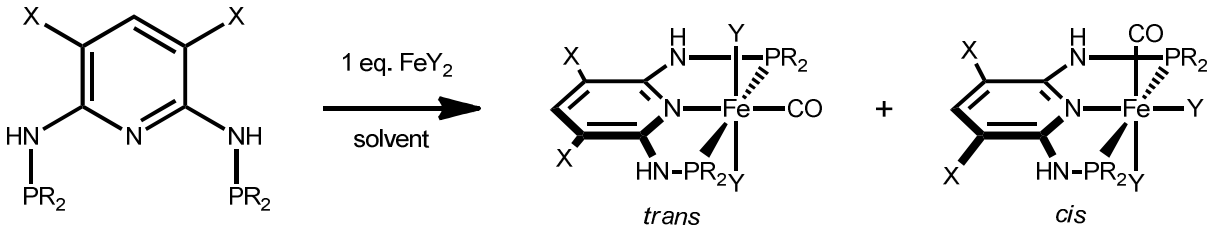

	R	X
2a	BIPOL	H
2b	Ph	H
3c	Ph	Cl
2d	Et	H

	R	X	Y
4a	BIPOL	H	Cl
4b	Ph	H	Cl
4c	Ph	Cl	Cl
4d	Et	H	Cl
5d	Et	H	Br

Scheme 6. Pathway for synthesis of mono-CO complexes

A series of octahedral mono-CO complexes of general formula [Fe(PNP)(Cl_2)CO] (**scheme 6)** were prepared (**4a-5d**)**.** They were easily available after conversion of PNP-ligand with FeY_2 (X = Cl, Br) in solution while CO-gas is bubbled through. A green species is initially formed which will be discussed in the section "κ^2,κ^3-[Fe(PNP)$_2$Y]$^+$-complexes". The conversion is typically finished within 1h and a stable diamagnetic 18e$^-$-complex is formed. The selectivity of the desired isomer is highly solvent dependent. IR is best suited for a rapid distinction between *cis*- and *trans*-isomers, but also $^{31}P\{^1H\}$ NMR and UV-Vis spectra were used for characterization. **Table 1** summarizes the IR and NMR data of the mono-CO complexes for differentiation between the isomers. Generally, the *cis*-isomers tend to be red colored and show lower wavenumbers (IR) as well as lower chemical shifts (NMR). With respect to IR this can be explained by the *trans*-influence, which is described as the tendency of ligands to selectively weaken bonds *trans* to one another.[30] It is assumed that the *trans*-influence of the pyridine-ring is larger than that of the coordinated chloride. Under this assumption, the Fe-C bond in *trans* position to the pyridine moiety is weakened. Hence π-backbonding is decreased and the C=O bond is shortened resulting in higher wavenumbers. Note that the stretching frequency of gaseous CO is 2143 cm^{-1}. **4a** makes an exception revealing an opposite trend. This may be due to the fact that the phosphine-moieties are now also stronger π-acceptors competing with the CO ligand, so that the *trans*-influence of pyridine is no longer as pronounced as in the other cases. Similar assumptions are made for $^{31}P\{^1H\}$ NMR as the CO in *cis* position is stabilizing the Fe-center by better π-backbonding. In return the phosphine-moieties are less deshielded because the Fe-center is withdrawing less electron density. One has to keep in mind that not only electronics affect chemical shifts in $^{31}P\{^1H\}$ NMR but sterics and especially bonding angles can also have critical influence. The strong π-accepting phosphite-moieties have significantly bigger deshielding effect than Ph-substituents since the chemical shift in $^{31}P\{^1H\}$ NMR is about 100

ppm shifted to lower field. **Table 1** summarizes the IR and $^{31}P\{^{1}H\}$NMR data of the mono-carbonyls including the known [Fe(PNP-*i*Pr)(CO)Cl_2] (**4e**).

Table 1. Selected IR, and NMR data for [Fe(PNP)(CO)Cl_2] complexes

compound	**IR [cm^{-1}]**	**$^{31}P\{^{1}H\}$ NMR [ppm]**	**color**	**electronic properties -PR_2**
trans-**4e**	1956	134.5 (DMSO-d_6)	blue	σ-donor
cis-**4e**	1947	123.5 (DMSO-d_6)	red	↓
trans-**4d**	1965	130.9 (acetone-d_6)	violet	
cis-**4d**	1960	119.5 (DMSO-d_6)	red	
trans-**4c**	1970	124.4 ($CDCl_3$)	pink	
cis-**4c**	1975	104.2 ($CDCl_3$)	red	
trans-**4a**	1991	202.7 (acetone-d_6)	pink	
cis-**4a**	2002	202.7 (acetone-d_6)	red-violet	π-acceptor

PNP-BIPOL

The mono-CO complexes of PNP-BIPOL are the only complexes where the distinction between the isomers was impossible by NMR. Nevertheless, this ligand-system was best suited for selective and quantitative preparation of both isomers. In DCM the *trans*-isomer precipitates as a bright pink solid. This also worked out in other solvents like CH_3CN and CH_3NO_2. *trans*-**4a** is good soluble in THF and reasonable soluble in acetone. The usage of *n*-Bu_4NCl dramatically changes the properties as *trans*-**4a** then dissolves in DCM, but is insoluble in THF. As shown by x-ray crystallography (**figure 9**) an ion-pair is formed with the ammonium-salt. Crystals were grown in THF by slow diffusion of *n*-pentane. The complex shows anionic-behavior with the chloride interacting with the NH-region.

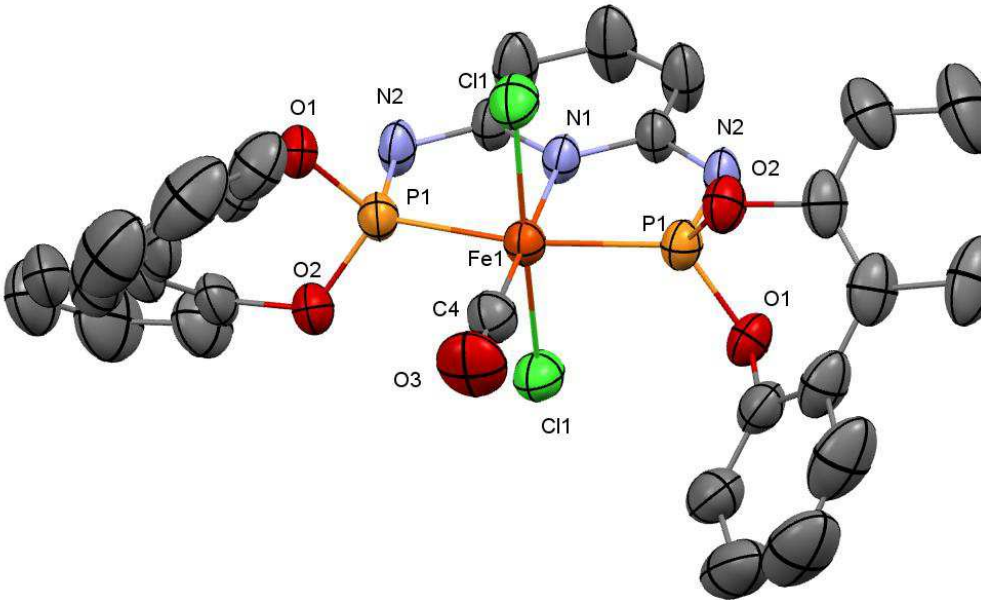

Figure 9. Structural view of *trans*-[Fe(PNP-BIPOL)(Cl)$_2$CO]·*n*Bu$_4$NCl (*trans*-4a·*n*Bu$_4$NCl) showing 50% thermal ellipsoids (H-atoms and nBu$_4$N omitted for clarity). Selected bond lengths (Å) and bond angles (deg): Fe(1)-P(1) 2.1765(9), Fe(1)-N(1) 2.007(4), Fe(1)-C(4) 1.778(6), Fe(1)-Cl(1) 2.305(1), P(1)-N(2) 1.653(3), N(2)-C(1) 1.358(4), C(4)-O(3) 1.132(7), P(1)-Fe(1)-P(1) 165.06(4), Fe(1)-C(4)-O(3) 180.0(5).

4a is labile in THF solution slowly releasing CO and forming the turquoise complex **10a** (*vide infra*). For crystal growth it is essential that the solution is saturated with CO before the diffusion. In the solid state, **4a** possesses longterm stability since no decomposition could be observed even after several months. This suggests that the coordination of solvent is crucial for the process of decarbonlyation.

In THF a red-violet solution of *cis*-**4a** is obtained. Small residues of *trans*-**4a** crystallize after refrigeration at -20°C and can be removed. In other solvents like DCM or CH_3CN, *cis*-**4a** isomerizes and precipitates again and the pink *trans*-isomer is isolated. The poor solubility is the driving force for the isomerization. THF is the only solvent in which *cis*-**4a** is stable, because of the good solubility of both isomers. Isomerization from *trans* to *cis* was not observed in THF. Furthermore, the synthesis in the presence of small amounts of DCM also yielded a mixture with *cis*-**4a** as the major compound. Preparing larger quantities (> 2g) in 10 mL of DCM, purging with CO gave red precipitate which turned out to be the *cis*-isomer. With the starting materials not dissolved from the beginning, a different intermediate and mechanism is proposed for the formation of the CO-complex. It is suggested that *trans*-**4a** is formed from the green intermediate species, while *cis*-**4a** results from another intermediate. Another option could be that *cis*-**4a** is always formed in the first place and then slowly isomerizes. With deficient solvent the solubility-limit is exceeded before full isomerization is accomplished.

UV-Vis experiments shown in **figure 10** provide additional distinction criteria. The graphic displays a difference of 10 nm of absorption maxima between *cis*-**4a** (555 nm) and *trans*-**4a** (545 nm).

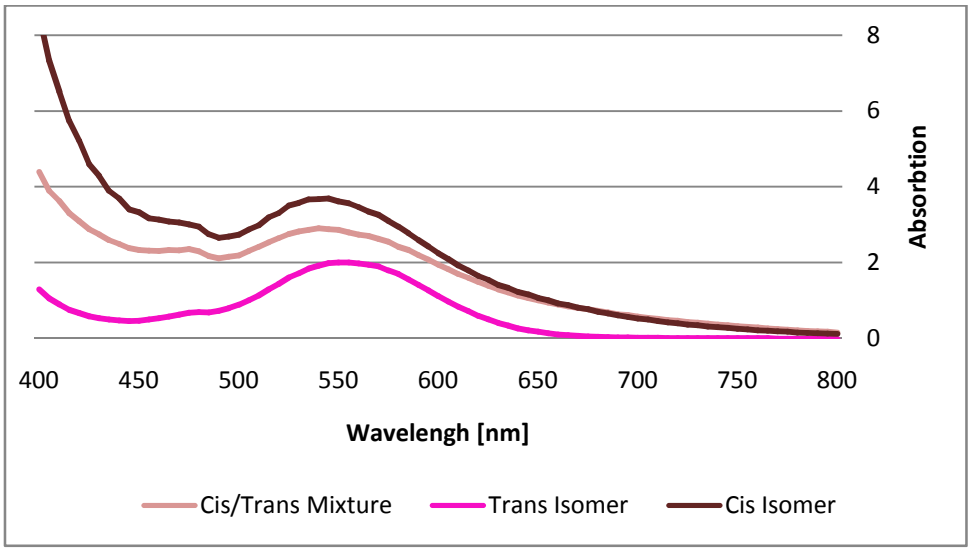

Figure 10. UV-VIS spectra of *cis*- and *trans*-[Fe(PNP-BIPOL)(Cl)$_2$CO] (4a)

Right inbetween, the spectra of a *cis/trans* mixture is depicted which was obtained after the synthesis with smaller amounts of DCM described *vide supra*. In the UV region below 400 nm the extinction of the ligand become dominant because of its aromatic building-blocks and was therefore cut off. A *cis/trans* mixture can also be indicated by IR showing a significantly broader CO-band than usual. Also the wavelength of ν_{CO} is located between the pure compounds, which show sharp signals for ν_{CO}.

Another crystal structure of *trans*-**4a** was obtained after refrigeration of a solution in THF at -20°C, but the data set was of poor quality due to molecule disorder. The violet crystals obtained by this method are very sensitive and turn black within a few minutes when exposed to air. An explanation for this phenomenon is delivered by the crystal structure which possesses incredible 14 solvent molecules per complex included in one unit cell.

PNP-Et

Trans-**4d** is obtained in THF as a violet precipitate. Due to its poor solubility in all common solvents, addition of *n*-Bu_4NCl was used for improvement. This complex is mixed with an excess of *n*-Bu_4NCl and stirred in CO-purged acetone. Remaining solids are filtrated over celite, and the violet solution was evaporated to dryness. With this method, a soluble modification of *trans*-**4a** is obtained, which is even better soluble in THF. A major drawback of this methodology is that the high-field region of ^{1}H-NMR is dominated by strong *n*-Bu-signals. However, this method is not suitable for crystal growth, since the compound becomes oily. The process can be inverted with DCM as *trans*-**4d** precipitates and *n*-Bu_4NCl can be washed away easily. Alternatively *trans*-**4d** can be dissolved in CO-purged DMSO for NMR-spectroscopy. Even though DMSO is strong coordinating, the compound has shown long term stability without observable decomposition over several days. Still no preparation of single crystals in DMSO was achieved by common techniques. The *trans*- configuration was finally proven after single crystals were grown in THF/DMSO by slow diffusion of Et_2O (**figure 11**).

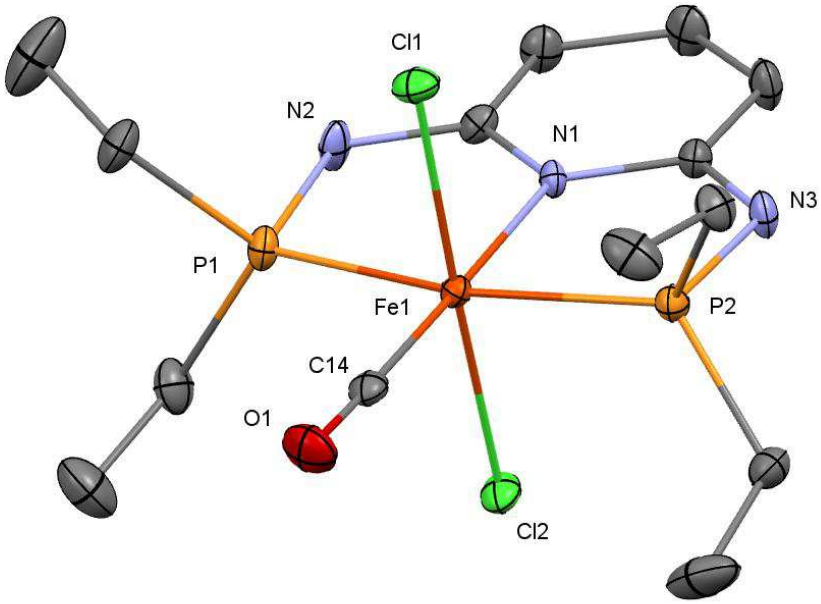

Figure 11. Structural view of *trans*-[Fe(PNP-Et)$(Cl)_2$CO] (*trans*-4d) showing 50% thermal ellipsoids (H-atoms omitted for clarity). Selected bond lengths (Å) and bond angles (deg): Fe(1)-P(1) 2.2273(8), Fe(1)-P(2) 2.2284(8), Fe(1)-N(1) 2.007(2), Fe(1)-C(14) 1.781(9), Fe(1)-Cl(1) 2.3179(7), Fe(1)-Cl(2) 2.3179(7), P(1)-N(2) 1.694(2), P(2)-N(3) 1.694(2), N(2)-C(1) 1.378(3), N(2)-C(5) 1.365(3), C(14)-O(1) 1.140(3), P(2)-Fe(1)-P(3) 166.80(3), Fe(1)-C(60)-O(10) 178.5(2).

When *trans*-**4d** is dissolved in DMSO and stored under exclusion of light, the color changes from violet to faint red. A comparison of the IR-spectra in solution shows a CO-stretch at lower wavenumbers. Also in NMR a new signal arises, shifted upfield. It is concluded, that the red compound matches with the corresponding *cis*-isomer. Single crystals of the blue bromide analogue *trans*-**5d** were grown by slow diffusion of Et_2O in DMSO/THF (**figure 12**).

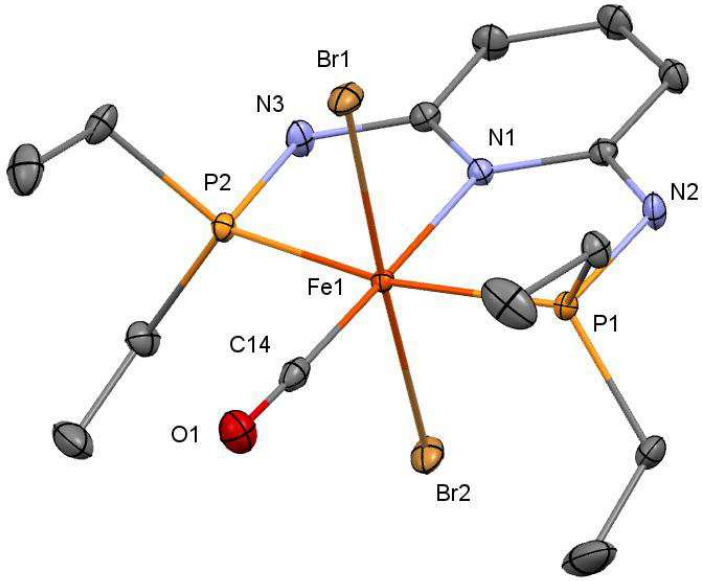

Figure 12. Structural view of *trans*-[Fe(PNP-Et)(Br)$_2$CO] (*trans*-5d) showing 50% thermal ellipsoids (H-atoms and DMSO omitted for clarity). Selected bond lengths (Å) and bond angles (deg): Fe(1)-P(1) 2.2383(6), Fe(1)-P(2) 2.2377(7), Fe(1)-N(1) 2.011(1), Fe(1)-C(14) 1.769(2), Fe(1)-Br(1) 2.4435(6), Fe(1)-Br(2) 2.4563(6), P(1)-N(2) 1.701(1), P(2)-N(3) 1.703(1), N(2)-C(1) 1.372(2), N(2)-C(5) 1.377(2), C(14)-O(1) 1.125(2), P(2)-Fe(1)-P(3) 166.91(2), Fe(1)-C(14)-O(1) 178.5(2).

Synthesis works in excellent yield in DCM, while in THF **12d** is the major by-product. Compared to *trans*-**4d**, the C=O bond is significantly longer and the Fe-C bond shorter. This, along with a lower wavenumbers of the C-O band in IR (1962 cm^{-1}), is explained by a better contribution of Br as a π-donor.

^{Cl2}PNP-Ph

Trans-**4c** was isolated selectively in THF as it precipitated as a pink solid. In solution *trans*-**4c** rapidly isomerizes, yet not completely, depending on the solvent. In CH_3CN both isomers are present in a 1:1 ratio, while in $CHCl_3$ *cis*-**4c** is the predominant species. The synthesis in DCM was not selective since the red solid obtained after evaporation contained both isomers along with a third compound presumably a *cis*-CO isomer (ν_{CO} = 2036 cm^{-1} and 1958 cm^{-1}).

Bis-CO-complexes $[Fe(PNP)(CO)_2Y]^+$

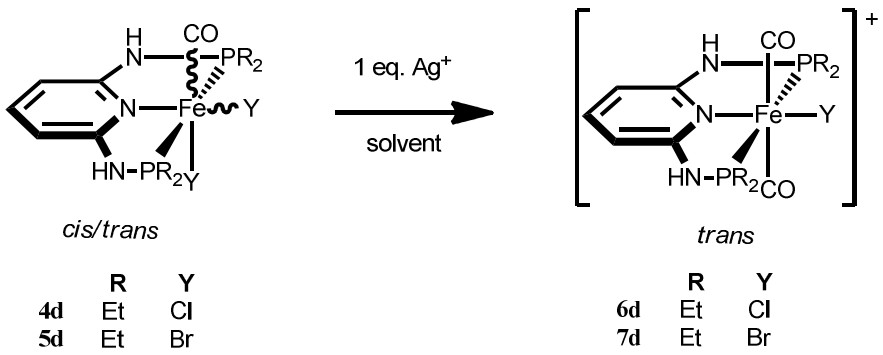

cis/trans

	R	Y
4d	Et	Cl
5d	Et	Br

trans

	R	Y
6d	Et	Cl
7d	Et	Br

Scheme 7. Pathway for synthesis of cationic *bis*-CO complexes $[Fe(PNP)(CO)_2Y]^+$

After treatment with stoichiometric amounts of Ag^+-salts, the corresponding mono-CO complex (**4d-5d**) is forming the cationic *bis*-CO-complexes (**6d-7d**) in a CO-purged solution (**scheme 7**). A direct approach starting from $FeCl_2$ and PNP ligand is also possible, but is less selective than starting from the pure mono-CO-complex. IR is well suited for a quick characterization of these complexes. A single CO-band for the *trans*-isomer and two CO-bands for a *cis*-isomer are expected, usually in a region higher than the corresponding mono-CO complex (>2000 cm^{-1}). Compared to the neutral $[Fe(PNP)(CO)Y_2]$ the metal center of the cationic complexes of general formula $[Fe(PNP)(CO)_2Y]^+$ become electron deficient with a lower HOMO. In addition, both coordinated CO's are competing for these less available orbitals.

PNP-Et

The synthesis in DCM delivered the best results for the bright orange *trans*-**6d** using AgOTf, $AgBF_4$ or $AgSbF_6$ as halide scavenger. By-products and starting material remain as a solid residue and can be removed by filtration. However, the solubility with BF_4^- as the counterion is rather poor so that other Ag-reagents are preferred. Characterization by IR shows a sharp single CO-band at 2008 cm^{-1}. *Trans*-**6d** is good soluble in acetone, and crystals could be grown by slow diffusion of *n*-pentane (**figure13**).

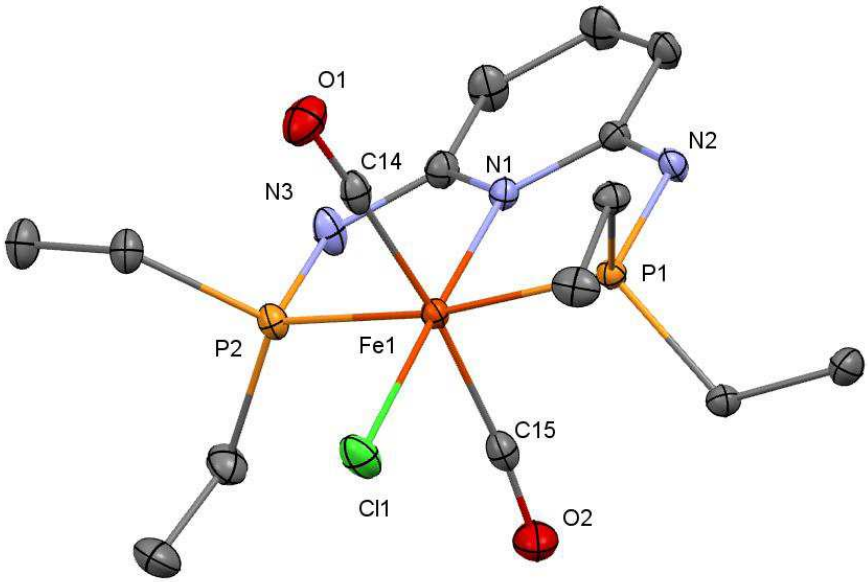

Figure 13. Structural view of *trans*-[Fe(PNP-Et)Cl(CO)$_2$]OTf (*trans*-6d) showing 50% thermal ellipsoids (H-atoms and OTf omitted for clarity). Selected bond lengths (Å) and bond angles (deg): Fe(1)-P(1) 2.2265(4), Fe(1)-P(2) 2.302(4), Fe(1)-N(1) 1.983(1), Fe(1)-C(14) 1.823(1), Fe(1)-C(15) 1.837(1), P(1)-N(2) 1.684(1), P(2)-N(3)1.685(1), N(2)-C(1) 1.356(2), N(3)-C(5) 1.358(1), P(1)-Fe(1)-P(2) 167.82(1), Fe(1)-C(14)-O(1) 177.6(1), Fe(1)-C(15)-O(2) 173.8(1).

Additionally the bromide-analogue *trans*-**7d** was fully characterized. (**figure14**).

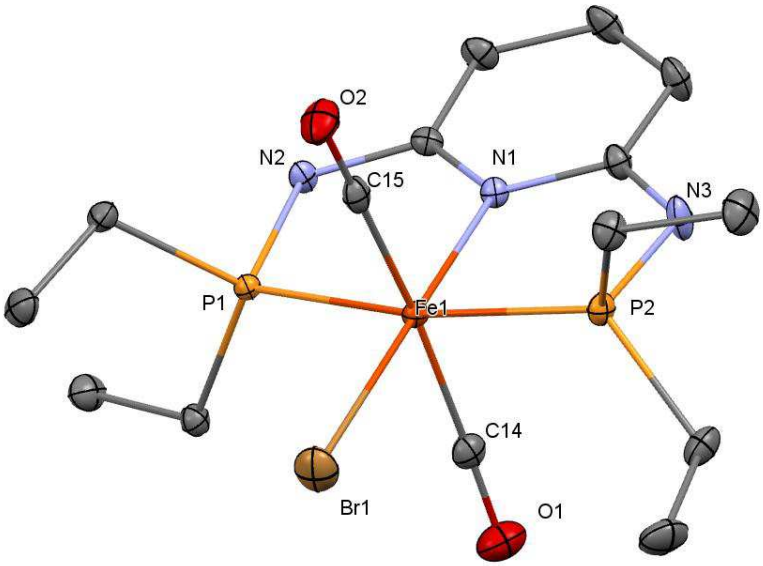

Figure 14. Structural view of *trans*-[Fe(PNP-Et)Cl(CO)2]OTf (*trans*-7d) showing 50% thermal ellipsoids (H-atoms and DMSO omitted for clarity). Selected bond lengths (Å) and bond angles (deg): Fe(1)-P(1) 2.2383(6), Fe(1)-P(2) 2.2377(7), Fe(1)-N(1) 2.011(1), Fe(1)-C(14) 1.769(2), Fe(1)-Br(1) 2.4435(6), Fe(1)-Br(2) 2.4563(6), P(1)-N(2) 1.701(1), P(2)-N(3) 1.703(1), N(2)-C(1) 1.372(2), N(2)-C(5) 1.377(2), P(2)-Fe(1)-P(3) 166.91(2), Fe(1)-C(14)-O(1) 178.5(2).

^{Cl2}PNP-Ph and PNP-BIPOL

In the case of PNP-BIPOL these conditions led to unselective side reactions and no *bis*-CO-complex could be isolated or characterized independent of the starting isomer. Analysis of the crude red product via $^{31}P\{^{1}H\}$ NMR indicated a mixture of several materials. An orange species was observed after separation over basic Al_2O_3 exhibiting two small CO-bands (2080 cm^{-1}, 2040 cm^{-1}) when $AgBF_4$ was used. Most dominant was another species showing two doublets in the $^{31}P\{^{1}H\}$ NMR in the range of free ligand, which could neither be isolated nor selectively characterized. Similar problems occurred with ^{Cl2}PNP-Ph, which was the main reason why this ligand was not further investigated. Throughout the research both ligand-systems turned out to be sensitive toward P-N bond cleavage. Assumptions have been made that a octahedral $[Fe(PN)_2Cl_2]$ type complex is formed. Replacement of Ag^+ by Tl^+-salts made no difference. Na^+-salts with weakly coordinating counterions like BPh_4^- or BAr^F were also not suitable for abstraction of the chloride.

Decarbonylation – pentacoordinated $[Fe(PNP)Cl_2]$

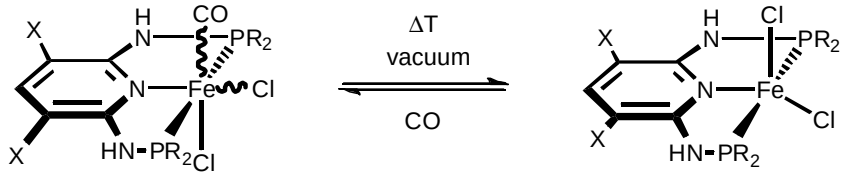

cis/trans

	R	X
4a	BIPOL	H
4c	Ph	Cl
4d	Et	H
4e	*i*Pr	H

	R	X
8a	BIPOL	H
8c	Ph	Cl
8d	Et	H
8e	*i*Pr	H

Scheme 8. Procedure for reversible coordination of CO

Under harsh conditions up to 250°C and more, plus vacuum of 1 mbar, coordinated CO of the complexes **4a-4d** was removed. This results in the formation of pale olive or yellow paramagnetic complexes without any observable CO-band in the IR. The process, independent of the isomer, is reversible and van be easily monitored by IR. The actual structure of these complexes of general formula $[Fe(PNP)Y_2]$ remains still in question. Characterization by NMR was impossible and crystal growth failed since rearrangements occur in solution. The fact that the process is fully reversible in solid state supports a pentacoordinated structure. Nevertheless, the analysis of the magnetic moment provides some insightful information which was estimated via faraday scale. The mass susceptibility χ_{mass} was determined by a magnetic scale and the effective magnetic moment μeff was calculated according to Hoppeé.[31] The results are listed in **table 2**. All values of μ_{eff}

correspond to 4 unpaired electrons and a spin state (S = 2) which does fit to the proposed complexes in **scheme 8**.

Re-carbonylation was achieved by purging the flask with CO gas. Surprisingly, for [Fe(PNP-BIPOL)$(Cl)_2$CO] a decrease of the CO-band occurs only at temperatures above 200°C although the BIPOL is the better EWG. The product is white, but no re-carbonylation was observed, neither in the solid state nor in solution. It is unclear whether decarbonylation or also decomposition takes place. Experimental data like the short Fe-CO bonding distance of 1.779 Å in the crystal structure (1.778 Å, **figure 9**) reveal that the Fe-C bond is tighter than for *trans*-**4d** (1.782Å, **figure 11**) in solid state. The magnetic moment would however match 4 unpaired electrons provided that the molecular weight for the compound is correct.

The decarbonylation of [Fe(PNP-Et)$(Cl)_2$CO] also needed higher temperatures than expected (> 250 °C), forming a yellow complex (**8d**). These conditions, even more intense than in the case of **8e** suggest, that decarbonylation is also steric driven to a high degree. After re-carbonylation in solid state, also trans-**4d** is afforded which is in contrast to **8e**, where *cis*-**4d** is obtained.

Table 2. Measured magnetic susceptibilities for 7a, 7c and 7d

proposed complex	color	χ_{mass} [$10^{-5}cm^3g^{-1}$]	μ_{eff}
7d (PNP-Et)$FeCl_2$	yellow		
7c (^{Cl2}PNP-Ph)$FeCl_2$	beige	1,78	5,29
7a (PNP-BIPOL)$FeCl_2$	off-white	1,58	4,95

κ^2-bonding mode - κ^2,κ^3-[Fe(PNP)$_2$Y]$^+$-complexes

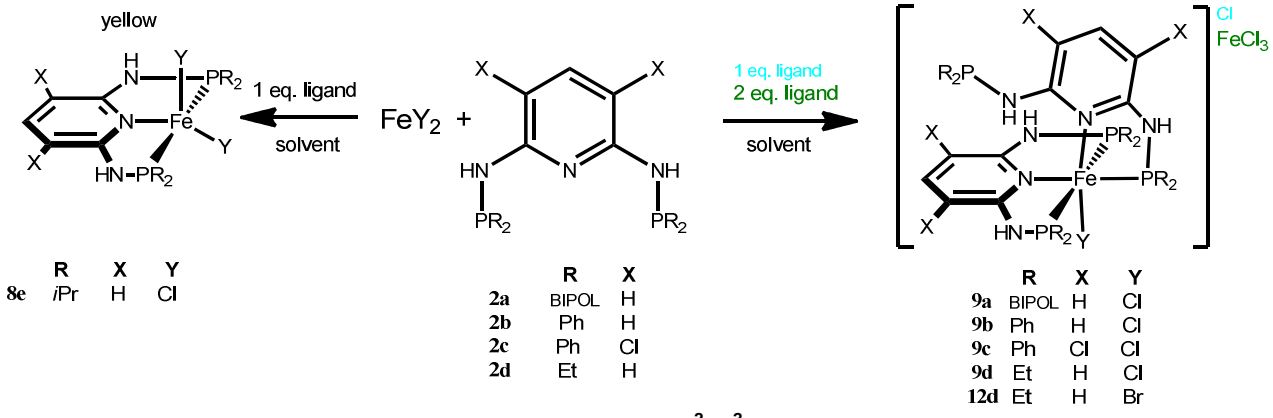

Scheme 9. Synthetic pathway for κ^2, κ^3-type complexes

As already implied in the section discussing mono-carbonyls a green intermediate is observed during synthesis of **9a-12d** (**scheme 9**). In the absence of CO, the green compound can be isolated as the octahedral, cationic, and diamagnetic complex of the general formula κ^2,κ^3-[Fe(PNP)$_2$Y]$^+$. Formation occurred even with substoichiometric

amounts of ligand. Using one equiv of the ligand the paramagnetic chloroferrate anion $FeCl_{3*}(THF)^-$, as evidenced by an x-ray structure, is formed while two equivalents afford the compound with the expected Cl^- counter ion. The exchange of the counter-ion strongly depends on the nature of the PNP ligand. **9b** requires Ag^+-salts, while weaker reagents such as Na^+-salts are not suitable. For **9d** counter-ion exchange works also with $NaBPh_4$, while for **8a** none of these methods proved to be successful. Excess of ligand or **4a** as a starting material (described in experimental section) is another option to suppress the formation of $FeCl_{3*}(THF)^-$. The $^{31}P\{^1H\}$ NMR is very characteristic for these complexes, exhibiting a triplet, a doublet, and a singlet resonance.

The reactions described above, may also be carried out with $FeBr_2$ as starting material but they differ in terms of reactivity. For **9a** and **9d** the reaction is faster and conversion is completed after 15 minutes while it takes 2 h with $FeCl_2$. Also, the solvent has particular influence on the reaction rate since the conversion runs faster in THF than in DCM. The bromide compounds also tend to have slightly higher stability. While **9a** turns brown on air in solution, the corresponding bromide compound is stable and solvent can slowly evaporate without any change of color.

PNP-Ph

9b was handled in the same way as previously discussed, and a crystal structure was obtained (**figure 15**).

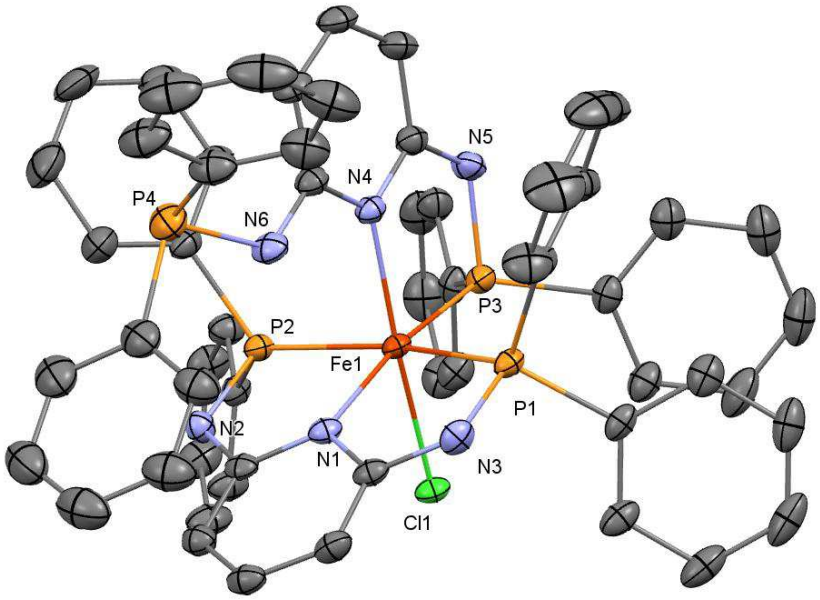

Figure 15. Structural view of $\kappa^2\kappa^3$-[Fe(PNP-Ph)$_2$Cl]BF_4 (9b) showing 50% thermal ellipsoids (H-atoms, solvents and BF_4^- omitted for clarity). Selected bond lengths (Å) and bond angles (deg): Fe(1)-P(1) 2.2438(6), Fe(1)-P(2) 2.2531(7), Fe(1)-P(3) 2.1845(7), Fe(1)-N(1) 2.065(2), Fe(1)-N(4) 2.085(2), Fe(1)-Cl(1) 2.3330(6), P(1)-N(3) 1.693(2), P(2)-N(2) 1.692(2), P(3)-N(5) 1.679(2), P(4)-N(6) 1.742(3), N(2)-C(1) 1.372(3), N(3)-C(5) 1.364(4), N(5)-C(30) 1.376(4), N(6)-C(34) 1.371(4), P(1)-Fe(1)-P(2) 163.32(3), N(1)-Fe(1)-P(3) 170.02(6), Cl(1)-Fe(1)-N(4) 170.50(4).

PNP-BIPOL and ^{Cl2}PNP-Ph

9a is obtained in good yield after conversion in DCM or THF. Solubility is very good in THF, but several trials for crystal growth were unsuccessful and ended up in polycrystalline solids. Exchange of the counter ion with Ag^+-salts frequently led to sideproducts and reagents like $NaBF_4$/$NaPF_6$ were not strong enough to remove the halide. Remarkably, the spectrum of **9a** always consists of 2 doublets for κ^3 PNP, a broad triplet for the κ^2 PNP and a singlet for the vacant PR_2 (**figure 16**). The other signals arise from partially hydrolyzed complex **10a** as discussed in the section "reactivity of - κ^2,κ^3[$(PNP)_2FeY]^+$-complexes". Even careful usage of dried solvents couldn't suppress the hydrolysis of the P-N bond.

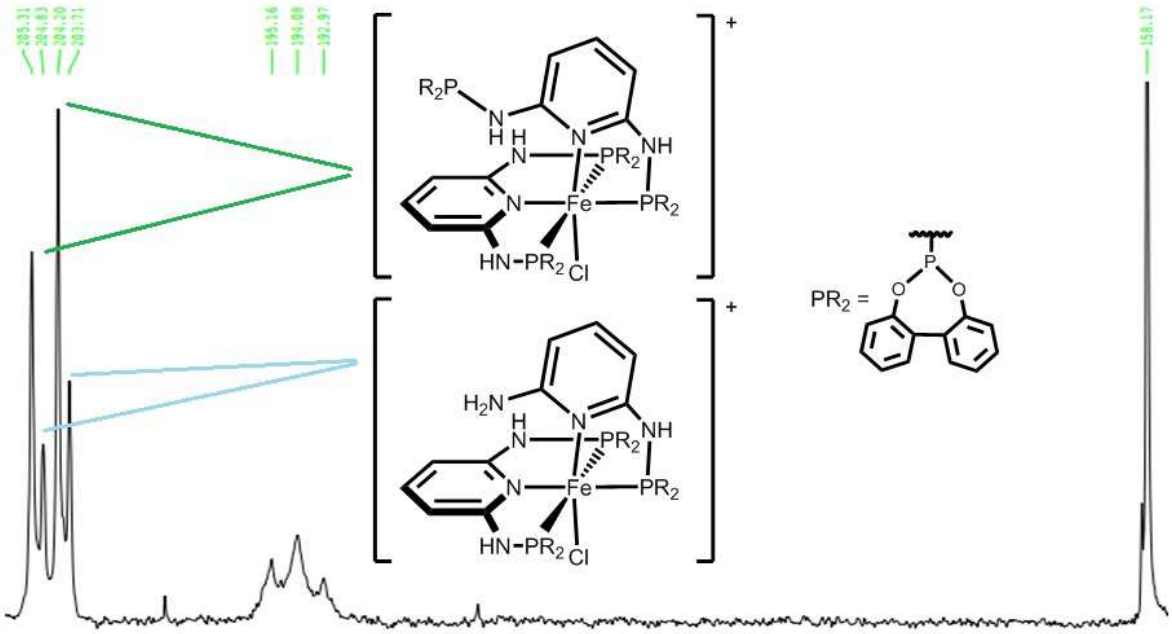

Figure16 . $^{31}P\{^1H\}$ NMR of κ^2,κ^3-[Fe(PNP-BIPOL)Cl]Cl (9a) with significant amounts of 10a

During a rough survey of the reactivity of **9c**, a similar sensitivity of the P-N bond towards hydrolysis has been noticed. An X-ray structure of the putative complex **9c**, obtained in THF by slow diffusion of Et_2O, shows full P-N bond cleavage (**10c**) and the formation of an $FeCl_4^-$ anion (**figure 17**).

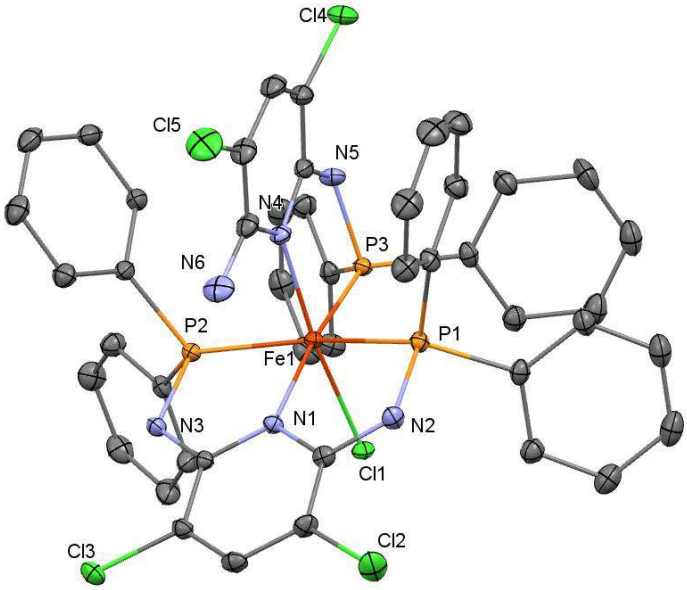

Figure17 . Structural view of κ^2,κ^3-[Fe(^{Cl2}PNP-Ph)(^{Cl2}PN-Ph)Cl]$FeCl_4$ (10c) showing 50% thermal ellipsoids (H-atoms, solvents and $FeCl_4^-$omitted for clarity). Fe(1)-P(1) 2.2696(5), Fe(1)-P(2) 2.2621(5), Fe(1)-P(3) 2.1781(5), Fe(1)-N(1) 2.050(2), Fe(1)-N(4) 2.070(2), Fe(1)-Cl(1) 2.3258(5), P(1)-N(2) 1.699(2), P(2)-N(3) 1.702(2), P(3)-N(5) 1.687(2), N(2)-C(1) 1.361(3), N(3)-C(5) 1.361(2), N(5)-C(30) 1.380(2), N(6)-C(34) 1.343(3), P(1)-Fe(1)-P(2) 163.84(2), N(1)-Fe(1)-P(3) 170.57(5), Cl(1)-Fe(1)-N(4) 173.20(5).

PNP-Et

9d with Cl^- as a counter ion quantitatively precipitates in THF and can be purified easily after several washing steps. The poor solubility in common solvents has to be overcome for characterization by exchange of Cl^-. Some Na^+-salts as well as stoichiometric amounts of Ag^+-salts generally work, with formation of **14a** (*vide infra)* to some degree. Solubility after exchange by BF_4^- and $NaBPh_4$ is still low, while decomposition occurred with $NaPF_6$. At last, $NaBPh^{Me}_4$ turned out to be the best reagent for full characterization. Crystals were grown in THF by slow diffusion of Et_2O (**figure 18**).

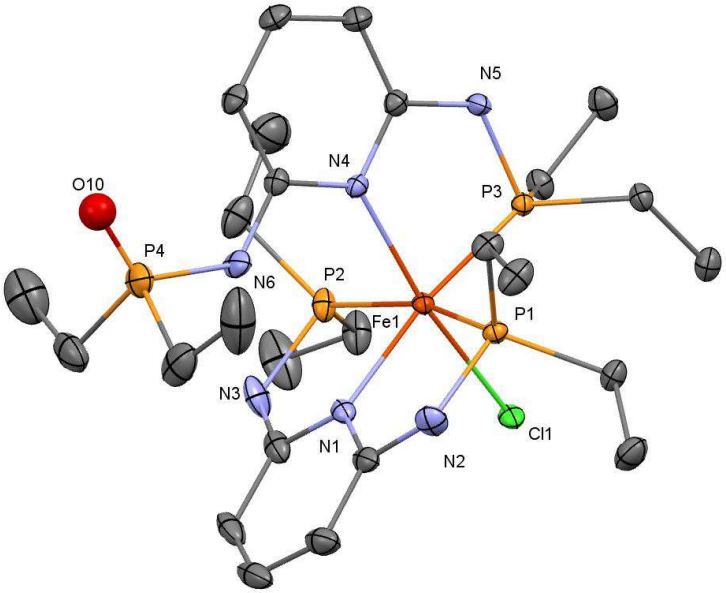

Figure 18. Structural view of $\kappa^2\kappa^3$-[Fe(PNP-Et)$_2$Cl](BPh$^{Me}_4$)$_2$ (9d) showing 50% thermal ellipsoids (H-atoms, solvents and BPh$^{Me}_4^-$ omitted for clarity). Selected bond lengths (Å) and bond angles (deg): Fe(1)-P(1) 2.2406(6), Fe(1)-P(2) 2.2461(7), Fe(1)-P(3) 2.1858(6), Fe(1)-N(1) 2.059(1), Fe(1)-N(4) 2.117(1), Fe(1)-Cl(1) 2.3504(6), P(1)-N(2) 1.706(2), P(2)-N(3) 1.711(2), P(3)-N(5) 1.687(1), P(4)-N(6) 1.722(2), N(2)-C(1) 1.362(2), N(3)-C(5) 1.355(3), N(5)-C(14) 1.375(2), N(6)-C(18) 1.383(2), P(1)-Fe(1)-P(2) 163.85(2), N(1)-Fe(1)-P(3) 171.59(4), Cl(1)-Fe(1)-N(4) 170.50(4).

According to the X-ray structure, there is some additional electron density in the vicinity of the non-coordinated –PEt$_2$ which discomplies with about 15% phosphineoxide formed during crystallization. $^{31}P\{^1H\}$ NMR of the crystals is in agreement with these results exhibiting a singlet at 55 ppm besides the singlet of the pendant -PEt$_2$ arm (48 ppm). The difference in chemical shift of 7 ppm resembles the observations for the pure free ligand PNP-Et **2d** (52 ppm *vs*. 45 ppm). The extremely short bond distance of P=O in the structure (1.2 Å) is debatable. It remains unclear whether oxidation occurs during handling of the crystals or during preparation of the crystals. Additionally, a crystal structure of the bromide analogue **12d** was obtained. Bond angles and lengths are almost identical to **9d**, but no oxidation of the free phosphine residue is observed (**figure 19**).

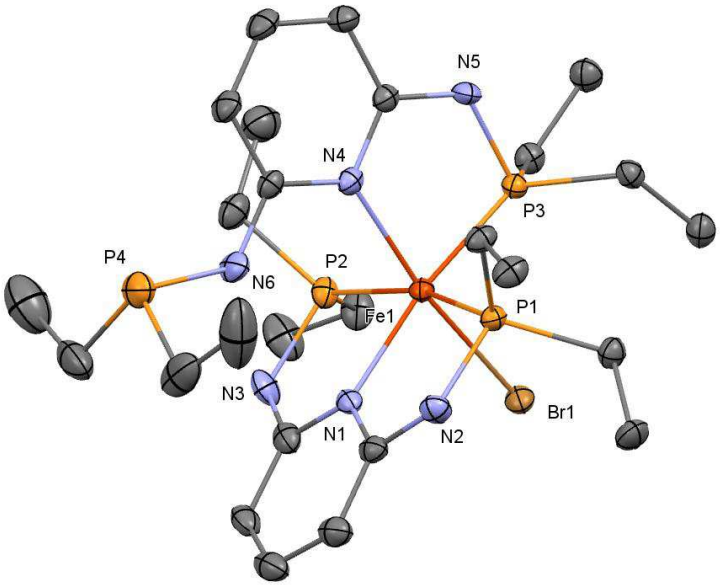

Figure 19. Structural view of κ^2,κ^3-[Fe(PNP-Et)$_2$Br](BPh$^{Me}_4$)$_2$ (12d) showing 50% thermal ellipsoids (H-atoms, solvents and BPh$^{Me}_4$$^-$ omitted for clarity). Selected bond lengths (Å) and bond angles (deg): Fe(1)-P(1) 2.243(1), Fe(1)-P(2) 2.2521(9), Fe(1)-P(3) 2.189(1), Fe(1)-N(1) 2.063(2), Fe(1)-N(4) 2.117(2), Fe(1)-Br(1) 2.4878(9), P(1)-N(2) 1.702(2), P(2)-N(3) 1.708(2), P(3)-N(5) 1.688(2), P(4)-N(6) 1.740(3), N(2)-C(1) 1.361(3), N(3)-C(5) 1.370(4), N(5)-C(14) 1.373(3), N(6)-C(18) 1.366(3), P(1)-Fe(1)-P(2) 163.98(3), N(1)-Fe(1)-P(3) 171.38(6), Br(1)-Fe(1)-N(4) 171.03(6).

Reactivity of - κ^2,κ^3[Fe(PNP)$_2$Y]$^+$-complexes

Reactivity towards oxygen and moisture

In solid state, the complexes **9a-9d** are inert towards air and moisture. In solution, these complexes are sensitive towards oxidation and partial oxidation at the vacant –PEt$_2$ site takes place (**scheme 10**).

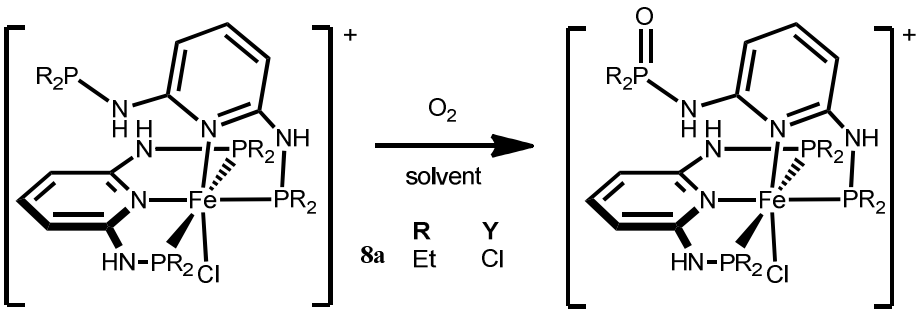

Scheme 10. Oxidation of the vacant phosphorus arm

As proven by X-ray crystallography, the complexes **9a** and **9c**, are very sensitive towards traces of H_2O. The hydrolyzation of 9a was monitored by $^{31}P\{^1H\}$ NMR as the vacant phosphine is vanishing (**figure 20**). The hydrolysed by-procucts are removed by subsequent washing steps with Et_2O

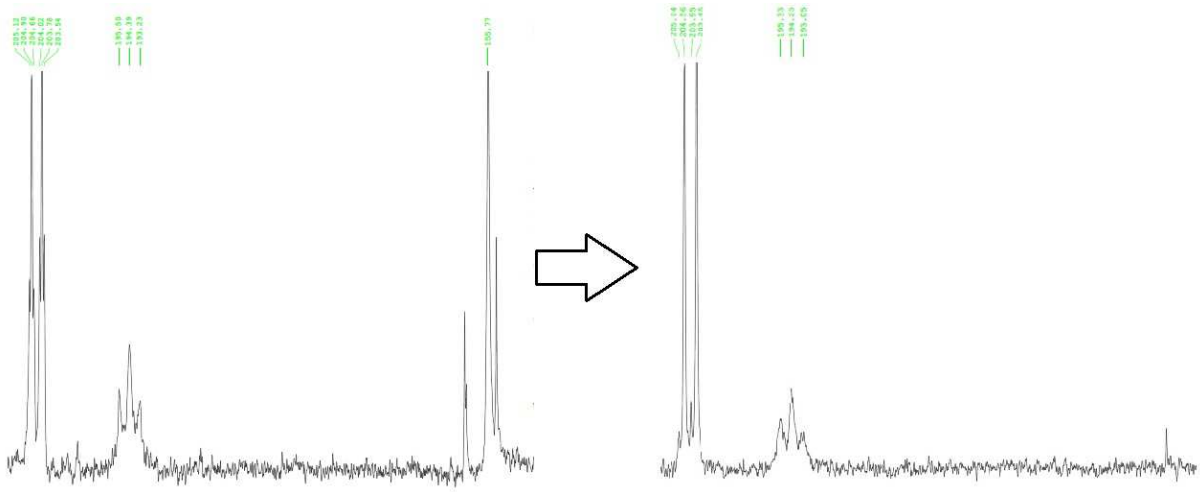

Figure 20. Monitoring of the hydrolysis of the P-N bond of 9a --> 10a

A gradual vanishing of the -PR_2 singlet is observed and the doublet shifts to high field. A quantitative preparation of the hydrolyzed complex **9a** is possible in wet acetone. **9a** precipitates as a turquoise solid which is filtered off, while the dark green impurities (good soluble, $FeCl_3^-$ presumed as counter ion) remain in solution. The hydrolyzed complex is only soluble in DCM.

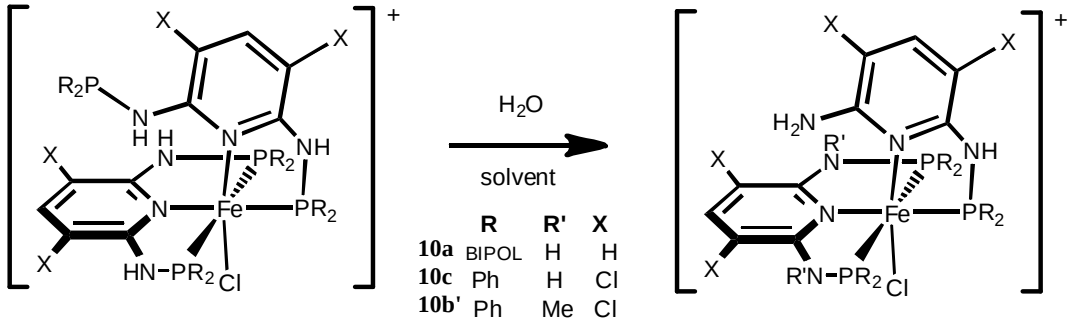

Scheme 11. Hydrolysis of pendant -PR_2

This procedure works in good quantity only with Cl^- as the counter-ion and the reaction-times are short (20 min). Longer reaction-times lead to a red, sticky by-product which was not further characterized. The P-N bond hydrolysis did not take place in the case of **9b** and **9d**. **10a** exhibits the same reactivities as the non-hydrolyzed complex **9a**, which will be discussed in the next sub-section. The extreme sensitivity of the P-N bond for **9a** compared to the other complexes **9** is presumably electronically driven.

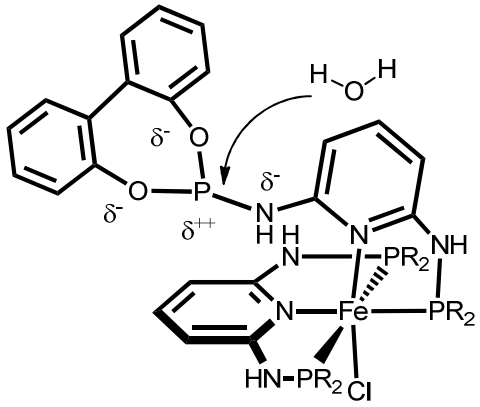

Figure 21. Proposed reason for sensitivity of 9a

Due to the high grade of polarization of the P-N bonding combination with a weak steric shielding **9a** is predestinated for hydrolysis through nucleophilic attack (**figure 21**).
Other nucleophiles can react in a similar fashion. That is the reason why synthesis in EtOH totally failed. Aprotic polar solvents favor nucleophilic attack, which could be the source of the unwanted side-reactions in CH_3CN.

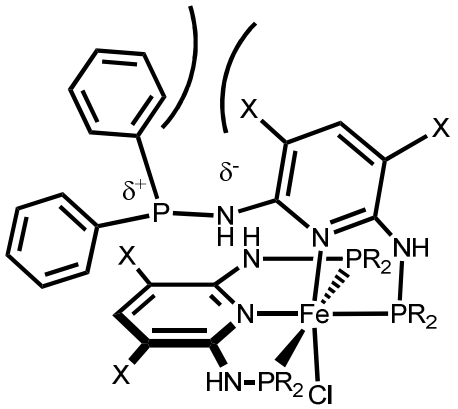

Figure 22: proposed source for sensitivity of 9c

Compared to the others, the sensitivity of **9c** is explained by the steric repulsion between vacant R_2P- and the chloride of py[3,5] (**figure 22**). **9b** already exhibits the highest degree of strain of all crystal structures (**table 3**) indicated by an angle N^{Py}-Fe-N^{Py} of almost 106°. The additional repulsion caused by the chloride might be sufficient for the P-N bond cleavage.

Reactivity towards CO

Remarkable is the reaction in a CO purged solution shown in **scheme 12**. The PNP ligand in κ^2 bonding mode dissociates, and a neutral CO complex is formed. The pendant $-PR_2$ does not need to be fully intact as it will be shown for **10a**.

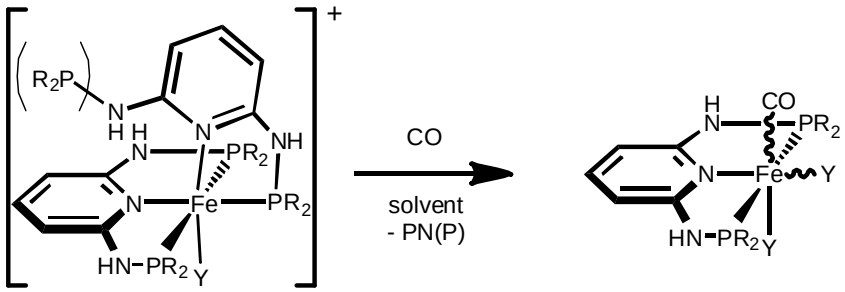

	R	Y
9a	BIPOL	Cl
10a	BIPOL	Cl
9d	Et	Cl

	R	Y
4a	BIPOL	Cl
4d	Et	Cl

Scheme 12. Dissociation of κ^2 bonded ligand by CO

The reaction and its outcome are similar to those discussed in section mono-carbonyls. Solvent is not only influencing the *cis/trans* ratio, as well as the reaction-rate. In the case of **9a**, the conversion takes significantly longer than in THF.

PNP-BIPOL

The weakly coordinating solvent DCM has a stabilizing effect on **4a**. This was observed when a solution of $FeCl_2$ was stirred with an excess (> 4 equivs) of **2a**. After CO was bubbled through, no reaction could be observed in DCM as the green color didn't change after all. On the other hand, the same reaction performed in THF led to formation of a CO complex, since the solution turned violet. Of course, conversion in this case is not quantitative. These effects suggested that the reaction with CO is reversible under certain conditions. Indeed this idea was proven by an additional experiment. Mono-CO-complex *trans*-**4a** was mixed with 1 equiv of free ligand **2a** in a mixture of THF/DCM. THF is necessary for better solubility, but neat THF is also suitable. After stirring for 24 h the solution turns from original pink over blue to green. Slow evaporation of the solvent under mild vacuum promotes the full conversion, because the CO is removed from equilibrium. The blue colored species was expected to be an intermediate. But NMR proved, that this is simply a mixture of pink *trans*-**4a** and green **9a**. Usage of red *cis*-**4a** however results in a brown color. Also, the hydrolyzed complex **10a** shows the same behavior. Altogether these reactions can be connected in an elegantly way, performing a cyclic process in which a selective hydrolyzed PNP-BIPOL ligand (**3a**) is generated (**figure 23**).

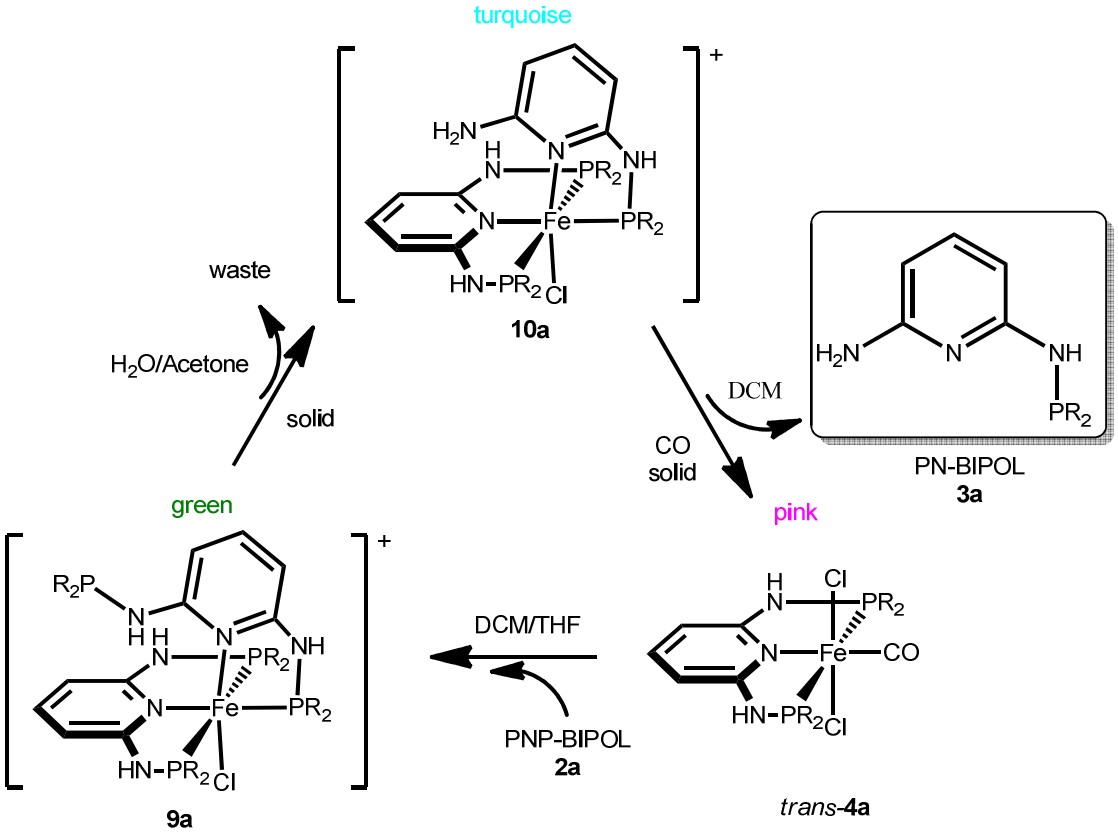

Figure 23. Selective hydrolysis of PNP-BIPOL using a Fe(II) complex as an template

3a was characterized by NMR and the recycling throughout the process works up to 80% based on Fe. Conventional synthesis of **3a** would probably need bulky protection groups. BIPOL is a very small residue and mono-phosphorylation would probably be accompanied by di-phosphorylation.

Some observations have been made concerning the role of the counter-ion in the mechanism for the formation of **4a**. Already marked out in section “Reactivity oxygen and moisture”, the green waste-solution of the reaction **9a** ->**10a** is believed to contain **9a**·$FeCl_3^-$. Dissolved in DCM and purged with CO no reaction occurred after all. From that viewpoint, the necessity of a counter-ion with a moderate coordinative behavior is suggested.

Rearrangements

When using $NaBPh_4$/$NaBPh^{Me}_4$ for exchange of counter-ion another unique reactivity of **9a/10a** was observed. When stirred overnight, the color changed from green to red. **Scheme 13** displays the proposed reaction.

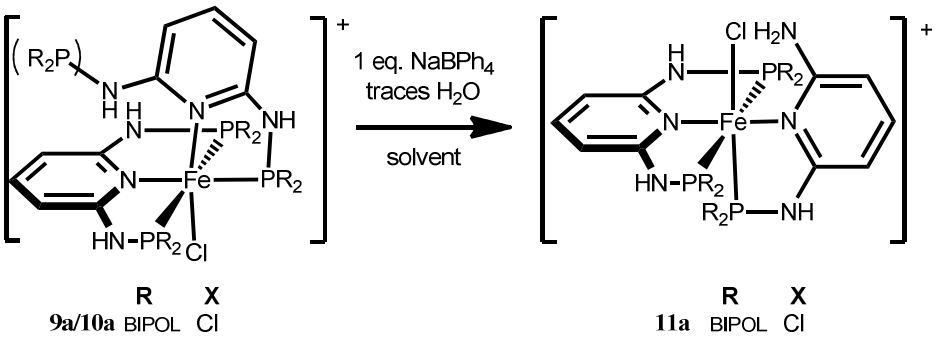

Scheme 13. Synthesis of 11a with pyridine-rings in *trans*-position

Since no crystal of **11a** could be grown, the structure is based on $^{31}P\{^{1}H\}$ NMR data. There is a striking difference in the spectrum of **11a** compared to **9a/10a** (**figure 24**). Remarkably, the triplet shifts to low field and the signal of the pendant $-PR_2$ disappears.

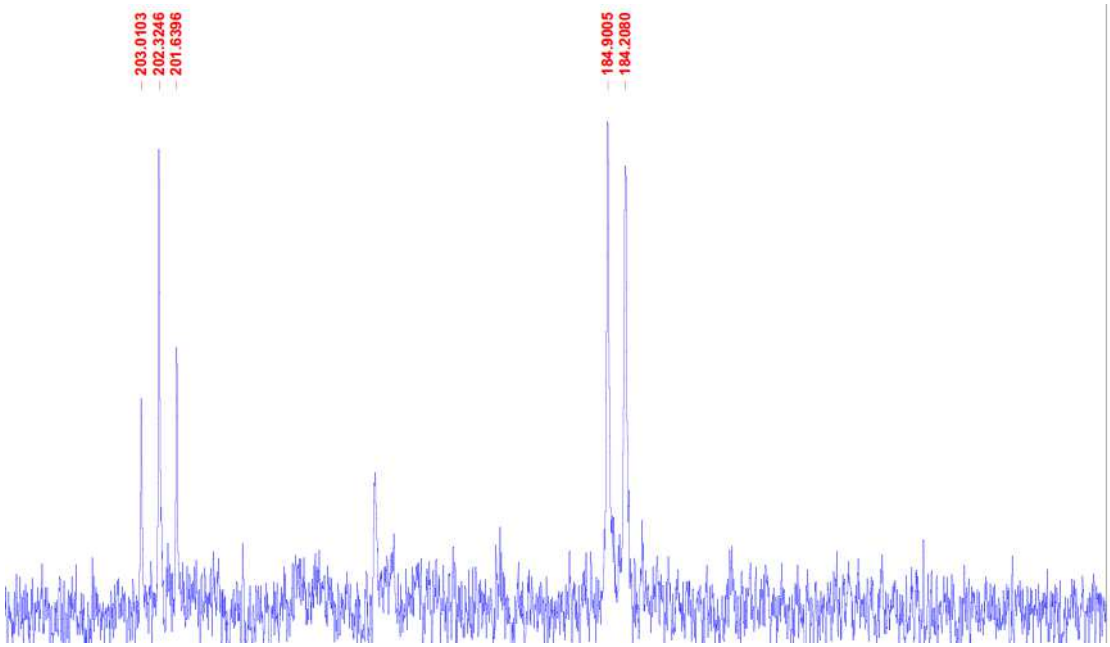

Figure 24.Pattern of the $^{31}P\{^{1}H\}$ NMR spectra of 11a

From a theoretical viewpoint, the κ^2 bound P gives rise to a triplet in *trans*-position to the Cl^-, being weak σ-donor. Therefore a better σ-bonding/π-backbonding interaction with the Fe-center is expected and the P is deshielded. This is confirmed by the experimental data. No rearrangement to reform **9a** was observed in presence of Cl^- upon addition of an excess of *n*-Bu_4NCl. When CO is bubbled through a solution of **11a** no reaction occurred at all, even after addition of *n*-Bu_4NCl. The similarity in color and reactivity to κ^3,κ^3-type complexes supports the estimation, of two pyridines being in *trans*-position.

Origins of lability and stability

Table 3. Characteristic crystal data of κ^2,κ^3-type complexes

compound	N^{Py}-N^{H} distance [Å]	N^{Py}..H^{N} distance [Å]	angle N^{Py1}-N^{Py2} [deg]
10c	2.870	2.072	104.43
9d	2.907	2.148	104.35
9b	2.941	2.184	105.91
10b'	2.802	1.977	104.61
12d	2.910	2.075	104.06

As already mentioned, the distortion of **9a-9d** results from unfavorable steric interactions between the NH of the pending -PR_2 moiety and the pyridine-ring. Although no X-ray structure of the hydrolyzed complex **10a** available, a similar distortion is expected because of the free amine group NH_2. The model compound **13b** was designed which resembles the κ^2,κ^3-type complexes structurally and electronically (**scheme 14**).

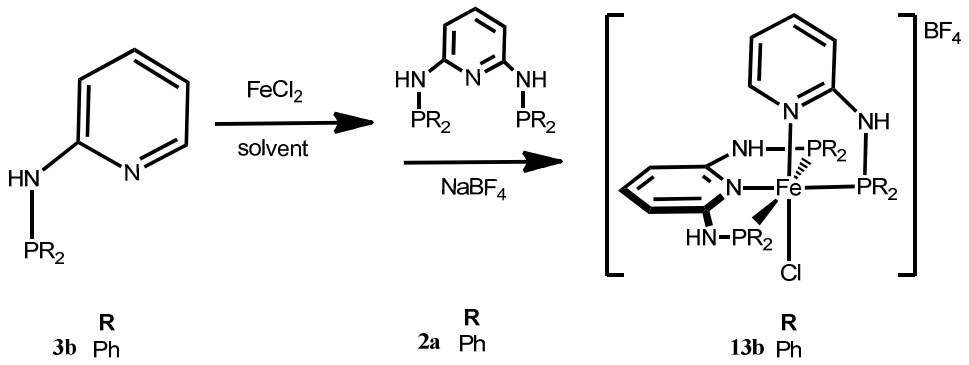

Scheme 14. Synthetic pathway of 13b

However, the model compound lacks a free phosphinoamine arm. Notably, the synthesis only was selective for R = Ph, while BIPOL led to mixtures. However, this is a perfect probe for comparison, and as the crystal structure shows, **13b** is almost perfectly octahedral (**figure25**).

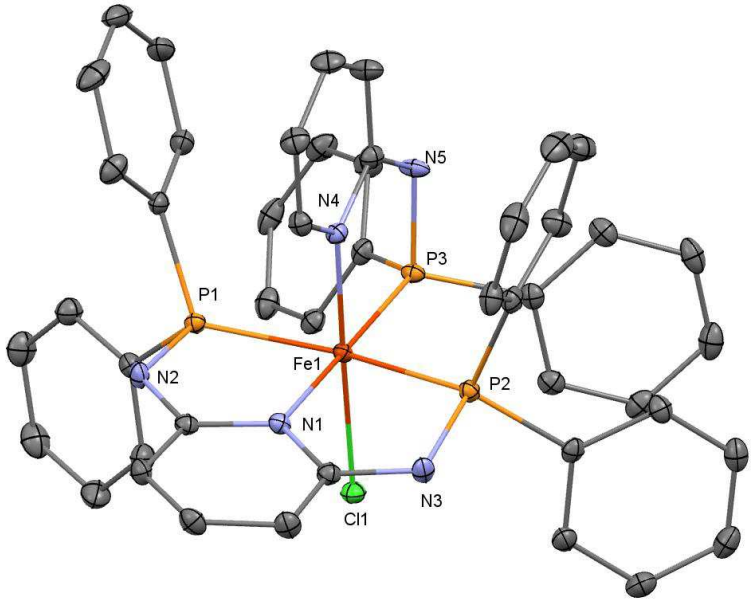

Figure 25. Structural view of κ^2,κ^3-[Fe(PN-Ph)(PNP-Ph)Cl]BF_4 (13b) showing 50% thermal ellipsoids (H-atoms, solvents and BF_4^- omitted for clarity). Selected bond lengths (Å) and bond angles (deg): Fe(1)-P(1) 2.2784(4), Fe(1)-P(2) 2.2533(4), Fe(1)-P(3) 2.1862(4), Fe(1)-N(1) 2.0172(9), Fe(1)-N(4) 1.9930(9), Fe(1)-Cl(1) 2.3331(4), P(1)-N(2) 1.696(1), P(2)-N(3) 1.690(1), P(3)-N(5) 1.686(1), N(2)-C(1) 1.370(2), N(3)-C(5) 1.377(2), N(5)-C(30) 1.380(2), P(1)-Fe(1)-P(2) 163.99(1), N(1)-Fe(1)-P(3) 178.08(3), Cl(1)-Fe(1)-N(4) 178.83(3).

Experimental data show that **13b** does not react with CO. With this evidence, it can be concluded that the lability (and also reactivity) of the κ^2,κ^3-type complexes **9a-12d** is a consequence of steric repulsion between the NH and the pyridine-ring. In the beginning, κ^2,κ^3-type complexes were only observed using π-acceptor PNP ligands **2a-2b**. Therefore when searching for the driving force of the formation of these complexes, we sided with the argument that the tendency to form an $18e^-$-complex increases with the π-acceptor strength of the ligands. The testing of PNP-Et showed, that κ^2,κ^3-type complexes were also possible with small, σ-donating ligands. According to the series of ligands used, it can be assumed that the formation of the κ^2,κ^3-type complexes only needs sterically little demanding phosphines. The existing of 18 valence electrons additionally is thermodynamically favored for octahedral complexes. With bulkier residues like *i*Pr attached, the pentacoordinated 16 e^- complex **8e** is formed. It seems legit, that the coordination of a second bulky ligand is kinetically disfavored. The influence of the N-H bridges and the role of the pyridine-ring e.g. forming N-H—N^{Py}-interactions, was rudimentary investigated in this research. An attempt to suppress the formation of a κ^2,κ^3-type complex by alkylation of the NH branch was unsuccessful. Instead, a new green variation of these complexes was formed, proved by crystal structure (**figure 26**).

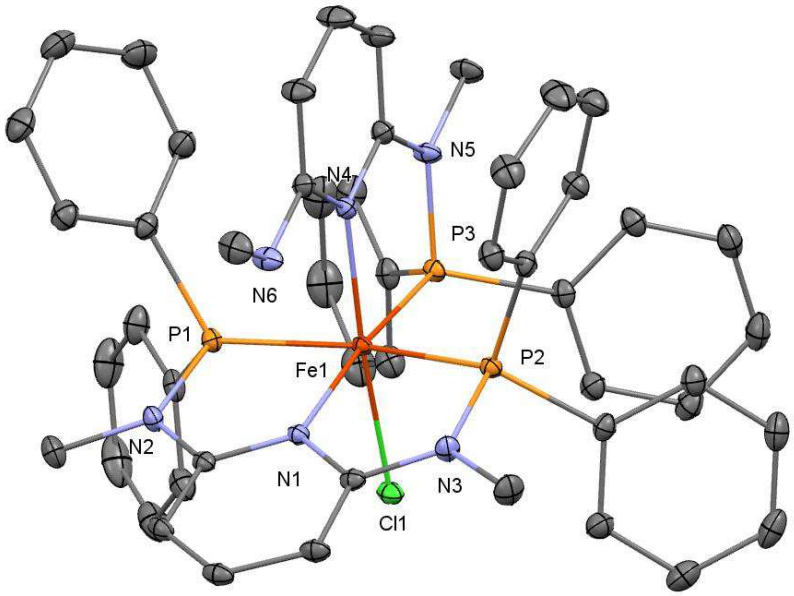

Figure 26. Structural view of hydrolysed $\kappa^2\kappa^3$-[Fe(PNP-Ph)$_2$Cl](BF$_4$) (10b') showing 50% thermal ellipsoids (H-atoms and BF$_4^-$ omitted for clarity). Selected bond lengths (Å) and bond angles (deg): Fe(1)-P(1) 2.2333(4), Fe(1)-P(2) 2.2410(4), Fe(1)-P(3) 2.1833(4), Fe(1)-N(1) 2.0472(9), Fe(1)-N(4) 2.0668(9), Fe(1)-Cl(1) 2.3323(3), P(1)-N(2) 1.7059(9), P(2)-N(3) 1.7055(9), P(3)-N(5) 1.6908(9), N(2)-C(1) 1.381(1), N(3)-C(5) 1.381(2), N(5)-C(32) 1.398(1), N(6)-C(36) 1.354(1), P(1)-Fe(1)-P(2) 163.97(1), N(1)-Fe(1)-P(3) 171.60(3), Cl(1)-Fe(1)-N(4) 173.32(3).

The initial assumption was, that the repulsion of the pyridine-ring and an N-R (R = Me) is too big, so that a pentacoordinated complex similar to **8e** is preferred. What truly happened was a hydrolysis of the P-N bond similar to **9a/9c** resulting in **10b'** (**scheme 15**).

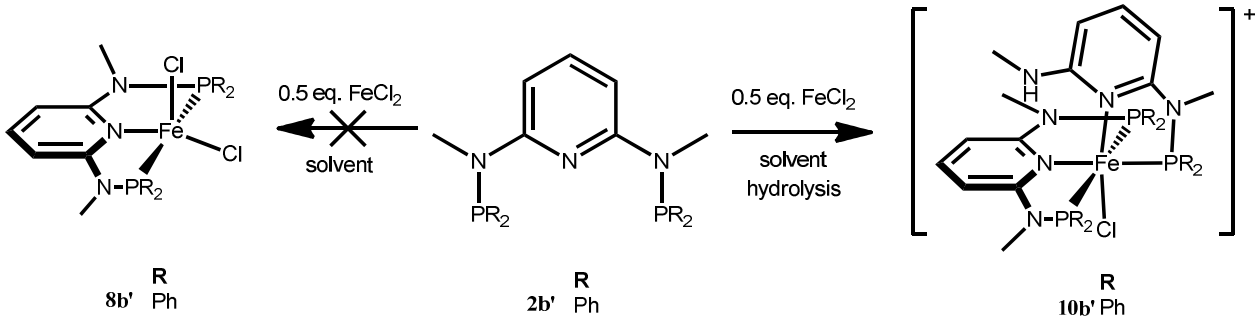

Scheme 15. Formation of 10b' by hydrolysis of P-N bond

This outcome is unexpected since the R$_2$P-N bond (R = Ph) was stable in the case of **9b** even in solution under atmospheric conditions.

Mixed type $\kappa^2,\kappa^3[Fe(PNP)_2Y]^+$-complexes

A few attempts were made to obtain κ^2,κ^3-type complexes based on PNP ligands with two different phosphine moieties (-PR_2, -PR'_2). The motivation was to get further insight into the stability of these complexes and to see whether the smaller PNP ligand ends up in κ^2or in κ^3 bonding mode. An attempt starting from $FeCl_2$, PNP-BIPOL **4a** and PNP-*i*Pr **4a** led to the formation of the complexes **4a** and **4a** already known. Similar results were achieved using PNP-Et and PNP-Ph as the corresponding complexes κ^2,κ^3-$[Fe(PNP)_2Y]^+$ were formed separately (**scheme 16**).

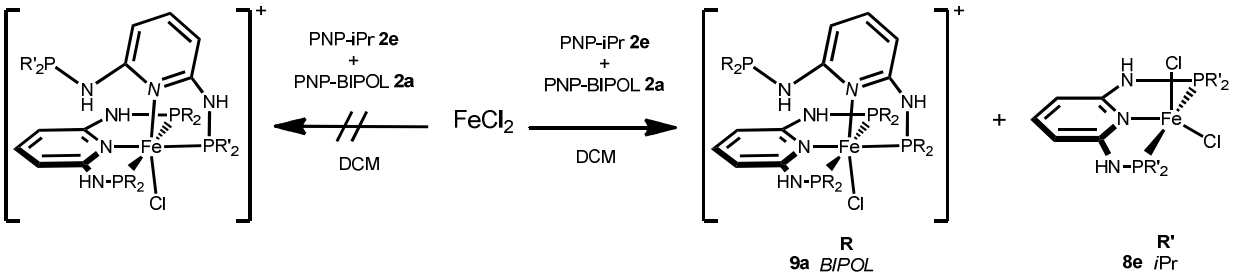

Scheme 16. Attempt to afford mixed κ^2,κ^3-type complexes

The attendance of two different PNP ligands seems to be disfavored. The outcomes of these experiments were monitored by $^{31}P\{^1H\}$ NMR for a quick screening and were not further investigated.

The same approaches starting from the *trans*-**4a** led to quantitative precipitation of *trans*-**5a** (**scheme 17**).

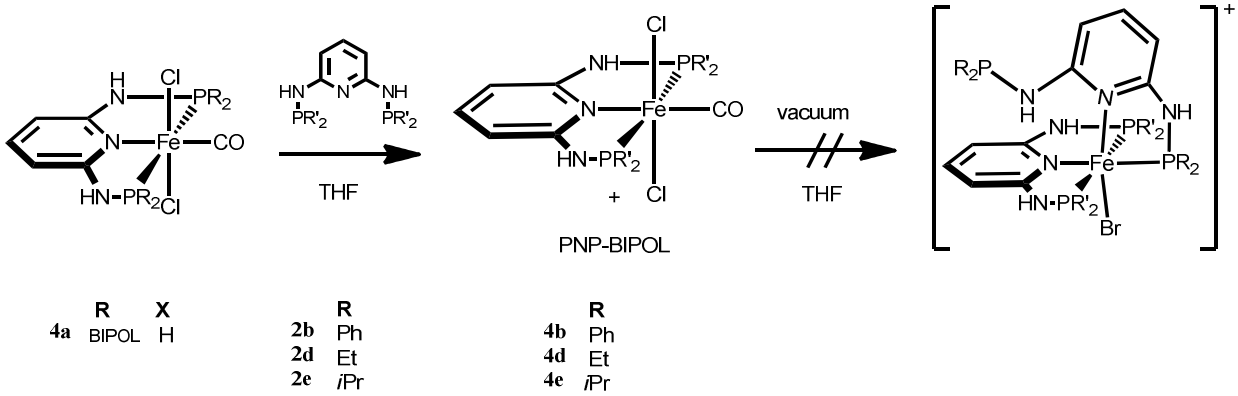

Scheme 17. 2nd attempt to get mixed κ^2,κ^3-type complexes

Although no new compound could be identified, this study revealed two facts. First, PNP-BIPOL is somehow weakly bound to the Fe center as it is immediately substituted by PNP ligands with better σ-donor strength. Secondly, the reversibility between κ^2,κ^3-type complexes and *mono*-CO complexes truly limited to very good π-acceptors like **2a**.

κ^3,κ^3-$[Fe(PNP)_2Y]^{2+}$-complexes

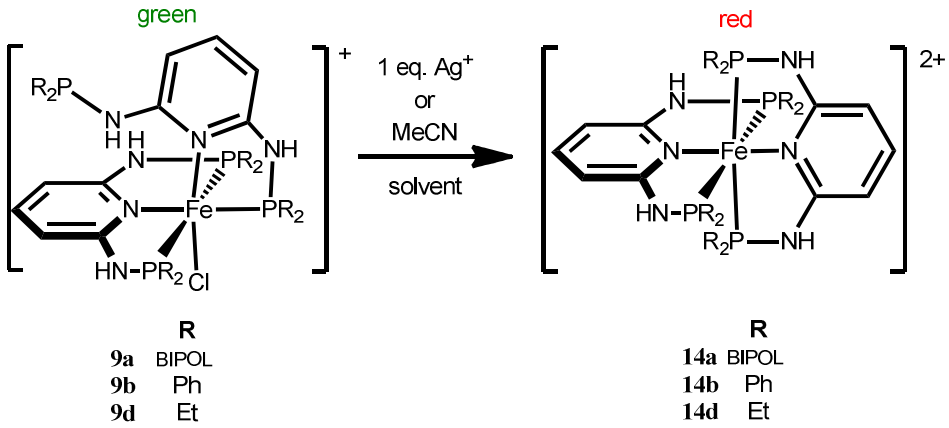

Scheme 18. Formation of κ^3,κ^3-type complexes by halide abstraction

After treatment of **9a-9d** with Ag^+-salts the octahedral, red colored complex of the general formula $[Fe(PNP)_2X]^{2+}$ is obtained (**scheme 18**). In case of **8b**, even the usage of coordinating solvents is sufficient. In CH_3CN conversion is completed within a few minutes, while THF takes several days. The formation of a κ^3,κ^3-type-complex is within expectation, but it is unclear why this one is not formed primarily. The singlet $^{31}P\{^1H\}$ NMR resonance occurs at lower field than the doublets of κ^2,κ^3-type-complexes, indicating a stronger deshielding of the phosphorus. **14b** is already literature known, synthesized and characterized by Kirchner *et. al*. using an alternative pathway (**scheme 19**).

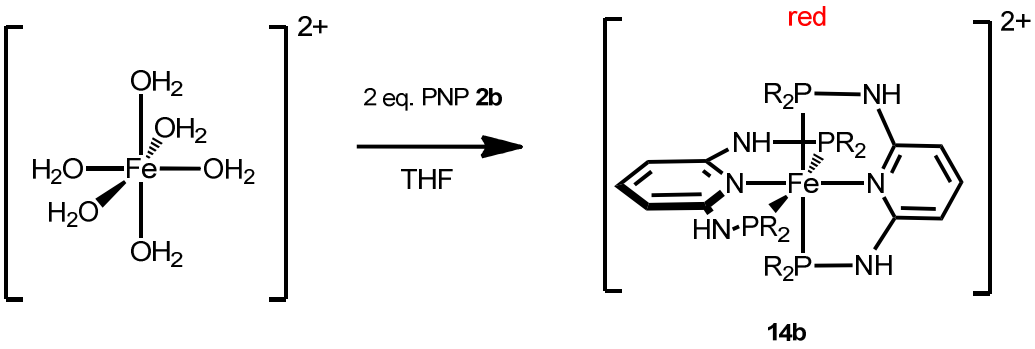

Scheme 19. Alternative pathway for the formation κ^3,κ^3-type-complexes

This procedure with $[Fe(H_2O)_6](BF_4)_2$ as a starting material works well as long as the free ligand is stabile towards water and works in 90% yield for PNP-Ph.

PNP-BIPOL

The PNP-BIPOL based ligand system, already known for its ailing in presence of Ag^+-salts led to crude and inseparable mixtures. Byproducts were the vast majority, also when dissolved in CH_3CN. So, originally the existence of **14a** was out of question, also because 6 π-accepting ligands around the Fe(II)-center were considered as very disadvantageous. Trials using method 2 starting from $[Fe(H_2O)_6](BF_4)_2$ using different solvents was of no avail. While in CH_3CN only $[Fe(PNP\text{-}BIPOL)(CH_3CN)_3](BF_4)_2$ (already literature known[19]) plus non-coordinated ligand was formed, DCM and THF led to mixtures. However, measurable crystals of **6a** were grown out of a mixture in THF after evaporation in the glove-box. The structure is shown in **figure 27**.

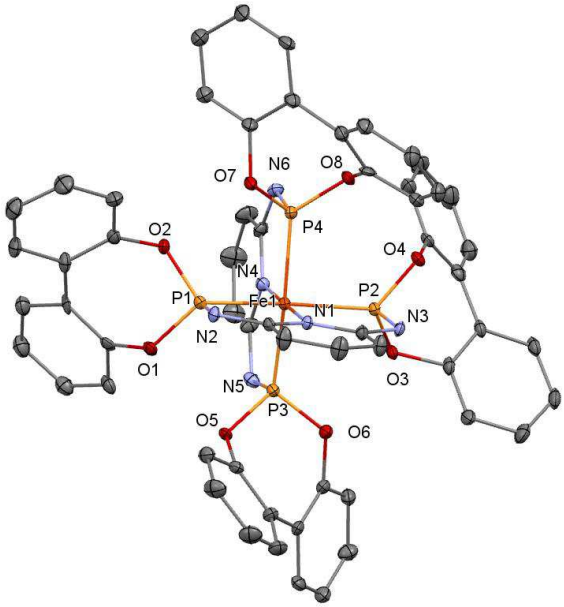

Figure 27. Structural view of $[(PNP\text{-}BIPOL)_2Fe](OTf^-)_2$ (14a) (H-atoms, solvent molecules and OTf^- omitted for clarity). Selected bond lengths (Å) and bond angles (deg): Fe(1)-P(1) 2.181(2), Fe(1)-P(2) 2.182(2), Fe(1)-P(3) 2.189(2), Fe(1)-P(4) 2.180(3), Fe(1)-N(1) 1.969(6), Fe(1)-N(4) 1.968(6), P(1)-N(2) 1.658(6), P(2)-N(3) 1.654(7), P(3)-N(5) 1.659(6), P(4)-N(6) 1.598(6), N(2)-C(1) 1.38(1), N(3)-C(5) 1.39(1), N(5)-C(30) 1.39(1), N(6)-C(34) 1.392(9), P(1)-Fe(1)-P(2) 167.5(1), P(3)-Fe(1)-P(4) 167.4(1).

Notably, the crystals were isolated from a different attempt using 1 equiv. of *trans*-**4a**, 1 eq. **2a** and 2 equivs. of AgOTf. Unfortunately there was not enough substance left for characterization by NMR-analysis. Further the crystal growth was not reproducible. The presumed chemical shift of $^{31}P\{^1H\}$ NMR is 208.97 ppm in acetone-d_6.

PNP-Ph

14b is the κ^3,κ^3-type-complex investigated in most detail with considerable reactivity under certain conditions. A rearrangement to the κ^2,κ^3-type-complexes **9b** is achieved, when a solution of **14b** is stirred for 9h in presence of *n*-Bu_4NCl. According to the data received from the crystal-structure, there is no source of steric repulsion observable. Hence, it is assumed that more likely electronic influences are decisive for stability. The two pyridine-rings in *trans*-position are very unfavorable and -PPh_2 is also a decent p-acceptor increasing this effect. Apparently, the accompaniment of a coordinating counter-ion is crucial for the lability of **14b**, because using BF_4^- as counter ions the complex is unreactive and stable. This statement was strengthened after CO was bubbled through a solution of **14b** in presence of Cl^-, which was either managed by Bu_4NCl or usage of CH_3CN for the synthesis. The outcome of the reaction is a mixture of **4b** and **6b** with the *bis*-CO complex as the major product. This might be a hint for the fact that **6b** could be formed in first place as a reactive intermediate during the direct synthesis of **6b**.

PNP-Et

14d is obtained by multiple pathways in good yield. Synthesis via Ag^+-salts works well, but still not completely selective. Due to the sensitivity of the noncoordinated -PR_2 oxidized byproducts are expected. It is also observed in small amounts after exchange of the counterion of **9d** with $AgBF_4$, AgOTf, and $NaBPh^{Me}_4$. Interestingly, κ^2,κ^3-type-complex **9d** is stable when dissolved in CH_3CN and no visual rearrangement is observed during a period of a few days. The direct conversion of 2 equivs **2d** and $FeCl_2$ in CH_3CN instantly delivers **14d**, with Cl^- as the counter ion. The best and most selective method however is method 2 with $[Fe(H_2O)_6](BF_4)_2$ in THF. **14d** precipitates as a purple solid and may be washed properly. For analysis and crystal growth the Cl^- counter ion is exchanged with $NaBPh_4$. Crystals for X-ray diffraction were grown in acetone by slow ether diffusion (**figure 28**).

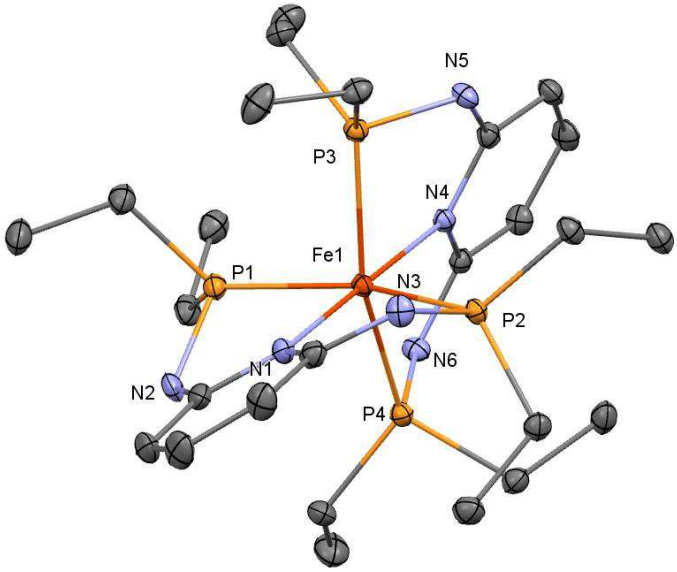

Figure 28. Structural view of Fe(PNP-Et)$_2$](BPh$_4$)$_2$ (13d) (H-atoms, solvents and BPh$_4^-$ omitted for clarity). Selected bond lengths (Å) and bond angles (deg): Fe(1)-P(1) 2.2804(4), Fe(1)-P(2) 2.2873(4), Fe(1)-P(3) 2.2898(6), Fe(1)-P(4) 2.3096(6), Fe(1)-N(1) 2.025(1), Fe(1)-N(4) 2.013(1), P(1)-N(2) 1.709(2),P(2)-N(3) 1.704(1), P(3)-N(5) 1.709(1), P(4)-N(6) 1.712(2), N(2)-C(1) 1.381(2), N(3)-C(5) 1.378(2), N(5)-C(14) 1.383(2), N(6)-C(18) 1.393(2), P(1)-Fe(1)-P(2) 157.93(2), P(3)-Fe(1)-P(4) 158.39(2).

Unlike **14b**, the structure of **14d** is extremely distorted, with the two pyridine-rings twisted in a 42° torsion angle. The coordination geometry of the PNP is almost planar indeed, but the NH bridges are pointing out of the plane. The Fe-N and Fe-P bonding distances are slightly shorter for **14b** (~0.02 Å), although -PEt$_2$ is sterically less demanding. From this viewpoint, electronic properties are crucial here, and -PPh$_2$ as a good π-acceptor is coordinated tighter to the metal center.

[(PNP)Fe(CH$_3$CN)$_3$]$^{2+}$complexes

The synthesis of the orange octahedral *tris*-acetonitrile-complexes (**scheme 20**) of general formula [Fe(PNP)(CH$_3$CN)$_3$]$^{2+}$ is literature known. The procedure has already been carried out for **16a-b** and **5e**. by Kirchner *et. al*. including crystallographic data.[19]

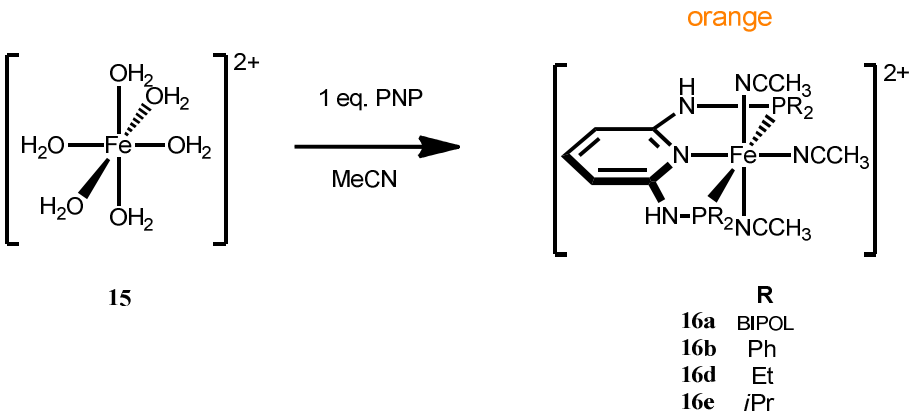

Scheme 20. Synthesis of complexes [Fe(PNP)(CH$_3$CN)$_3$]$^{2+}$

These complexes are of fundamental interest, because they offer an effective probe-compound to study specific characteristics of the PNP ligands. The complex-system is easy to prepare, rather stable, cationic and therefore rather willing to crystallize. Acetonitrile as a linear weakly π-accepting spectator ligand is well qualified to compare electronic and steric influence of a series of ligands.

After conversion of **2d** with [Fe(H$_2$O)$_6$](BF$_4$)$_2$ in CH$_3$CN **16d** is isolated in viable yield Several washing steps (DCM/Et$_2$O) are necessary before crystal growth since the product is oily and sticky. Nice needle shaped crystals were grown in CH$_3$CN by slow diffusion of Et$_2$O. The structure is displayed in **figure 29**.

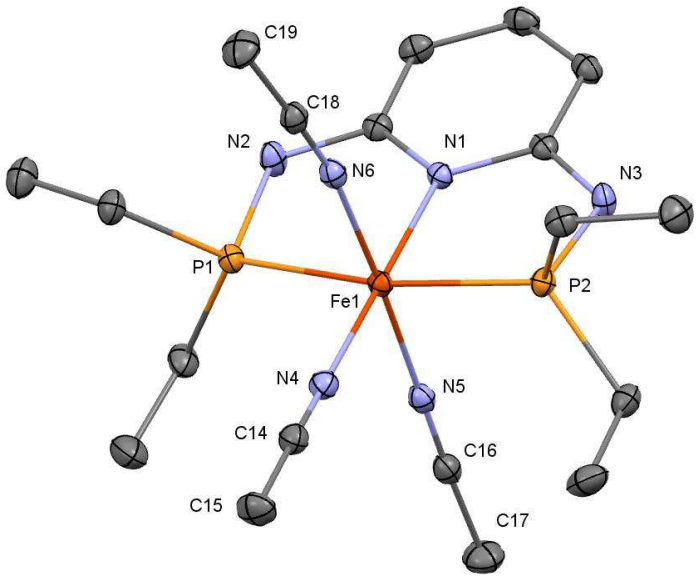

Figure 29. Structural view of [Fe(PNP-Et)(CH3CN)3]$(BF_4)_2$ (16d) showing 50% thermal ellipsoids (H-atoms and BF_4^- omitted for clarity). Selected bond lengths (Å) and bond angles (deg): Fe(1)-P(1) 2.2436(4), Fe(1)-P(2) 2.2355(4), Fe(1)-N(1) 1.9851(9), Fe(1)-N(4) 1.9315(9), Fe(1)-N(5) 1.922(1), Fe(1)-N(6) 1.927(1), P(1)-N(2) 1.694(1), P(2)-N(3) 1.694(1), N(2)-C(1) 1.373(2), N(3)-C(5) 1.377(2), N(4)-C(14) 1.136(1), N(5)-C(16) 1.143(2), N(6)-C(18) 1.143(2), P(1)-Fe(1)-P(2) 167.60(1), N(4)-C(14)-C(15) 179.2(1), N(5)-C(16)-C(17) 177.8(1), N(6)-C(18)-C(19) 177.8(1).

Table 4 shows a comparison of characteristic values of **16a-16e**, based on their crystal structures. The bonding distance of the C-N triple bond is equivalent to the extent of π-backbonding by the metal, while the degree of linearity of the coordinated CH_3CN reflects the steric repulsion with the surrounding residues. The comparison shows, that the ligands are tighter bond to the Iron, the better the π-acceptor and activation of the C-N bond increases with is better σ-donors, which is consistent with our expectations. Interestingly **16d** is exhibiting a longer nitrile bond than **16e**. **16a-16d** show only subtle bending of the CH_3CN ligand, differ a few degrees from perfect 180°C. Far more prominent is the distortion of the N-C-C angle for **16e**, validating the obvious difference in size between these PNP ligands.

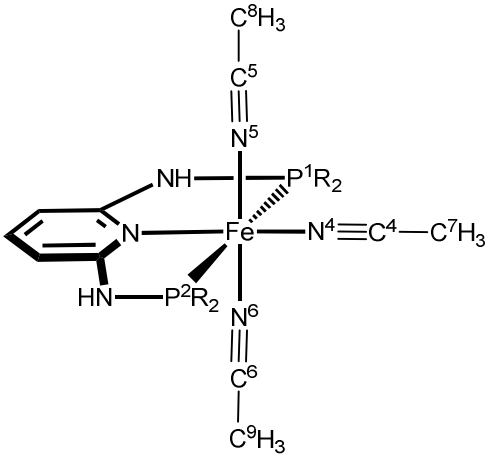

Figure 30. Designated bonding distances and angles for table 4

Table 4.Selected bonding distances and angles of complexes 16a-16e

	16a	**16b**	**16d**	**16e**
Fe-P1 (Å)	2.1895(6)	2.2339(9)	2.2436(4)	2.2581(9)
Fe-P2 (Å)	2.1881(5)	2.2275(8)	2.2355(4)	2.2682(7)
Fe-N1(Å)	1.975(1)	1.977(2)	1.9851(9)	1.988(2)
Fe-C1 (Å)	1.931(2)	1.934(3)	1.9315(9)	1.932(3)
Fe-C2 (Å)	1.917(1)	1.903(2)	1.922(1)	1.914(2)
Fe-C3 (Å)	1.913(1)	1.920(2)	1.927(1)	1.926(3)
N4-C4 (Å)	1.136(2)	1.137(4)	1.136(1)	1.123(6)
N5-C5 (Å)	1.137(2)	1.128(4)	1.143(2)	1.134(4)
N6-C6 (Å)	1.126(2)	1.135(4)	1.143(2)	1.140(4)
N4-C4-C7 (deg)	179.4(2)	179.4(4)	179.2(1)	174.4(6)
N5-C5-C8 (deg)	178.1(2)	178.9(4)	177.8(1)	178.0(4)
N6-C6-C9 (deg)	179.0(3)	177.9(4)	177.8(1)	176.7(4)

Catalytic activity for coupling of aromatic aldehydes with ethyldiazoacetate (EDA) is reported for **16e.**[32] Smaller phosphine residues of **16d** could enhance the substrate binding which would therefore be valuable of reinvestigation.

Conclusions and Outlook

- An inexpensive and solvent-economic synthesis for Et_2PCl (**1d**), a rather expensive reagent, was re-established based on literature back from 1961. Conversion with 2,6-DAP delivered a new PNP ligand **2d** which was fully characterized. Applied on a basis probe-complex **16d** the steric and electronic properties could be compared to resembling ligands of frequent usage. There is a lot of room for a series of *n*-alkyl- and cycloalkyl-chlorophosphines R_2PCl extend the scope for modifications of PNP ligands. The number of variations even grown larger when the diphosphine is transformed into other reactants.[33]
- A series of three basic PNP pincer ligands, based on a 2,6-diaminophosphine-pyridine scaffold were applied on Fe(II)-precursors. The steric demand of PNP-ligands wassimilar, but they strongly varied in terms of electronics. The phosphine-residues range from strong π-accepors to σ-donors (-$P(OR)_2$, -PPh_2, -PEt_2). These modifications had significant influence on the investigated complexes.
- Octahedral CO complexes of general formula $Fe(PNP)COCl_2$ plus corresponding $[Fe(PNP)(CO)_2Cl]^+$ were isolated. The configuration highly relied on the solvent used and also the phosphine-residue –PR_2. Some of the mono-CO complexes were capable of reversible coordination of CO, even in solid phase. In addition these complexes are useful precursors for preparation for Fe^{II}-hydrides and Fe^0-carbonyls.
- A new class of green, diamagnetic PNP-Fe^{II} pincer complex of general formula κ^2,κ^3-$[Fe(PNP)_2Cl]^+$ was characterized. One ligand is in tridentate κ^3-(*P,N,P*) bonding mode, while the other is in bidentate κ^2-(*P,N*) bonding mode, with a pendant phosphine-residue –PR_2. Analysis of the crystal structures with comparable compounds reveal information of certain driving forces. The distorted octahedral geometry is a main factor responsible for several reactivities. These include hydrolysis of the vacant –PR_2, rearrangement in bonding mode and ligand exchange with CO in solution.
- The phosphite-based PNP **2a** was figured out as inappropriate for Fe^{II} systems, at least not for those tackled in this survey. Many fundamental transformations were disturbed by side-reactions, e.g. hydrolysis. The few isolated complexes are not crystallizing well and are labile compared to alkyl/aryl based PNP ligands. But, applied in a cyclic reaction sequence a single phosphorylated 2,6-DAP can be isolated selectively. After further optimization and upscaling this can be utilized for preparation of non-symmetric PNP ligands. A replacement by less electron withdrawing, isoelectronic amine-analogues of BINOL is worthy of investigation, since they have successfully been applied for asymmetric Cu-catalysis[34].

Experimental Section

General Procedures

All syntheses were performed under inert condition under argon atmosphere using standard Schlenk-techniques for handling air- and moisture-sensitive compounds.[35] The solvents used were dried over sodium (THF, diethylether, toluene, *n*-pentane, *n*-hexane) or CaH_2 (DCM, CH_3CN, CH_3NO_2). ^{1}H, $^{13}C\{^{1}H\}$, and $^{31}P\{^{1}H\}$ NMR spectra were recorded on Bruker AVANCE-250 and AVANCE-300 DPX spectrometers. ^{1}H and $^{13}C\{^{1}H\}$ NMR spectra were referenced internally to residual protio-solvent, and solvent resonances, respectively, and are reported relative to tetramethylsilane (δ = 0 ppm). $^{31}P\{^{1}H\}$ NMR spectra were referenced externally to H_3PO_4 (85%) (δ = 0 ppm).

Preparation of Ligands

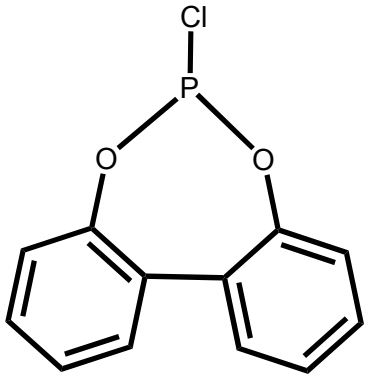

BIPOL-PCl (1a). Method 1: A suspension of biphenol (10.0 g, 53.7 mmol) in toluene (50 ml) is cooled down to 0°C. A mixture of PCl_3 (6.9 ml, 79 mmol) and NEt_3 (22 ml, 159 mmol) in Toluene (50 ml) is slowly added by a drop-funnel to the suspension. After the addition the suspension is allowed to warm to room temperature and stirred for further 18 hours. The white solid is removed by filtration over celite, washed with 30 ml Toluene before the solvent is evaporated. The remaining yellow oil is purified by bulb-to-bulb distillation (1.6 mbar, 240°C) resulting a colorless oil. Yield 5.5 g (52%). Method 2: A suspension of biphenol (15.0 g, 80.6 mmol) in toluene (40 ml) is cooled down to 0°C and PCl_3 (14.1 ml, 161.2 mmol) is added dropwise by a syringe. The mixture is gently warmed with an oilbath (50°C oilbath temperature) for 10 h until the solution is clear. The formed HCl gas is bubbled through water by a gas-wash-bottle. The solvent is evaporated and the remaining slightly yellow oil is purified by bulb-to-bulb distillation (1.6 mbar, 240°C). The resulting colorless oil crystallizes over night at RT. Yield 11.7 g (77%) (white crystalline solid, MW: 250.62).

$C_{12}H_8ClO_2P$, elemental analysis (calc): C, 57.51; H, 3.22; Cl, 14.15; O, 12.77; P, 12.36

^1H NMR (δ, CD_2Cl_2, 20°C): 7.57 (d, J_{HH} = 2.2 Hz, 1H), 7.54 (d, J_{HH} = 2.1 Hz, 1H), 7.51-7.38 (m, 4H), 7.28 (s, 1H), 7.26 (s, 1H). $^{13}C\{^1H\}$ NMR (δ, CD_2Cl_2, 20°C): 149.15 (d, J_{CP} = 5.5 Hz, Ph^1), 130.85 (d, J_{CP} = 3.4 Hz, Ph^2), 130.21 (d, J_{CP} = 1.3 Hz, Ph^6), 129.5 (s, Ph^3), 126.36 (d, J_{CP} = 1.3 Hz, Ph^5), 122.13 (d, J_{CP} = 2.0 Hz, Ph^4). $^{31}P\{^1H\}$ NMR (δ, CD_2Cl_2, 20°C): 191.17 (s).

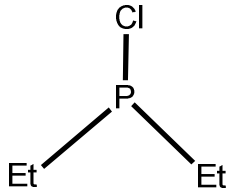

Et_2-PCl (1d)

Step 1: Preparation of thiophosphorylchloride ($S=PCl_3$). A distillation apparatus with column is prepared. Sulfur (18.0 g, 561 mmol) and PCl_3 (41 ml, 469 mmol) are mixed in the 3-necked distillation flask and heated up to 70°C. $AlCl_3$ (3.36 g, 25.2 mmol) before the suspension is further heated up to 110°C. The exothermal reaction itself runs rapidly and is finished within a few seconds. The colorless oily product is obtained after distillation at 123°C. The first 5 ml of the distillate may contain remaining PCl_3 and are brushed away. Yield 67.9 g (74 %) (colorless liquid, MW: 169.40).

$^{31}P\{^1H\}$ NMR (δ, $CDCl_3$, 20°C): 43.6 (s).

Step 2: Preparation of tetraethyl-diphosphine-disulfide ($Et_2P_2S_2$). A Grignard-solution is prepared using Mg (24.3 g, 1 mol), EtBr (74,6 ml, 1 mol) and 250 ml Et_2O. The solution is refluxed for 1h before it is cooled do 0°C. Then the $S=PCl_3$ (53 g, 0.32 mol) is slowly added via dropfunnel, holding the temperature between 0-5 °C. After addition, further 350 ml of THF are added dropwise before the reaction-mixture is refluxed for 2h. The mixture is cooled again to 0°C and quenched with 500 ml of 0.25M sulfuric acid. The organic phase is separated by a separating funnel and the aqueous phase extracted with further 100 ml of Et_2O. The combined organic phases are dried over Na_2SO_4 before evaporation of the solvent. 20 ml of EtOH are added to the remaining liquid before refrigeration at -20°C. The product crystallizes as white needles and is separated by filtration. Yield 22.9 g (70%) (white crystals, MG: 240.32).

^1H NMR (δ, $CDCl_3$, 20°C): 1.85 (dq, J_{HH} = 7.4 Hz, J_{HP} = 14.3 Hz, 8H), 1.18 (dt, J_{HH} = 7.6 Hz, J_{HP} = 15.3 Hz, 12H, CH_3). $^{13}C\{^1H\}$ NMR (δ, $CDCl_3$, 20°C): 21.46 (t, J_{CP} = 26.5 Hz, CH_2), 6.56 (s, CH_3). $^{31}P\{^1H\}$ NMR (δ, $CDCl_3$, 20°C): 62.8 (s).

Step 3: Preparation of tetraethyl-disphospine (Et_4P_2). A distillation apparatus is prepared with multiple receiving-flasks but without column. In the 25 ml distillation-flask $Et_4S_2P_2$ (10.0 g, 41.3 mmol) is mixed and homogenized with activated Fe-powder (9.2 g, 165.1 mmol). The mixture is heated with a sand bath quickly to >200°C.After that, the product is obtained by fractional distillation. The 1st fraction (60 °C) is brushed away. The temperature rises up to 180°C and the 2nd fraction containing the Et_4P_2 is collected. The highly reactive product is used right away for the next synthesis step. Yield 6.0 g (82 %) (colorless oil, MW: 178.19).

Step 4: Preparation of diethylphospinechloride (Et_2P-Cl). The diphosphine Et_4P_2 (6.0 g, 33.6 mmol) is cooled to 0°C and 2 eq. of Ph_2P-Cl (6.3 g, 34.4 mmol) is added dropwise under stirring. After 30 min the icebath is removed and the mixture is allowed to reach room temperature. Finally the Et_2P-Cl is obtained after distillation. The colorless oil is refrigerated at -20°C, forcing impurities to precipitate. Yield 6.78 g (81 %) (colorless liquid, MW: 124.55).
$C_4H_{10}ClP$, elemental analysis (calc): C, 38.57; H, 8.09; Cl, 28.47; P, 24.87
^1H NMR (δ, $CDCl_3$, 20°C): 1.86 (dq, J_{HH} = 7.4 Hz, J_{HP} = 14.3 Hz, 8H), 1.17 (dt, J_{HH} = 7.6 Hz, J_{HP} = 15.3 Hz, 12H). $^{13}C\{^1H\}$ NMR (δ, $CDCl_3$, 20°C): 26.3 (broad, CH_2), 8.39 (d, J_{CP} = 12.4 Hz, CH_3). $^{31}P\{^1H\}$ NMR (δ, $CDCl_3$, 20°C): 123.80 (s).

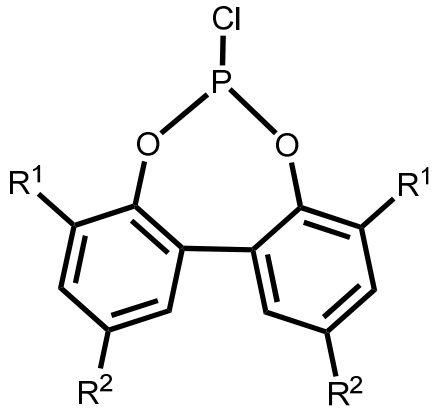

^{tBuOMe}BIPOL-PCl (1f)

Step 1: Preparation of 3,3'-di-tert-butyl-5,5'di-methoxy-[1,1'-biphenyl]-2,2'-diol(2,2'-Biphenol^{tButOMe}). 3-tert-butyl-hydroxyanisole (10.0 g, 55.5 mmol) is dissolved in 250 ml MeOH. A solution of KOH (11.0 g, 196.0 mmol) and $K_3[Fe(CN)_6]$ (18.5 g, 56.2 mmol) in 250 ml H_2O is added dropwise. The suspension is stirred for 2 h before extraction with 600 ml EtOAc. The combined organic phases are washed with 100 ml of brine, dried with Na_2SO_4 and evaporated to dryness by the rotary evaporator. The crude red product is washed 3 times with cold acetone. Yield 7.92 g (79 %) (white powder, MW: 358.47).

^{1}H NMR (δ, $CDCl_3$, 20°C): 6.97 (d, J_{HH} = 3.1 Hz, 2H), 6.63 (d, J_{HH} = 3.1 Hz, 2H), 5.05 (s, 2H, OH), 3.79 (s, 6H, OMe), 1.44 (s, 18H, tBu). $^{13}C\{^1H\}$ NMR (δ, $CDCl_3$, 20°C): 153.19 (s, Ph^4), 145.88 (s, Ph^1), 138.91 (s, Ph^1), 123.20 (s, Ph^2), 115.26 (s, Ph^5), 111.74 (s, Ph^3), 55.72 (s, OMe), 35.16 (s, C_q), 29.48 (d, Me).

Step 2: 2,2'Biphenol^{tBuOMe} (5.0 g, 14.0 mmol) is suspended in 30 ml toluene and cooled to 0°C. PCl_3 (2.44 ml, 27.9 mmol) is added quickly to the suspensionand NEt_3 (4.0 ml, 29.3 mmol) is added slowly by a dropfunnel. The suspension is stirred for further 30 min at 0°C before it is allowed to reach room temperature. After another 2 h the suspension is filtrated, and the solution evaporated to dryness. The remaining orange solid is purified by bulb-to bulb distillation at 260 °C. Yield 4.93 g (85 %) (white crystalline solid, MW: 422.88).

$C_{22}H_{28}ClO_4P$,elemental analysis (calc): C, 62.48; H, 6.67; Cl, 8.38; O, 15.13; P, 7.32

^{1}H NMR (δ, $CDCl_3$, 20°C): 7.02 (d, J_{HH} = 3.1 Hz, 2H), 6.73 (d, J_{HH} = 3.1 Hz, 2H), 3.84 (s, 6H, OMe), 1.47 (s, 18H, tBu). $^{13}C\{^1H\}$ NMR (δ, $CDCl_3$, 20°C): 156.31 (s, Ph^4), 142.95 (d, J_{CP} = 2.5 Hz, Ph^6), 141.31 (d, J_{CP} = 5.8 Hz, Ph^1), 133.60 (d, J_{CP} = 4.2 Hz Ph^2), 114.72 (s, Ph^5), 113.07 (s, Ph^3), 55.60 (s, OMe), 35.52 (s, C_q), 31.27 (d, J_{CP} = 2.7 Hz, Me). $^{31}P\{^1H\}$ NMR (δ, CD_2Cl_2, 20°C): 184.18 (s).

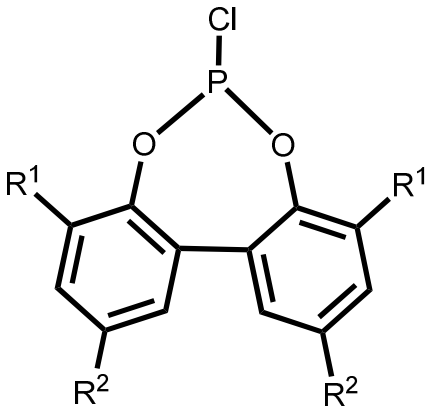

R^1 = *t*Bu
R^2 = *t*Bu

^{tButBu}BIPOL-PCl (1g)

Step1: Preparation of 3,3',5,5'-tetra-tert-butyl-[1,1'-biphenyl]-2,2'-diol (2,2' Biphenol^{tButBu}). The synthesis was performed analogously to procedure of **1f** using 2,4-tert-butyl-phenole (11.4 g, 55.5 mmol), KOH (11.0 g, 196.0 mmol) and $K_3[Fe(CN)_6]$ (18.5 g, 56.2 mmol). Yield 3.12 g (27 %) (white powder, MW: 410.63).

^{1}H NMR (δ, $CDCl_3$, 20°C): 7.40 (s, 2H, Ph^3), 7.12 (s, 2H, Ph^5), 5.23 (s, 2H, OH), 1.47 (s, 18H, tBu^2), 1.34 (s, 18H, tBu^4).

Step 2: The synthesis was performed analogously to procedure of **1f** using 2,2'Biphenol^{tButBu} (2.0 g, 4.2 mmol), PCl_3 (0.8 ml, 8.4 mmol) and NEt_3 (1.2 ml, 8.5 mmol). Yield 1.62g (81%) (white crystalline solid, MW: 475.04).

$C_{28}H_{40}ClO_2P$, elemental analysis (calc): C, 70.79; H, 8.49; Cl, 7.46; O, 6.74; P, 6.52

^{1}H NMR (δ, $CDCl_3$, 20°C): 7.44 (s, 2H, Ph^3), 7.09 (s, 2H, Ph^5), 5.23 (s, 2H, OH), 1.43 (s, 18H, tBu^2), 1.25 (s, 18H, tBu^4). $^{31}P\{^1H\}$ NMR (δ, CD_2Cl_2, 20°C): 183.36 (s).

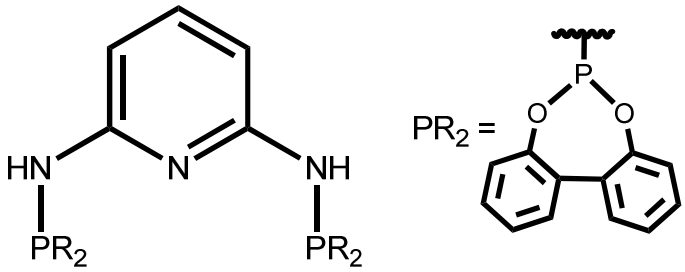

PNP-BIPOL (2a)

A suspension of 2,6-diaminopyridine (2.53 g, 23.25 mmol) in toluene (80 ml) is cooled down to 0°C before addition of NEt_3 (6.5 ml, 47 mmol). A solution of **1a** (11.7 g, 46.5 mmol) in 40 ml toluene is slowly added via a drop-funnel. After the addition the mixture is allowed to reach RT and stirred for 7 h, then heated to 80°C and stirred for another 10 h. The mixture is cooled to RT, the white solid filtrated and washed with 35 ml toluene. The solution is evaporated to dryness, to get the white powdery product. Yield 11.5 g (92 %) (white powder, MW: 537.44).

^{1}H NMR (δ, $CDCl_3$, 20°C): 7.50-7.15 (m, ~17 H), 6.40 (d, J_{HH} = 7.5 Hz, 2H, $Py^{3,5}$), 5.87 (d, J_{HP} = 2.5 Hz, 2H, NH). ^{13}C{^{1}H} NMR (δ, $CDCl_3$, 20°C): 154.30 (d, J_{CP} = 17.0 Hz, $Py^{2,6}$), 149,60 (d, J_{CP} = 4.4 Hz, Ph^{1}), 139.95 (s, Py^{4}), 131.65 (d, J_{CP} = 3.0 Hz, Ph^{2}), 129.79 (s, Ph^{6}), 129.05 (s, Ph^{3}), 125.28 (s, Ph^{5}), 122.27 (s, Ph^{4}), 101.00 (d, J_{CP} = 11.6, $Py^{3,5}$). ^{31}P{^{1}H} NMR (δ, $CDCl_3$, 20°C): 157.65 (s).

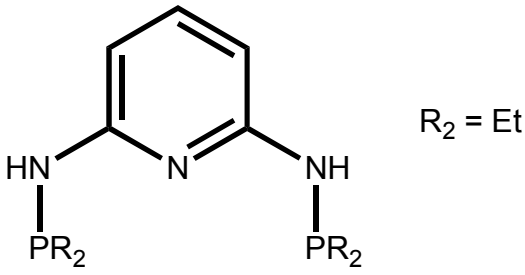

(PNP-Et) (2d)

A suspension of 2,6-diaminopyridine (590 mg , 5.4 mmol) in toluene (15 ml) is cooled down to 0°C before addition of NEt_3 (1,5 ml, 10.8 mmol). A solution of **1b** (1.34 g, 10.8 mmol) in 10 ml toluene is slowly added via a drop-funnel. After the addition the mixture is allowed to reach RT and stirred for 12 h. The mixture is filtrated over celite and washed with 15ml toluene. The solution is evaporated to dryness to obtain a pale red oil, which crystallizes in the freezer at -20°C. Yield 1.46 g (96 %) (white crystalline solid, MW: 285.31).

$C_{13}H_{25}N_3P_2$, elemental analysis (calc): C, 54.73; H, 8.83; N, 14.73; P, 21.71

^1H NMR (δ, $CDCl_3$, 20°C): 7.25 (t, J_{HP} =8.4 Hz, 1H, Py^4), 6.37 (d, J_{HP} = 8.1 Hz, 2H, $Py^{3,5}$), 4.26 (d, J_{HP} = 9.3 Hz, 2H, NH). $^{13}C\{^1H\}$ NMR (δ, $CDCl_3$, 20°C): 158.70 (d, J_{CP} = 18.1 Hz, $Py^{2,6}$),139.24 (s, Py^4), 98.10 (d, J_{CP} = 17.7 Hz, $Py^{3,5}$), 23.55 (d, J_{CP} = 11.9 Hz, CH_2), 8.50 (d, J_{CP} = 13.0 Hz, CH_3). $^{31}P\{^1H\}$ NMR (δ, $CDCl_3$, 20°C): 44.97 (s).

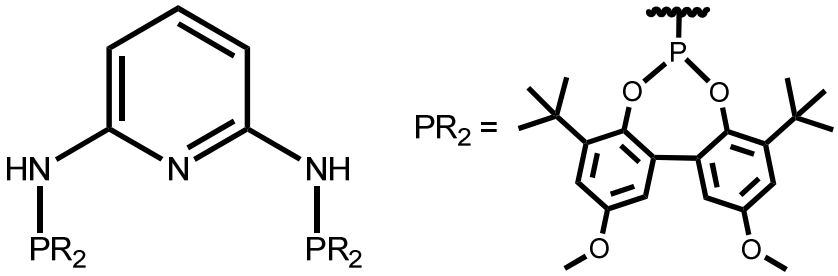

PNP-^{tBuOMe}BIPOL (2f)

The synthesis was performed analogously to procedure of **2a**, using **1f** (1 g, 2.36 mmol), NEt_3 (0.66 ml, 4.72 mmol) and 2,6-DAP (130 mg, 1.18 mmol). The reaction-mixture was stirred over night at 60°C. Yield 0.68 g (65 %) (white powder, MW: 881.97).

$C_{49}H_{61}N_3O_8P_2$, elemental analysis (calc): C, 66.73; H, 6.97; N, 4.76; O, 14.51; P, 7.02

$^{31}P\{^1H\}$ NMR (δ, $CDCl_3$, 20°C):151.21 (s).

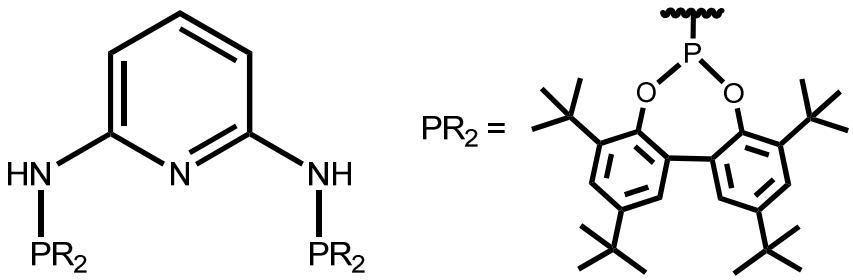

PNP-^{tBuBu}BIPOL (2g)

The synthesis was performed analogously to procedure of **2a**, using **1g** (1 g, 2.11 mmol), NEt_3 (0.60 ml, 4.22 mmol) and 2,6-DAP (115 mg, 1.05 mmol). The reaction-mixture was stirred over night at 60°C. Yield 0.54 g (52 %) (white powder, MW: 986.92).

$C_{61}H_{85}N_3O_4P_2$, elemental analysis (calc): C, 74.28; H, 8.69; N, 4.26; O, 6.49; P, 6.28

$^{31}P\{^1H\}$ NMR (δ, $CDCl_3$, 20°C): 144.34 (s).

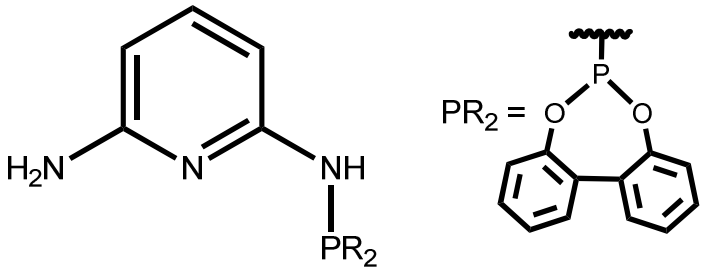

PN-BIPOL (3a)

CO is bubbled through a solution of **13a** (1 g, 1.0 mmol) in DCM (10 ml) and stirred for 4 h. The pink solid *trans*-**4a** is filtrated and the solution evaporated to dryness. The slightly turquoise solid is dissolved in diethylether (20 ml) and filtrated over celite. The clear solution is evaporated to dryness to get the clean white powder. Yield 291 mg (89 %) (white powder, MW: 323.29).

$C_{17}H_{14}N3O_2P$, elemental analysis (calc): C, 63.16; H, 4.36; N, 13.00; O, 9.90; P, 9.58

^{1}H NMR (δ, CD_2Cl_2, 20°C): 7.53-7.17 (m, ~10 H), 6.39 (d, J_{HH} = 7.5 Hz, Py^3), 5.84 (d, J_{HP} = 5 Hz, NH), 5.34 (s, NH_2). $^{31}P\{^1H\}$ NMR (δ, CD_2Cl_2, 20°C): 158.02 (s).

Preparation of Complexes

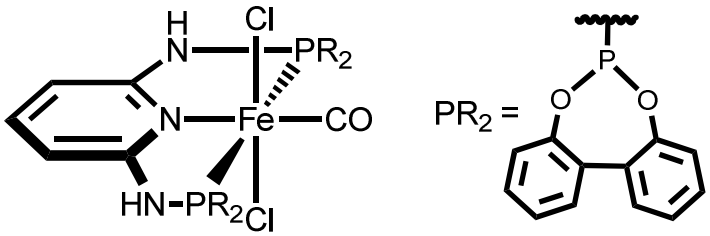

***trans*-[Fe(PNP-BIPOL)Cl_2(CO)] (*trans*-4a)**

CO is bubbled through a green solution of **2a** (500 mg, 0.93 mmol) and $FeCl_2$ (118 mg, 0.93 mmol) in DCM (10 ml). The solution is stirred for further 4 h. The pink solid is filtrated by a glass frit and washed with 10 ml DCM. The pink product is then dried over vacuum. Yield 644 mg (91 %) (pink powder, MW: 693.21). Crystals were grown in THF after refrigeration at -20°C.

$C_{30}H_{22}C_{l2}FeN_3O_5P_2$, elemental analysis (calc): C, 51.98; H, 3.20; Cl, 10.23; Fe, 8.06; N, 6.06; O, 11.54; P, 8.94

^{1}H NMR (δ, acetone-d_6, 20°C): 9.70 (s, 2H, NH), 7.77 (d, J_{HP} = 6.6 Hz, 5H), 7.52 (s, 5H), 6.82 (d, J_{HP} = 7.9 Hz, 2H, $Py^{3,5}$). $^{13}C\{^1H\}$NMR (δ, acetone-d_6, 20°C): 216.52 (t, J_{CP} = 32.3 Hz, CO), 158.65 (t, J_{CP} = 14.4 Hz, $Py^{2,6}$), 149.90 (d, J_{CP} = 4.7 Hz, Ph^1), 141.29 (s, Py^4), 130.21 (s, Ph^2), 129.82 (s, Ph^6), 129.69 (s, Ph^3), 126.38 (s, Ph^5), 122.60 (s, Ph^4), 101.38 (t, J_{CP} = 4.8 Hz, $Py^{3,5}$). $^{31}P\{^1H\}$NMR (δ, acetone-d_6, 20°C): 202.68 (s). IR (ATR, cm^{-1}): $\nu_{C=O}$ 1991.

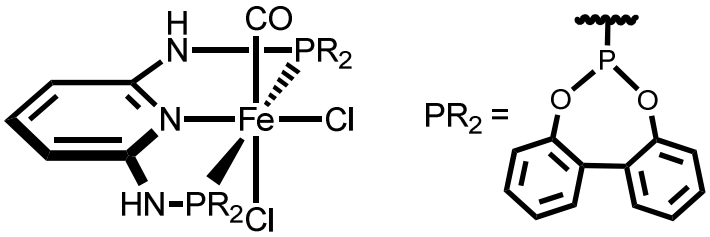

***cis*-[Fe(PNP-BIPOL)Cl_2(CO)] (*cis*-4a)**

CO is bubbled through a green solution of **2a** (500 mg, 0.93 mmol) and $FeCl_2$ (118 mg, 0.93 mmol) in THF (10 ml). The solution turns red immediately and is stirred for 60 min. The solvent is then evaporated, the red solid washed with 10 ml toluene, 10 ml Et_2O and dried over vacuum. Yield 630 mg (89 %) (red powder, MW: 693.21).

$C_{30}H_{22}C_{l2}FeN_3O_5P_2$, elemental analysis (calc): C, 51.98; H, 3.20; Cl, 10.23; Fe, 8.06; N, 6.06; O, 11.54; P, 8.94

^{1}H NMR (δ, acetone-d_6, 20°C): 9.69 (s, 2H, NH), 7.77 (s, 5H), 7.51 (s, ~5H), 6.82 (s, 2H, $Py^{3,5}$). $^{13}C\{^1H\}$NMR (δ, acetone-d_6, 20°C):216.50 (t, J_{CP} = 34.0 Hz, CO), 158.49 (s, $Py^{2,6}$), 149.62 (s, Ph^1), 141.04 (s, Py^4), 130.22 (s, Ph^2), 130.11 (s, Ph^6), 129.99 (s, Ph^3), 126.79 (s, Ph^5), 122.65 (s, Ph^4), 101.69 (t, J_{CP} = 4.8 Hz, $Py^{3,}$). $^{31}P\{^1H\}$ NMR (δ, acetone-d_6, 20°C): 202.68 (s). IR (ATR, cm^{-1}): $v_{C=O}$ 2002.

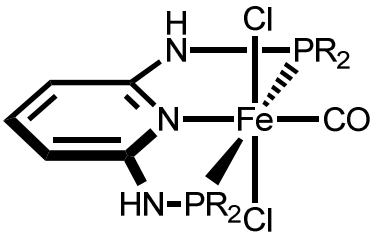

R = Et

***trans*-[Fe(PNP-Et)Cl_2(CO)] (*trans*-4d)**

CO is bubbled through a solution of **2d** (200mg, 0.70 mmol) and $FeCl_2$ (85 mg, 0.67 mmol) in THF (8 ml). The solution turns slightly red, is stirred for 30 min until a violet precipitate is formed. The violet solid is washend with 10 ml THF and 10 ml Et_2O before evaporation to dryness. Yield 644 mg (93 %) (violet powder; MW: 441.07). Note: the product is bad soluble in common solvents. Addition of Bu_4NCl improved solubility and was used for NMR in acetone-d_6.

$C_{14}H_{26}Cl_2FeN_3OP_2$, elemental analysis (calc): C, 38.12; H, 5.94; Cl, 16.08; Fe, 12.66; N, 9.53; O, 3.63; P, 14.04

^{1}H NMR (δ, DMSO-d_6, 20°C): 8.61 (s, 2H, NH), 7.37 (s, broad, 1H, Py^4), 6.30 (d, J_{HP} = 6.0 Hz, 2H, $Py^{3,5}$), 2.08(s, broad, 8H, CH_2), 1.26 (s, 12H, CH_3). $^{13}C\{^1H\}$NMR (δ, DMSO-d_6, 20°C):221.13 (t, J_{CP} = 23.5 Hz, CO), 160.53 (t, J_{CP} = 9.9 Hz, $Py^{2,6}$), 138.17 (s, Py^4), 96.77 (t, J_{CP} = 4.8 Hz, $Py^{3,5}$), 15.37 (t, J_{CP} = 14.0 CH_2), 6.12 (s, CH_3). $^{31}P\{^1H\}$NMR (δ, acetone-d_6, 20°C): 130.94 (s). IR (ATR, cm^{-1}): $\nu_{C=O}$ 1965.

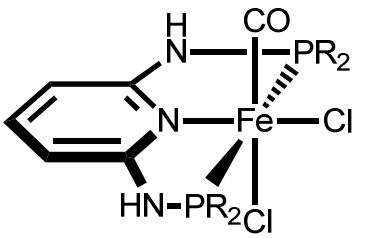

R = Et

***cis*-[Fe(PNP-Et)Br_2(CO)] (*cis*-4d)**

cis-**4d** was detected in solution when a sample of *trans*-**4d**, stored in DMSO-d_6 was avoided of light for 1 week. The solution turned from violet to red. $^{31}P\{^1H\}$NMR (δ, DMSO-d_6, 20°C): 119.54 (s). IR (ATR, cm^{-1}): $\nu_{C=O}$ 1960.

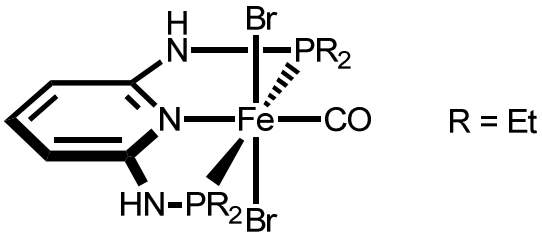

***trans*-[Fe(PNP-Et)Br_2(CO)] (*trans*-5d)**

The synthesis was performed analogously to procedure of **4d** using $FeBr_2$ (150 mg, 0.70 mmol) and **2d** (200 mg, 0.70 mmol) in DCM (10 ml). Yield 250 mg (95 %) (blue powder; MW: 529.98). Single crystals were grown in DMSO/THF by slow diffusion of *n*-pentane.

$C_{14}H_{26}Br_2FeN_3OP_2$, elemental analysis (calc): C, 31.73; H, 4.94; Br, 30.15; Fe, 10.54; N, 7.93; O, 3.02; P, 11.69

^{1}H NMR (δ, DMSO-d_6, 20°C) IR (ATR, cm^{-1}): $\nu_{C=O}$ 1962.

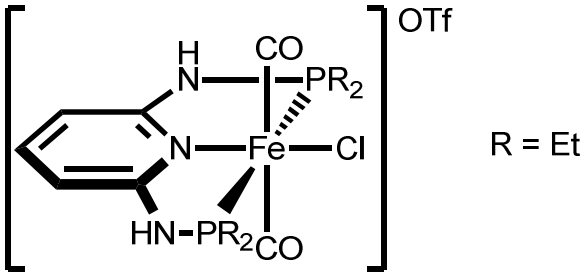

***trans*-[Fe(PNP-Et)(CO)$_2$Cl]OTf (*trans*-6d)**

trans-**4d** (72 mg, 0.16 mmol) and AgOTf (44 mg, 0.17 mmol) are dissolved in DCM (20 ml) upon CO is bubbled through the solution. The solution turns from red to orange and is stirred for further 30 minutes. The orange solution is then filtrated over celite, evaporated to dryness and washed with 10 ml Et_2O. Yield 85 mg (91 %) (orange powder; MW: 583.71). Crystals were grown in acetone by slow diffusion of Et_2O.

$C_{16}H_{27}ClF_3FeN_3O_5P_2S$, elemental analysis (calc): C, 32.92; H, 4.66; Cl, 6.07; F, 9.76; Fe, 9.57; N, 7.20; O, 13.70; P, 10.61; S, 5.49

^{1}H NMR (δ, acetone-d_6, 20°C): 8.49 (s, 2H, NH), 7.63 (s, 1H, Py^4), 6.31 (d, J_{HP} = 5.2 Hz, 2H, Py ^{3,5}), 2.90-2.78(m, J_{HP} = 45.6 Hz, 8H, CH_2), 1.51 (s, 12H, CH_3). ^{13}C{^{1}H}NMR (δ, acetone-d_6, 20°C):210.53 (t, J_{CP} = 25.2 Hz, CO), 161.78 (t, J_{CP} = 6.9 Hz, Py^{2,6}), 141.07 (s, Py^4), 100.29 (s, Py^{3,5}), 23.37 (t, J_{CP} = 15.3 Hz, CH_2), 6.38 (s, CH_3).^{31}P{^{1}H}NMR (δ, acetone-d_6, 20°C): 112.70 (s). IR (ATR, cm^{-1}): $\nu_{C=O}$ 2008.

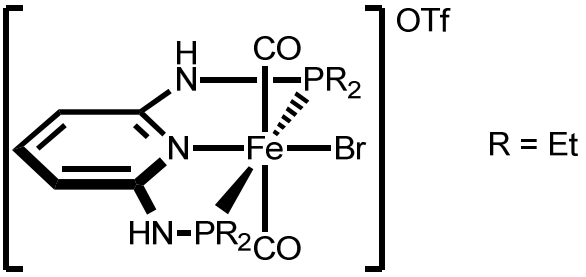

***trans*-[Fe(PNP-Et)(CO)$_2$Br]OTf (*trans*-7d)**

The synthesis was performed analogously to procedure of **6d**, using *trans*-**5d** (100 mg, 0.19 mmol) and AgOTf (51 mg, 0.20 mmol). Yield 110 mg (92 %) (orange powder; MW: 629.17). Crystals were grown in acetone by slow diffusion of Et_2O.

$C_{16}H_{27}BrF_3FeN_3O_5P_2S$, elemental analysis (calc): C, 30.54; H, 4.49; Br, 12.70; F, 9.06; Fe, 8.88; N, 6.68; O, 12.71; P, 9.85; S, 5.10

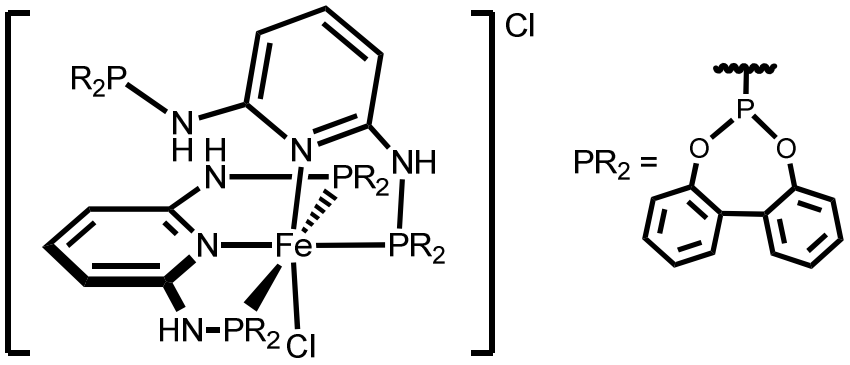

κ^2,κ^3-[Fe(PNP-BIPOL)$_2$Cl]Cl (9a)

Method 1: **2a** (500 mg, 0.93 mmol) and $FeCl_2$ (50 mg, 0.39 mmol) are dissolved in DCM (15 ml) and stirred for 4 h. The green solution is evaporated to dryness and the remaining green solid washed with 30 ml diethylether. Yield 422 mg (90 %). Method 2: *cis*-**4a** or *trans*-**4a** (500 mg, 0.72 mmol) and **2a** (388 mg, 0.72 mmol) are dissolved in a THF/DCM mixture (10ml/10ml) and stirred for 12 h. The green solution is then evaporated to dryness under very gentle vacuum for 3 h. The green product is washed with 10 ml Et_2O. Yield 735 mg (85%) (green powder; MW: 1201.64).

$C_{58}H_{42}Cl_2FeN_6O_8P_4$, elemental analysis (calc): C, 57.97; H, 3.52; Cl, 5.90; Fe, 4.65; N, 6.99; O, 10.65; P, 10.31

^{1}H NMR (δ, CD_2Cl_2, 20°C): 7.66-7.00 (m, ~31 H), 6.85 (d, J_{HH} = 7.5 Hz, 4H, $Py^{3,5}Py^{3',5'}$), 6.56 (d, J_{HP} = 7.5 Hz, 3H, NH), 6.40 (t, 2H, Py^4 $Py^{4'}$), 6.13 (d, J_{HP} = 7.5 Hz, 1H, NH') . $^{13}C\{^1H\}$ NMR (δ, $CDCl_3$, 20°C): 158.26 (t, J_{CP} = 13.0 Hz, $Py^{1,6}$), 151.60 (d, J_{CP} = 12 Hz, Ph^1), 150.55 (s, $Py^{6'}$), 149.90 (m, $Ph^{1'}$), 140.10 (s, Py^4), 137.71 (s, $Py^{4'}$), 130.2-128.12 (m, Ph Ph'), 125.74 (s, Ph^5), 124.84 (s, $Ph^{5'}$), 123.19 (s, Ph^4), 122.53 (s, $Ph^{4'}$), 116.03 (m, $Py^{5'}$), 100.71 (m, $Py^{3,5}$ $Py^{3'}$) . $^{31}P\{^1H\}$ NMR (δ, CD_2Cl_2, 20°C): 205.3-203.71 (dd, J_{PP} = 48.4 Hz, P^{K3}), 194.07 (t, J_{PP} = 112 Hz, P^{K2}), 158.17 (s, P^{free}).

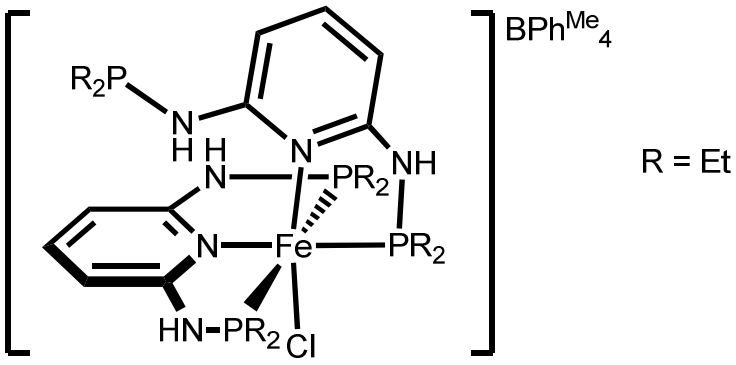

κ^2,κ^3-[Fe(PNP-Et)$_2$Cl]BPh$^{Me}_4$ (9d).

2d (200 mg, 0.70 mmol) and $FeCl_2$ (44 mg, 0.35 mmol) are dissolved in THF (10 ml) and stirred for 1 h. The green product with Cl^- as a counter-ion precipitates, is filtrated and washed with further 5 ml of THF. The green precipitate is suspended with 8 ml THF again and $NaBPh^{Me}_4$ is added (139 mg, 0.35 mmol). Upon stirring for 30 min the solution is evaporated to dryness, the residue resolved in 10 ml DCM and filtrated over celite. The solvent is removed and the solid washed with 8 ml *n*-hexane and dried over vacuum.Yield 323 mg (89%) (green powder; MW: 1037.24). Crystals were grown in THF by slow diffusion of Et_2O or *n*-pentane.

$C_{54}H_{78}BClFeN_6P_4$, elemental analysis (calc): C, 62.53; H, 7.58; B, 1.04; Cl, 3.42; Fe, 5.38; N, 8.10; P, 11.94

^{1}H NMR (δ, CD_2Cl_2, 20°C): 8.21 (s, 2H, NH^{k3}), 7.92 (s, 1H, NH^{k2}), 7.54 (t, J_{HP} = 8.1 Hz, 1H, $Py^{4\ k3}$), 7.30 (m, 8H, $Ph^{2,6}$), 7.06 (t, J_{HP} = 7.8 Hz, 1H, $Py^{4\ k2}$), 6.79 (m, 8H, $Ph^{3,5}$), 6.64 (d, J_{HP} = 8.0 Hz, 2H, $Py^{3,5\ k3}$), 6.36 (dd, J_{HP} = 4.8 Hz, 1H, $Py^{3\ k2}$), 6.07 (d, J_{HP} = 7.7 Hz, 1H, $Py^{5\ k2}$), 4.91 (d, J_{HP} = 9.5 Hz, 1H, NH^{free}), 2.85-2.54 (m, ~8H, $CH_2{}^{k3}$), 2.51-2.34 (m, ~4H, $CH_2{}^{k2}$),2.15 (s, ~12H, Ph^{Me}), 2.07-2.00 (m, ~18H, $CH_3{}^{k3,k2}$), 1.38-1.31 (m, $CH_2{}^{free}$), 1.10-0.85 (m, $CH_3{}^{free}$).^{13}C{^{1}H} NMR (δ, $CDCl_3$, 20°C): 158.26 (t, J_{CP} = 13.0 Hz, $Py^{2,6}$), ^{13}C{^{1}H} NMR (δ, CD_2Cl_2, 20°C): 165.20 (d, J_{CP} = 19.1 Hz, $Py^{2\ k2}$),163.15 (t, J_{CP} = 8.1 Hz, $Py^{2,6\ k3}$), 162.23 (d, J_{CP} = 10.8 Hz, $Py^{6\ k2}$), 160.80 (q, J_{CB} = 48.2 Hz, Ph^1), 140.78 (d, J_{CP} = 11.3 Hz, $Py^{4\ k3}$), 138.92 (d, J_{CP} = 9.5, $Py^{4\ k2}$), 135.94 (s, Ph^4), 130.27 (s, $Ph^{2,6}$), 126.48 (s, $Ph^{3,5}$), 99.90 (d, J_{CP} = 11.3 Hz,$Py^{3,5\ k3}$), 98.5 (d, J_{CP} = 5.9 Hz, $Py^{3\ k2}$),98.40 (d, J_{CP} = 5.7 Hz, $Py^{5\ k2}$),27.90 (d, J_{CP} = 26.4, $CH_2{}^{free}$), 23.05 (d, J_{CP} = 11.8 Hz, $CH_2{}^{k2}$), 21.36 (s, Ph^{Me}), 17.26 (t, J_{CP} = 9.8 Hz, $CH_2{}^{k3}$), 9.05 (d, J_{CP} = 9.1 Hz, $CH_3{}^{free}$), 7.55 (d, J_{CP} = 6.5 Hz, $CH_3{}^{k2}$), 7.42 (s, $CH_3{}^{k3}$).^{31}P{^{1}H} NMR (δ, CD_2Cl_2, 20°C): 127.05 (d, J_{PP}= 50.0 Hz, PNP^{k3}), 123.64 (t, J_{PP} = 47.5 Hz, PNP^{k2}), 48.32 (s, P^{free})

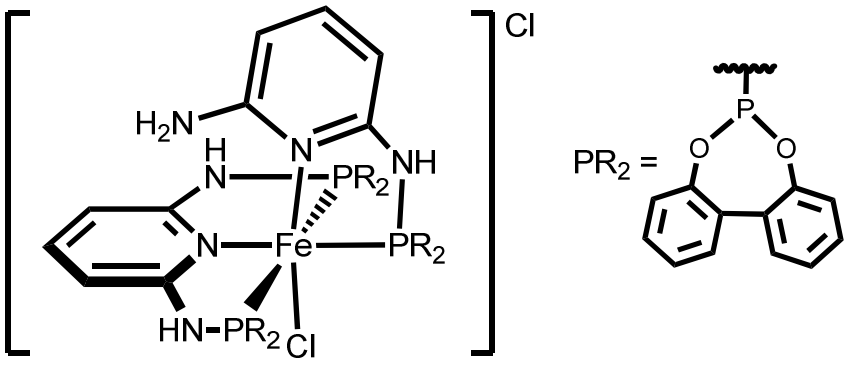

[PNP-BIPOL)(PN-BIPOL)FeCl]Cl (10a).

9a (500 mg, 0.42 mmol) is dissolved in cold technical acetone (15 ml) and stirred for 15 min. The turquoise product is filtrated, washed with technical diethylether (15 ml) and dried over vacuum. Yield 370 mg (90%) (turquoise powder; MW: 987.48).

$C_{46}H_{35}Cl_2FeN_6O_6P_3$, elemental analysis (calc): C, 55.95; H, 3.57; Cl, 7.18; Fe, 5.66; N, 8.51; O, 9.72; P, 9.41

^{1}H NMR (δ, CD_2Cl_2, 20°C): 7.69-7.01 (m, ~24 H), 6.89-6.84 (m, 3H, $Py^{3,5}Py^3$), 6.56 (d, J_{HP} = 7.5 Hz, 3H, NH, NH'), 6.38 (s, 2H, NH_2), 6.10 (t, J_{HH} = 78.0 Hz, 1H, $Py^{4'}$), 5.27 (d, J_{HH} = 8.2 Hz, $Py^{2'}$). $^{13}C\{^1H\}$ NMR (δ, $CDCl_3$, 20°C): 158.28 (t, J_{CP} = 13.0 Hz, $Py^{1,6}$ $Py^{1'}$), 151.55 (d, J_{CP} = 12 Hz, Ph^1), 151.20 (d, J_{CP} = 12 Hz, $Ph^{1'}$), 150.55 (s, $Py^{6'}$), 149.90 (m, $Ph^{1'}$), 140.16 (s, Py^4), 137.66 (s, $Py^{4'}$), 130.25-128.78 (m, Ph Ph'), 125.76 (s, Ph^5), 124.64 (s, $Ph^{5'}$), 123.30 (s, Ph^4), 122.90 (s, $Ph^{4'}$), 105.00 (m, $Py^{5'}$), 100.80 (m, $Py^{3,5}$ $Py^{3'}$) . $^{31}P\{^1H\}$ NMR (δ, CD_2Cl_2, 20°C): 204.72-203.45 (d, J_{PP} = 112 Hz, P^{K3}), 194.25 (t, J_{PP} = 108 Hz, P^{K2}).

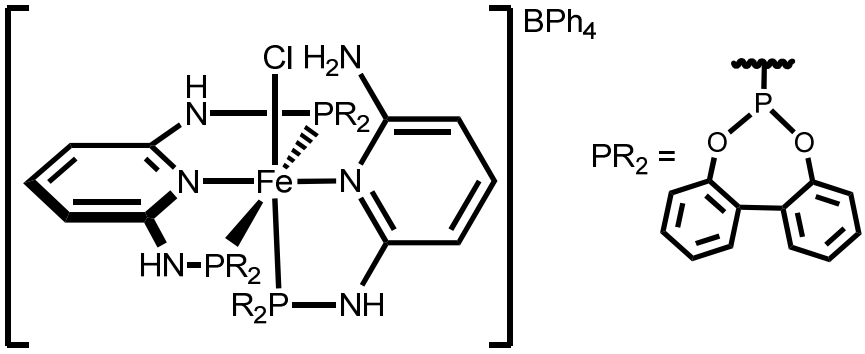

***trans*-κ^2,κ^3-[Fe(PNP-BIPOL)$_2$Cl]BPh$_4$ (11a)**.

2a (200 mg, 0.37 mmol) and $FeCl_2$ (22 mg, 0.18 mmol) are dissolved in DCM (15 ml) and stirred for 1 h before addition of $NaBPh_4$ (60 mg, 0.37 mmol). The red solution is evaporated to dryness washed with 5 ml toluene and 10 ml diethylether. Yield 170 mg (74%). (red powder; MW: 1271.25).

$C_{70}H_{55}BClFeN_6O_6P_3$, elemental analysis (calc): C, 66.14; H, 4.36; B, 0.85; Cl, 2.79; Fe, 4.39; N, 6.61; O, 7.55; P, 7.31

^{1}H NMR (δ, CD_2Cl_2, 20°C): 7.66-7.15 (m, ~24 H, BIPOL), 7.05-6.85 (m, ~20H,BPh_4), 6.69 (t, J_{HP} = 8.2 Hz, 1H, Py^4), 6.48 (d, J_{HP} = 8.9 Hz, 2H, Py^{3,5}), 6.28 (s, broad, 2H, NH_2), 5.96 (d, J_{HP} = 7.8 Hz, NH^{k3}), 5.70 (t, J_{HP} = 7.9 Hz, Py$^{4'}$), 5.40 (d, J_{HP} = 8.0 Hz, 1H, Py$^{3'}$), 5.28 (d, J_{HP} = 8.4, 1H, Py$^{3'}$). ^{13}C{^{1}H} NMR (δ, $CDCl_3$, 20°C): 158.26 (t, J_{CP} = 13.0 Hz, Py^{1,6}), ^{31}P{^{1}H} NMR (δ, CD_2Cl_2, 20°C): 224.33 (d, J_{PP} = 110 Hz, P^{K3}), 196.6 (t, J_{PP} = 112 Hz, P^{K2}).

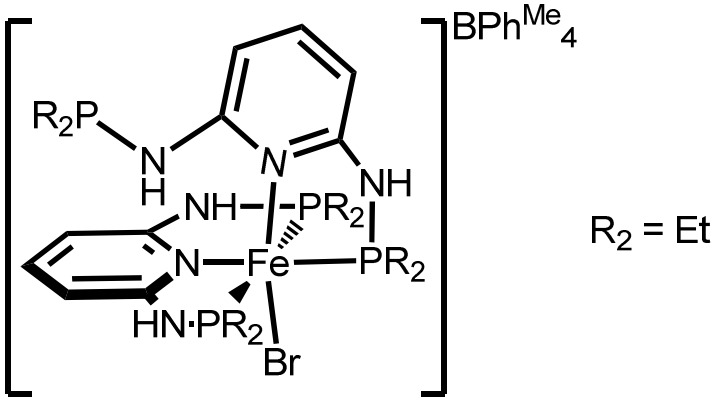

κ^2,κ^3-[Fe(PNP-Et)$_2$Br](BPh$^{Me}_4$) (12d)

The synthesis was performed analogously to procedure of **8d**, using **2d** (200 mg, 0.70 mmol), $FeBr_2$ (151 mg, 0.35 mmol) and THF (10 ml).Yield 352 mg (93%) (green powder; MW: 1081.72). Crystals were grown in THF by slow diffusion of Et_2O.

$C_{54}H_{78}BBrFeN_6P_4$, elemental analysis (calc): C, 59.96; H, 7.27; B, 1.00; Br, 7.39; Fe, 5.16; N, 7.77; P, 11.45

^{1}H NMR (δ, acetone-d_6, 20°C): 8.25 (s, 2H, NH^{k3}), 7.98 (s, 1H, NH^{k2}), 7.50 (t, J_{HP} = 8.0 Hz, 1H, Py$^{4\ k3}$), 7.23 (m, 8H, Ph^{2,6}), 7.09 (t, J_{HP} = 7.8 Hz, 1H, Py$^{4\ k2}$), 6.74 (m, 8H, Ph^{3,5}), 6.65 (d, J_{HP} = 8.0 Hz, 2H, Py$^{3,5\ k3}$), 6.40 (dd, J_{HP} = 4.0 Hz, 1H, Py$^{3\ k2}$), 6.09 (d, J_{HP} = 7.0 Hz, 1H, Py$^{5\ k2}$), 4881 (d, J_{HP} = 10.0 Hz, 1H, NH^{free}), 2.85-2.54 (m, ~8H, CH_2 ^{k3}), 2.51-2.34 (m, ~4H, CH_2^{k2}),2.15 (s, ~12H, Ph^{Me}), 2.07-2.00 (m, ~18H, $CH_3^{k3,k2}$), 1.38-1.31 (m, CH_2^{free}), 1.10-0.85 (m, CH_3^{free}). ^{13}C{^{1}H} NMR (δ, acetone-d_6, 20°C): 166.60 (d, J_{CP} = 17.7 Hz, Py$^{2\ k2}$),164.67 (m, Py$^{2,6\ k3}$), 162.38 (m, Py$^{6\ k2}$), 160.80 (q, J_{CB} = 50.1 Hz, Ph^1), 141.10 (s, Py$^{4\ k3}$), 139.37 (s, Py$^{4\ k2}$), 137.06 (m, Ph^4), 129.94 (s, Ph^{2,6}), 126.75 (q, J_{HB} = 2.9 Hz, Ph^{3,5}), 100.40 (s, Py$^{3,5\ k3}$), 99.40 (m, Py$^{3\ k2}$),98.80 (m, Py$^{5\ k2}$), 23.63 (d, J_{CP} = 10.4, CH_2^{free}), 22.27 (d, J_{CP} = 2.8 Hz, CH_2^{k2}), 21.36 (s, Ph^{Me}), 20.00 (t, J_{CP} = 12.2 Hz, CH_2^{k3}), 9.60 (d, J_{CP} = 15.6 Hz, CH_3^{free}), 8.45 (d, J_{CP} = 13.8 Hz, CH_3^{k2}), 7.83 (s, CH_3^{k3}). ^{31}P{^{1}H} NMR (δ, acetone-d_6, 20°C): 126.75 (s), 48.47 (s, P^{free})

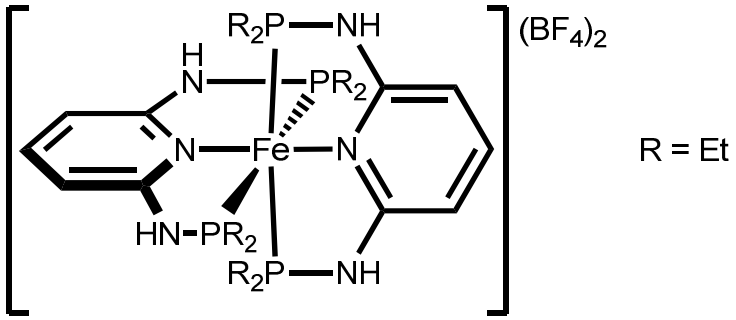

[Fe(PNP-Et)$_2$](BF$_4$)$_2$ (14d).

Method 1: **2d** (200 mg, 0.70 mmol) and $FeCl_2$ (44 mg, 0.35 mmol) are dissolved in Acetone (10 ml) and stirred for 1 h. $AgBF_4$ (136 mg, 0.70 mmol) is added to the suspension which turns purple upon. After 1 h the solution is filtrated over celite and the solvent removed. The purple solid is washed with 15 ml hexane before it is dried over vacuum. Yield 265 mg (95%) (purple powder; MW: 800.08).

Method 2: **2d** (85 mg, 0.30 mmol) and **15** $[Fe(H_2O)_6]^{2BF4}$ (47 mg, 0.14 mmol) are dissolved in THF (8 ml) and stirred for 3 h. The purple solid, is separated from solvent and washed with further 8 ml of THF. The purple product is dried over vacuum. Yield 102 mg (91%) (purple powder; MW: 800.08). Crystals were grown in Acetone by slow diffusion with Et_2O after exchange of the counter-ion with $NaBPh_4$.For NMR analysis and crystal growth **13d** with the BPh_4^-counter-ion was used because of better solubility.

$C_{26}H_{50}B_2F_8FeN_6P_4$, elemental analysis (calc): C, 39.03; H, 6.30; B, 2.70; F, 19.00; Fe, 6.98; N, 10.50; P, 15.49

^{1}H NMR (δ, acetone-d$_6$, 20°C):7.86 (s, 4H, NH), 7.34 (m, 18H, Py^4, Ph^{2,6}), 6.89 (m, 16H, Ph^{3,5}), 6.77 (m, 8H, Ph^4), 6.37 (d, J_{HP} = 7.8 Hz, 4H, Py^{3,5}), 2.87 (d, broad, J_{HP} = 45.7 Hz, 16H, CH_2), 1.03 (s, 24H, CH_3). ^{13}C{^{1}H} NMR (δ, acetone-d$_6$, 20°C): 164.95 (q, J_{CB} = 49.5Hz, Ph^1), 163.30 (s, Py^{2,6}), 141.71 (s, Py^4), 127.05 (d, J_{CB} = 1.7 Hz, Ph^4), 126.00 (d, J_{CB} = 2.7, Ph^{2,6}), 122.22 (s, Ph^{3,5}), 100.60 (s, Py^{3,5}), 25.56 (s, broad, CH_2), 7.71 (s, CH_3).b^{31}P{^{1}H} NMR (δ, acetone-d$_6$, 20°C): 130.74.

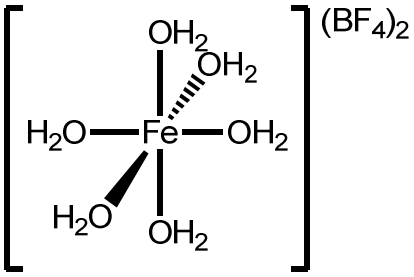

$[Fe(H_2O)_6](BF_4)_2$ (15).

15 was synthesized based on literature[36], suspending Fe-powder (5 g, 0.09 mmol) in H_2O (100 ml) and dropwise addition of HBF_4 (25 ml, 48% aqueous solution, 0.14 mmol). The suspension is stirred over for 16 h, filtrated and evaporated to saturation. The product crystallizes at -20°C and is washed with Et_2O (50 ml). Yield 21 g (70%) (off green crystals, MW: 337.47).

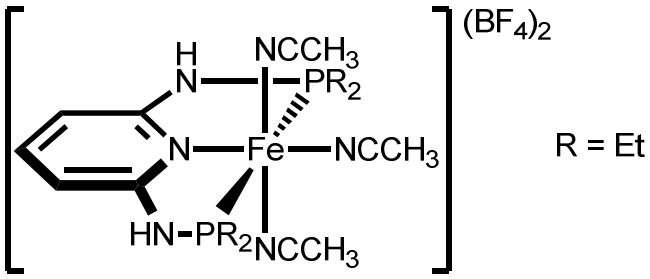

$[Fe(PNP\text{-}Et)(CH_3CN)_3](BF_4)_2$ (6d)

2d (340 mg, 1.2 mmol) and **15** $[Fe(H_2O)_6](BF_4)_2$ (440 mg, 1.3 mmol) are dissolved in CH_3CN (8 ml) and stirred for 2 h. The orange solution is evaporated to dryness, washed with DCM/Et_2O (15 ml ; 1:1) and dried over vacuum. Yield 490 mg (58%) (orange powder; MW: 637.92). Crystals were grown in MeCN by slow Et_2O diffusion.

$C_{19}H_{34}B_2F_8FeN_6P_2$, elemental analysis (calc): C, 35.77; H, 5.37; B, 3.39; F, 23.83; Fe, 8.75; N, 13.17; P, 9.71

^1H NMR (δ, CD_3CN, 20°C): 7.27 (t, J_{HP} = 8.1 Hz, 1H, py[4]), 7.23 (s, 2H, NH), 6.19 (d, J_{HP} = 8.0 Hz, 2H, py[3,5]), 1.98 (s, 9H, CH_3), 1.95 (dq, J_{HH} = 2.5 Hz, 8H, CH_2), 1.47 (dt, J_{HH} =7.4Hz, 12H, CH_3). $^{31}P\{^1H\}$ NMR (δ, CD_3CN, 20°C): 124.92 (s). IR (ATR, cm^{-1}): $\nu_{C=N}$ 2316, 2287.

Appendix

Literature

1. Morales-Morales, D. *Rev. Soc. Quím. Méx.* **2004,***48*, 338-346.
2. Moulton, C. J.; Shaw, B. L. *Chem. Soc., Dalton Trans.* **1976**, 1020–1024.
3. (a) Ewart; G.; Lane, A. P.; McKechnie, J.; Payne, D. S. *J. Chem. Soc.* **1964**, 1543-1547;(b) Lane, A. P.; Morton-Blake, D. A.; Payne, D. S. *J. Chem. Soc.* **1967**, 1492-1498.
4. Fei, Z.; Dyson, P. J. *Coord. Chem. Rev.* **2005**, 2056–2074.
5. Öztopçu, Ö.; Holzhacker, C.; Puchberger, M.; Weil, M.; Mereiter, K.; Veiros, L. F.; Kirchner, K. *Organometallics* **2013,***32*, 3042−3052.
6. (a) Casey, C. P.; Guan, H. *J. Am. Chem. Soc.* **2009,***131*, 2499-2507;(b) Casey, C. P.; Guan, H. *J. Am. Chem. Soc.* **2007,***129*, 5816-5817.
7. (a) Trovitch, R. J.; Lobkovsky, E.; Bill, E.; Chirik, P. J. *Organometallics* **2008,***27*, 1470–1478;(b) Trovitch, R. J.; Lobkovsky, E.; Chirik, P. J. *Inorg. Chem.* **2006,***45*.
8. Sui-Seng, C.; Haque, F. N.; Hadzovic, A.; Pütz, A.-M.; Reuss, V.; Meyer, N.; Lough, A. J.; Iuliis, M. Z.-D.; Morris, R. H. *Inorg. Chem.* **2009,***48*, 735-743.
9. (a) Langer, R.; Leitus, G.; Ben-David, Y.; Milstein, D. *Angew. Chem. Int. Ed.* **2011,***50*, 2120 –2124;(b) Langer, R.; Iron, M. A.; Konstantinovski, L.; Diskin-Posner, Y.; Leitus, G.; Ben-David, Y.; Milstein, D. *Chem. Eur. J.* **2012,***18*, 7196-7209;(c) Zell, T.; Butschke, B.; Ben-David, Y.; Milstein, D. *Chem. Eur. J.* **2013,***19*, 8068-8072.
10. EPA. *EPA-452/R-09-004* **2009**.
11. Wang, B.; Zhao, Y.; Hu, L.; Cao, J.; Gao, F.; Liu, Y.; Wang, L. *Chin.Sci.Bull.* **2010,***55*, 228-232.
12. Tate, C. W.; Gee, A. D.; Kealey, S.; Vilar, R.; Whites, A. J. P.; Long, N. J. *Dalton Trans.* **2012,***41*, 83-89.
13. Wilson, A. D.; Fraze, K.; Twamley, B.; Miller, S. M.; DuBois, D. L.; DuBois, M. R. *J. Am. Chem. Soc.* **2008,***130*, 1061-1068.
14. Tate, C. W.; Geea, A. D.; Vilar, R.; White, A. J. P.; Long, N. J. *J. Orgmet. Chem.* **2012,***715*, 399-42.
15. Itou, M.; Araki, Y.; Ito, O.; Kido, H. *Inorg. Chem.* **2006,***45*, 6114−6116.
16. Moragues, M. E.; Esteban, J.; Ros-Lis, J. V.; Martinez-Manez, R.; Marcos, M. D.; Martinez, M.; Soto, J.; Sancenón, F. *J. Am. Chem. Soc.* **2011,***133*, 15762–15772.
17. Benito-Garagorri, D.; Puchberger, M.; Mereiter, K.; Kirchner, K. *Angew. Chem. Int. Ed.* **2008,***47*, 9142-9145.
18. (a) Benito-Garagorri, D.; Gonçalo-Alves, L.; Veiros, L. F.; Standfest-Hauser, C. M.; Tanaka, S.; Mereiter, K.; Kirchner, K. *Organometallics* **2010,***29*, 4932–4942;(b) Benito-Garagorri, D.; Alves, L. G.; Puchberger, M.; Mereiter, K.; Veiros, L. F.; José-Calhorda, M.; Deus-Carvalho, M.; Ferreira, L. P.; Godinho, M.; Kirchner, K. *Organometallics* **2009,***28*, 6902–6914.
19. Benito-Garagorri, D.; Becker, E.; Wiedermann, J.; Lackner, W.; Pollak, M.; Mereiter, K.; Kisala, J.; Kirchner, K. *Organometallics* **2006,***25*, 1900-1913.
20. Brown, T. L.; Lee, K. J. *Coord. Chem. Rev.* **1993,***128*, 89–116.
21. Rietveld, M. H. P.; Grove, D. M.; Koten, G. V. *New J. Chem.* **1997,***21*, 751-771.
22. Smith, D. A.; Roşca, D.-A.; Bochmann, M. *Organometallics* **2012,***31*, 5998−6000.

23. Qingchen Dong, M. J. R., Wai-Yeung Wong and Harry B. Gray. *Inorg. Chem.* **2011,***50*, 10213–10224.
24. Hayashi, A.; Okazaki, M.; Ozawa, F. *Organometallics* **2007,***26*, 5246-5249.
25. Jana, R.; Tunge, J. A. *J. Org. Chem.* **2011,***76*, 8376–8385.
26. Vallée, C.; Chauvin, Y.; Basset, J.-M.; Santini, C. C.; Galland, J.-C. *Adv. Synth. Catal.* **2005,***347*, 1835-1847.
27. (a) Niebergall, H. *Angew. Chem.* **1960,***72*, 210;(b) Niebergall, H.; Langenfeld, B. *Chem. Ber.* **1962,***95*, 64-76.
28. Wolfsberger, W. *J. Org. Chem.* **1986,** (317), 167-173.
29. Patel, N. K.; James-Harwood, H. *J. Org. Chem.* **1967,***32*, 2999-3003.
30. Coe, B. J.; Glenwright, S. J. *Coord. Chem. Rev.* **2000,***203*, 5-80.
31. Hoppee, J. J. *J. Chem. Ed.* **1972,***49*, 505.
32. Alves, L. G.; Dazinger, G.; Veiros, L. F.; Kirchner, K. *Eu. J. Inorg. Chem.* **2010,***20*, 3160-3166.
33. Cowley, A. H. *Chem. Rev.* **1965,***65*, 617-634.
34. Barta, K.; Eggenstein, M.; Hölscher, M.; Franciò, G.; Leitner, W. *Eu. J. Org. Chem.* **2009**, 6198-6204.
35. Komiya, S. *Synthesis of Organometallic Compounds* **1997,**(pp. 35-57), Wiley&Sons.
36. Dîrtu, M. M.; Schmit, F.; Naik, A. D.; Rotaru, A.; Marchand-Brynaert, J.; Garcia, Y. *Int. J. Mol. Sci.* **2011,***12*, 5339-5351.

List of Figures

List of Abbreviations

THF	Tetrahydrofurane
Et_2O	Diethylether
DCM	Dichloromethane
MeOH	Methanol
EtOAc	Ethylacetate
CH_3CN	Acetonitrile
OTf	Trifluoromethanesulfonate
2,6-DAP	2,6-Diaminopyridine
NEt_3	Triethylamine
BuLi	Butyl-lithium
BPh_4	Tetraphenylborate
BPh_4Me	Tetrakis(4-methylphenyl)borate
BF_4	Tetrafluoroborate
PF_6	Hexafluorophosphate
BAr^F	$[B[3,5\text{-}(CF_3)_2C_6H_3]_4]^-$
h	Hour(s)
min	Minute(s)
HOMO	Highest occupied molecule orbital
LUMO	Lowes unoccupied molecule orbital

List of Compounds

Ligand	
a	PNP-BIPOL
b	PNP-Ph
b‘	N-methyl-PNP-Ph (PNP^{Me}-Ph)
c	3,5-Dichloro-PNP-Ph (^{Cl2}PNP-Ph)
d	PNP-Et
e	PNP-*i*Pr
f	PNP-^{tBu,OMe}BIPOL
g	PNP-^{tBu,tBu}BIPOL
Compounds/Complexes	
1	Chlorophosphines
2	PNP-Ligand
3	Mono-posphorylated 2,6 DAP (PN^{NH2})
4	Di-chloro-mono-CO-Fe(PNP)
5	Di-bromo-mono-CO-Fe(PNP)
6	$[$Mono-chloro-bis-CO-Fe(PNP)$]^+$
7	$[$Mono-bromo-bis-CO-Fe(PNP)$]^+$
8	Di-chloro-Fe(PNP)
9	κ^2,κ^3-$[Fe(PNP)_2Cl]^+$
10	κ^2,κ^3-$[Fe(PNP)_2Cl]^+$ hydrolyzed
11	*trans*-κ^2,κ^3-$[Fe(PNP)_2Cl]^+$
12	κ^2,κ^3-$[Fe(PNP)_2Br]^+$
13	$[Fe(PNP)(PN)Cl]^+$
14	$[Fe(PNP)_2]^{2+}$
15	$[Fe(H_2O)_6]^{2+}$
16	$[Fe(PNP)(CH_3CN)_3]^{2+}$